CATALYTIC DEHYDROAROMATIZATION OF ALKANES BY

PINCER-LIGATED IRIDIUM COMPLEXES

By

ANDREW MURRAY STEFFENS

A dissertation submitted to the

Graduate School-New Brunswick

Rutgers, The State University of New Jersey

In partial fulfillment of the requirements

For the degree of

Doctor of Philosophy

Graduate Program in Chemistry and Chemical Biology

Written under the direction of

Alan S. Goldman

And approved by

_____

_____

_____

_____

New Brunswick, New Jersey

January 2016

ABSTRACT OF THE DISSERTATION

CATALYTIC DEHYDROAROMATIZATION OF ALKANES

BY PINCER-LIGATED IRIDIUM COMPLEXES

By

ANDREW MURRAY STEFFENS

Dissertation Director:

Alan S. Goldman

Further understanding of the activation of small molecules by metal complexes is an ongoing goal in organometallic chemistry, and expansion on previously reported reactions is of particular interest. This thesis will discuss expansion of transfer dehydrogenation reactions, specifically multiple transfer dehydrogenation reactions of alkanes leading to aromatic products in one pot.

The synthesis of the pincer catalyst used for dehydroaromatization reactions is presented along with full characterization of each step. Optimization of dehydroaromatization reactions was performed on a variety of *n*-alkane starting materials to maximize yield of alkylbenzene products. Kinetics and concentrations for each starting material are presented to highlight the complexity of these reactions.

Despite a mechanism that would suggest otherwise, dehydroaromatization reactions surprisingly yield benzene regardless of the starting *n*-alkane. This interesting appearance of benzene is discussed along with yields of benzene for various *n*-alkanes.

Mechanistic studies and DFT calculations were performed to elucidate the mechanism through which benzene is formed, and these studies show that benzene forms though a retro-ene mechanism. Attempts to limit or maximize benzene formation were performed by utilizing the information gained through the retro-ene mechanism.

Expansion of dehydroaromatization reactions is discussed through multiple dehydroaromatization reactions on the same starting material. Of particular emphasis was the formation of 1,5-dimethylnaphthalene, which is a precursor to the desirable polymer polyethylene naphthalate. 1,5-dimethylnaphthalene was observed as a product from dehydroaromatization reactions, and mechanistic studies were performed to understand the mechanism for the second dehydroaromatization reaction. Attempts to maximize yield of 1,5-dimethylnaphthalene and *o*-pentyltoluene, which is a precursor to 1,5-dimethylnaphthalene, were performed.

Further expansion of dehydroaromatization reactions is discussed through dehydroaromatization of branched alkanes to yield products not obtainable through dehydroaromatization of *n*-alkanes. Of particular focus is accessing *p*-xylene and *m*-xylene via dehydroaromatization. A new synthesis of *p*-xylene is presented using ethylene as a starting material and utilizing dehydroaromatization of 2-ethyl-1-hexene. Optimization of these reactions is also discussed.

Acknowledgement

I would first like to thank my adviser, Dr. Alan Goldman, for everything he has done to make this work possible. His unfailing guidance and continued willingness to have meaningful and helpful conversations have been of immeasurable value to me. Alan has helped me tremendously and I greatly appreciate the opportunities he has afforded to me.

I would like to thank Dr. Heinz Roth and Dr. Fuat Celik for their time and support in serving on my committee. I would also like to thank Dr. Karsten Krogh-Jespersen and Dr. Kai Hultzsch for being a part of my original committee. I am grateful to Dr. Nagarajan Murali for his expertise in NMR techniques and to Dr. Alexei Ermakov for his expertise in instrumental troubleshooting.

My graduate school experience would not have been possible without the wonderful experience I had at Gettysburg College for my undergraduate degree. I would particularly like to thank Dr. Timothy Funk for being such a driving force in my chemistry career, and both serving as my undergraduate adviser and on my graduate thesis committee. His love of organometallic chemistry was infectious and led me to pursue organometallic chemistry in my graduate career (particularly with iridium!).

I am extremely thankful to past and current members of the Goldman Group for making our lab a good place to work and spend five years doing research. The lab atmosphere was supportive and happy and I appreciate the help of the lab on any issues I may have faced. I would particularly like to thank Dr. Akshai Kumar, Dr. Jongwook Choi,

Dr. Thomas Dugan, Dr. Jason Hackenberg, Dr. David Wang, Dr. Kathleen Field, Dr. Michael Haibach, Michael Blessent, and Nicholas Lease for their discussions and ideas that helped form the work in this thesis.

I would like to thank my friends for their continued support throughout my graduate career and for maintaining connections and keeping me motivated. Particularly I would like to thank Dr .Gregory Bitto, Andrew Krasley, Gregory Purifoy, Aaron Deibler-Gorman, and Dr. Paul Smith. My future in-laws have been incredibly supportive of me and my work for a very long time and I owe them a great deal. Thank you Dr. Arun Kalyan-Masih, Mrs. Pamela Kalyan-Masih, and Dr. Priya Kalyan-Masih. My family has afforded me nothing but happiness and encouragement throughout my life and nothing I have achieved would be possible without them. Thank you Nancy Murray, Brad Steffens, and Kyle Steffens for making me into a better person and always believing that what I achieved was special.

And of course my deepest thanks and gratitude go to my fiancée, Sabeen Kalyan-Masih. My life has been so amazing since she entered it and I cannot fully express how truly thankful I am to her for being my rock and continually showing me how proud she is of me and my work. I love her with all my heart and this work would not have been possible without her.

Dedication

To Sabeen, Mom, Dad, and Kyle,

for always being there, no matter what.

Table of Contents

List of Figures

List of Schemes

List of Tables

Chapter 1

1.1 Introduction

Further understanding of the factors affecting the activation of small molecules by transition metal complexes is a major goal in organometallic chemistry due to the wide applicability of these reactions. The two fundamental transformations in organometallic chemistry are oxidative addition and the reverse reaction, reductive elimination.[1] Oxidative addition with a metal complex involves the cleavage of an X-Y bond along with formation of new M-X and M-Y bonds.[2] The desire to understand these processes is a result of the need to discover new chemistry to activate C-H bonds, which are typically thought of as bonds that cannot be activated.[3]

The earliest account of oxidative addition to a transition metal complex was reported by Vaska in 1962 with the complex that is now named after him (Scheme 1.1).[4]

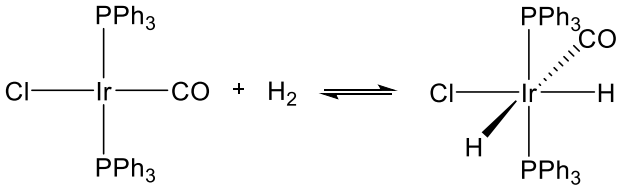

Scheme 1.1: Oxidative addition of H_2 to Vaska's Complex

The oxidative addition of H_2 to this complex was followed by a report where it was used in the catalytic hydrogenation of ethylene and acetylene.[5] In the same year, Wilkinson

reported the oxidative addition of H_2 via dissociation of a PPh_3 group with the similar hydrogenation catalyst that now bears his name (Scheme 1.2).[6,7]

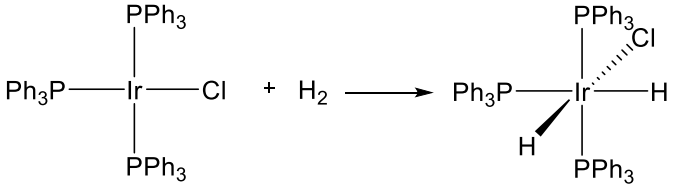

Scheme 1.2: Oxidative addition of H_2 to Wilkinson's Catalyst

This pioneering work in the field of small molecule activations, along with mechanistic studies of these transformations, led to an understanding that if oxidative addition of H_2 and subsequent hydrogenation and reductive elimination of olefins was possible, then perhaps C-H bond activation was also possible.[8-10]

The activation and functionalization of C-H bonds has been one of the major challenges of modern chemistry due to the strong nature of the C-H bond. In fact, C-H bonds are often thought of as the un-functional group; in organic shorthand, C-H bonds are completely omitted. The first example of the highly desirable activation of C-H bonds was reported in 1965 by Chatt and Davidson.[11] They found the aryl C-H activation of naphthalene with $Ru(0)(dmpe)_2$ yields a napthyl hydride complex (Scheme 1.3).

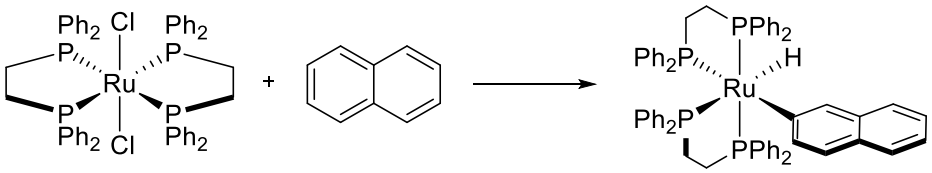

Scheme 1.3: Oxidative addition of naphthalene to $Ru(0)(dmpe)_2$

Several years later, Green and Knowles reported oxidative addition of benzene to a tungsten complex after photolytic loss of H_2 (Scheme 1.4).[12,13]

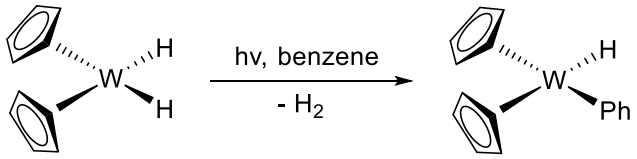

Scheme 1.4: Oxidative addition of benzene to Cp_2WH_2

It was not until 1982 that Bergman and Graham independently reported the C-H activation of alkyl bonds. Janowicz and Bergman reported C-H activation of cyclohexane resulting from photolytic loss of H_2 with $Cp^*Ir(PMe_3)(H)_2$ (Scheme 1.5).[14]

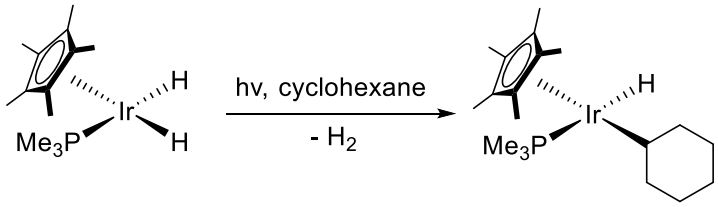

Scheme 1.5: C-H activation of cyclohexane

Similarly, Hoyano and Graham reported C-H activation of neopentane resulting from photolytic loss of CO with $Cp^*Ir(CO)_2$ (Scheme 1.6).[15]

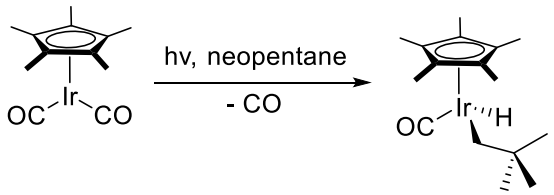

Scheme 1.6: C-H activation of neopentane

The first reports of C-H activation caused many researchers to question the selectivity of these reactions. Specifically, mechanistic studies of C-H activated alkane complexes by Bergman, Bercaw, and Jones showed that there is a surprising thermodynamic preference for C-H activation at the strongest C-H bonds (primary > secondary > tertiary) regardless of metal-ligand framework.[16-18] Similarly, despite arene C-H bonds being stronger than alkyl C-H bonds, C-H activation of arenes is thermodynamically favorable.[19, 20] All these observations were initially described as being

caused by steric effects, but more recently have been attributed to electronic effects.[16-18, 21-24]

The oxidative addition of alkyl C-H bonds to metal complexes is of particular emphasis here due to the importance of catalytic transfer dehydrogenation reactions. The ability to transform alkanes into higher value olefins is of great interest because of the importance of olefins for many synthetic reactions. Dehydrogenation is a thermodynamically uphill process, but when combined with the thermodynamically downhill hydrogenation reaction, catalytic dehydrogenation becomes a possibility under relatively mild conditions.[25] Crabtree reported the first example of dehydrogenation using the sacrificial hydrogen acceptor *tert*-butyl ethylene (TBE) and the cationic complex $[IrH_2(acetone)_2(PPh_3)_2][BF_4]$ to dehydrogenate cycloalkanes.[26] As more research was published, it became clear that "pincer"-type catalysts are exceedingly good transfer dehydrogenation catalysts.

Moulton and Shaw reported the first examples of pincer complexes in 1976, which are named after the meridionally-bound tridentate ligand that is coordinated to the metal (Figure 1.1).[27]

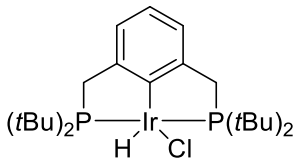

Figure 1.1: One of the first pincer complexes

Their novel ligand, κ^3-2,6-(tBu$_2$PCH$_2$)$_2$C$_6$H$_3$, was abbreviated to $^{t\text{Bu}4}$PCP; subsequent pincer ligands have been abbreviated based on the atoms that are bound to the metal center and by any non-carbon linkers. The field of pincer catalysts has expanded drastically in the decades following this report due to the multitude of applications for these catalysts, which can be attributed to their high thermal stability (>240 °C) and the ease with which the ligand system can be systematically tuned. Adaptations to the sterics or electronics of these complexes can have a dramatic change on the reactivity and selectivity of those catalysts (Figure 1.2).[28]

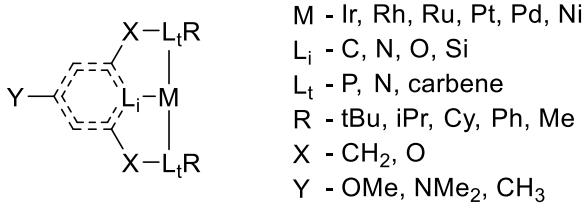

Figure 1.2: Variations to the pincer complex framework

For example, changing the R group from *tert*-butyl groups to *i*so-propyl or phenyl groups will change the sterics of the complex; sterically bulky complexes are typically more thermally stable and higher in selectivity whereas sterically less bulky complexes can be more reactive.[29, 30] Also, changing the L_t group from P to nitrogen or carbene can change the sterics and electronics of the complex and allow for those ligands to become hemilabile.[31, 32] Other modifications include changing the X linker from CH_2 to O, placing

electron donating or electron withdrawing groups in the L_i or Y positions to change the electronics or allow the catalyst to be supported onto silica or alumina, and changing the metal center.[33-41]

The research groups of Kaska and Jensen reported the first example of transfer dehydrogenation using a pincer complex in 1996, showing that ($^{t\text{Bu}4}$PCP)Ir(H_2) has high catalytic activity (Scheme 1.7).[42]

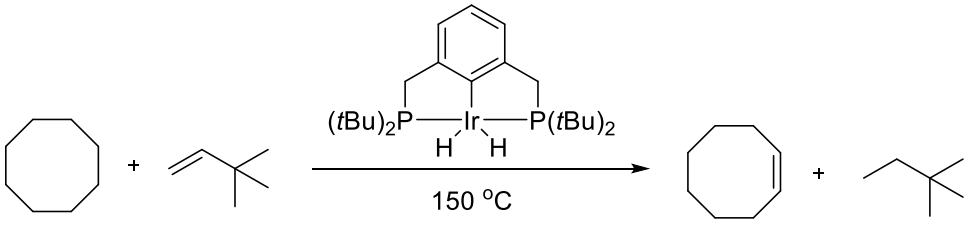

Scheme 1.7: Transfer dehydrogenation of cyclooctane

The corresponding rhodium complex was shown to be significantly less active for transfer dehydrogenation which is in agreement with a study by Goddard and coworkers stating that iridium is the best transition metal for dehydrogenation.[43] Following this work, Goldman and Jensen reported the selective transfer dehydrogenation of *n*-octane to yield 1-octene (Scheme 1.8).[44]

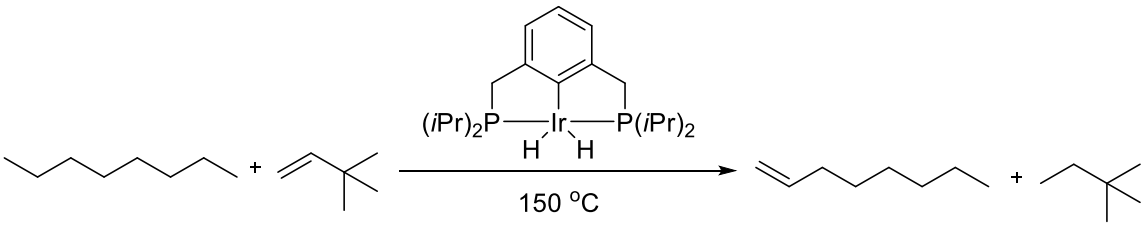

Scheme 1.8: Selective dehydrogenation of *n*-octane

The kinetically favored product is 1-octene, but isomerization of 1-octene by the catalyst under the reaction conditions rapidly yields the thermodynamically favored internal olefins. Around the same time, Goldman also reported that catalytic dehydrogenation is possible without an acceptor due to the thermal stability of these pincer catalysts.[45, 46] Mechanistic studies have since elucidated the mechanism for transfer dehydrogenation, which takes place through a 1,2 insertion of the acceptor (TBE) followed by reductive elimination of the hydrogenated acceptor (*tert*-butyl ethane or TBA), and oxidative addition of the alkane (cyclooctane or COA) followed by β-hydride elimination of the olefin (cyclooctene or COE) (Figure 1.3).[47, 48]

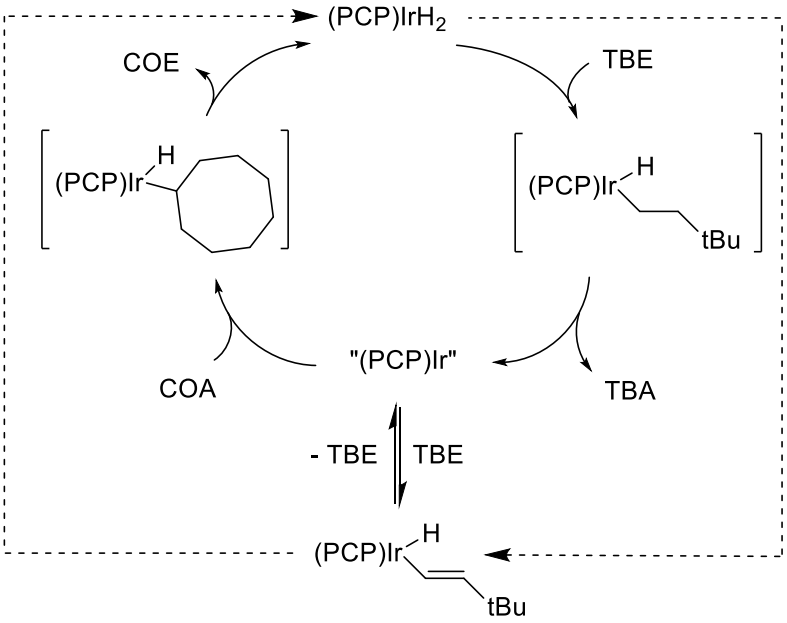

Figure 1.3: Mechanism for transfer dehydrogenation

The concept of alkane dehydrogenation has since been expanded to more ambitious multistep processes such as alkane metathesis and dehydroaromatization. Alkane metathesis is a tandem catalytic process that uses a dehydrogenation catalyst and an olefin metathesis catalyst to convert, for instance, two *n*-hexane molecules into *n*-decane and ethane. This process utilizes a pincer catalyst to dehydrogenate an *n*-alkane to an olefin, followed by olefin metathesis of two of those olefins to a single longer chain olefin, followed by hydrogenation of that longer chain olefin with the original pincer catalyst to give a longer chain *n*-alkane and a shorter chain *n*-alkane as the final products (Figure 1.4).[49, 50]

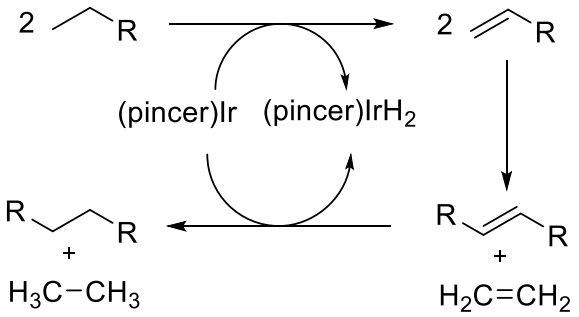

Figure 1.4: Alkane metathesis process

There are some limiting factors to the industrial viability of alkane metathesis. As noted before in the context of selectivity, pincer catalysts are highly selective for α-olefins kinetically, but because pincer catalysts are good isomerization catalysts, the α-olefins are quickly isomerized to the thermodynamically favorable internal olefins. This opens up the possibility for metathesis with chains of differing lengths which gives an unselective distribution of metathesized products. Studies have been done to enhance regioselectivity for dehydrogenation and increase overall selectivity for alkane metathesis.[51, 52]

The first example of homogeneous dehydroaromatization was published by Goldman and coworkers in 2011.[53] They reported that a pincer catalyst with four equivalents of hydrogen acceptor can convert *n*-alkanes into aromatics in one pot, which allows for conversion of relatively low value alkanes to relatively high value alkylaromatics (Scheme 1.9).

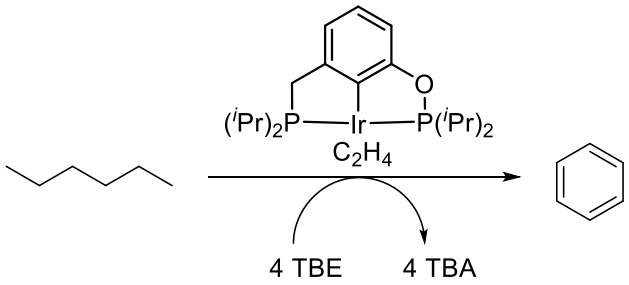

Scheme 1.9: Dehydroaromatization of *n*-hexane

Optimization and expansion of the dehydroaromatization process are the focus of this thesis.

1.2 Research Goals of this Thesis

Further understanding of the dehydroaromatization process is still a worthwhile goal in the Goldman lab. This thesis aims to better understand the dehydroaromatization process while also optimizing and expanding on the initially reported dehydroaromatization results. The rest of this thesis is organized into two parts. The first part includes Chapters 2 and 3 and focuses on optimizing and further understanding the dehydroaromatization reaction. The second part includes Chapters 4 and 5 and focuses on expanding dehydroaromatization reactions to other uses.

Chapter 2 discusses the synthesis of the ($^{i\text{Pr}}$PCOP)Ir(C_2H_4) catalyst which is the primary catalyst used for all dehydroaromatization reactions. Also, the previously reported dehydroaromatization results are enhanced with improved reaction methods

and with the addition of NaO^tBu. Higher yields and decreased reaction times were achieved through this work.

Chapter 3 discusses the surprising appearance of benzene for *n*-alkanes of increasing length. Mechanistic studies and density functional theory (DFT) calculations are performed to understand the mechanism through which benzene is formed. Attempts to control the amount of benzene formed are also discussed.

Chapter 4 presents the interesting formation of 1,5-dimethylnaphthalene from *n*-dodecane. This molecule is desirable because it is a precursor to a monomer of polyethylene naphthalate (PEN), which is a polymer that is superior to polyethylene terephthalate (PET) in many ways except for total cost. Attempts to maximize yield of 1,5-dimethylnaphthalene or *o*-pentyltoluene, which can be cyclized via zeolites to form 1,5-dimethylnaphthalene, are discussed. Biaromatic formation with *n*-tridecane as the starting material is also detailed.

Chapter 5 discusses the dehydroaromatization of branched starting materials to give products that are impossible to access via dehydroaromatization of *n*-alkanes. Specifically, dehydroaromatization to yield *p*-xylene and *m*-xylene are detailed, along with a process to synthesize *p*-xylene from ethylene starting material. Data to maximize yields of xylenes and minimize formation of dimerized side products are presented.

1.3 References

[1] Halpern, J. *Acc. Chem. Res.* **1970**, *3*, 386.
[2] Hartwig, J. F. *Organotransition Metal Chemistry: From Bonding to Catalysis*; University Science Books: Sausalito, CA, 2010.
[3] Golberg, K. I.; Goldman, A. S. *Activation and Functionalization of C-H Bonds*; Oxford University Press, 2004.
[4] Vaska, L; DiLuzio, J. W.; *J. Am. Chem. Soc.* **1962**, *84*, 679.
[5] Vaska, L.; Rhodes, R. E. *J. Am. Chem. Soc.* **1965**, *87*, 4970.
[6] Young, J. F.; Osborn, J. A.; Jardine, F. H.; Wilkinson, G. *Chem. Commun.* **1965**, 131.
[7] Osborn, J. A.; Jardine, F. H.; Young, J. F.; Wilkinson, G. *J. Chem. Soc., A* **1966**, 1711.
[8] Chock, P. B.; Halpern, J. *J. Am. Chem. Soc.* **1966**, *88*, 3511.
[9] Eberhardt, G. G.; Vaska, L. *J. Catal.* **1967**, *8*, 183.
[10] Halpern, J.; Wong, C. S. *J. Chem. Soc., Chem. Commun.* **1973**, 629.
[11] Chatt, J.; Davidson, J. M. *J. Chem. Soc.* **1965**, 843.
[12] Green, M. L. H.; Knowles, P. J. *J. Chem. Soc. D* **1970**, 1677.
[13] Green, M. L. H.; Knowles, P. J. *J. Chem. Soc. A* **1971**, 1508.
[14] Janowicz, J. A.; Bergman, R. G. *J. Am. Chem. Soc.* **1982**, *104*, 352.
[15] Hoyano, J. K.; Graham, W. A. G. *J. Am. Chem. Soc.* **1982**, *104*, 3723.
[16] Buchanan, J. M.; Stryker, J. M.; Bergman, R. G. *J. Am. Chem. Soc.* **1986**, *108*, 1537.
[17] Bryndza, H. E.; Fong, L. K.; Paciello, R. A.; Tam, W.; Bercaw, J. E. *J. Am. Chem. Soc.* **1987**, *109*, 1444.
[18] Northcutt, T. O.; Wick, D. D.; Vetter, A. J.; Jones, W. D. *J. Am. Chem. Soc.* **2001**, *123*, 7257.
[19] Janowicz, A. H.; Periana, R. A.; Buchanan, J. M.; Kovac, C. A.; Stryker, J. M.; Wax, M. J.; Bergman, R. G. *Pure and Appl. Chem.* **1984**, *56*, 13.
[20] Jones, W. D.; Feher, F. J. *J. Am. Chem. Soc.* **1984**, *106*, 1650
[21] Jones, W. D.; Hessell, E. T. *J. Am. Chem. Soc.* **1993**, *115*, 554.
[22] Bennett, J. L.; Wolczanski, P. T. *J. Am. Chem. Soc.* **1994**, *116*, 2179.
[23] Wick, D. D.; Jones, W. D. *Organometallics* **1999**, *18*, 495.
[24] Choi, G.; Morris, J.; Brennessel, W. W.; Jones, W. D. *J. Am. Chem. Soc.* **2012**, *134*, 9276.
[25] Crabtree, R. H.; Mellea, M. F.; Mihelcic, J. M.; Quirk, J. M. *J. Am. Chem. Soc.* **1982**, *104*, 107.
[26] Crabtree, R. H.; Mihelcic, J. M.; Quirk, J. M. *J. Am. Chem. Soc.* **1979**, *101*, 7738.
[27] Moulton, C. J.; Shaw, B. L. *J. Chem. Soc., Dalton Trans.* **1976**, 1020.
[28] Choi, J.; MacArthur, A. H. R.; Brookhart, M.; Goldman, A. S. *Chem. Rev.* **2011**, *111*, 1761.
[29] Rybtchinski, B.; Ben-David, Y.; Milstein, D. *Organometallics* **1997**, *16*, 3786.
[30] Punji, B.; Emge, T. J.; Goldman, A. S. *Organometallics*, **2010**, *29*, 2702.
[31] Flores, J. A.; Haibach, M. C.; Goldman, A. S. ACS: 2012, INOR 8.
[32] Nishiyama, H.; Niwa, E.; Inoue, T; Ishima, Y.; Aoki, K. *Organometallics* **2002**, *21*, 2572.
[33] Göttker-Schnetmann, I.; White, P. S.; Brookhart, M. *Organometallics* **2004**, *23*, 1766.
[34] Huang, Z.; Rolfe, E.; Carson, E. C.; Brookhart, M.; Goldman, A. S.; El-Khalafy, S. H.; MacArthur, A. H. R. *Adv. Synth. Catal.* **2010**, *352*, 125.
[35] Krogh-Jespersen, K.; Czerw, M.; Zhu, K.; Singh, B.; Kanzelberger, M.; Darij, N.; Achord, P. D.; Renkema, K. B.; Goldman, A. S. *J. Am. Chem. Soc.* **2002**, *124*, 10797.
[36] Huang, Z.; Brookhart, M.; Goldman, A. S.; Kundu, S.; Ray, A.; Scott, S. L.; Vincente, B. C. *Adv. Synth. Catal.* **2009**, *351*, 188.
[37] Ben-Ari, E.; Gandelman, M.; Rozenberg, H.; Shimon, L. J. W.; Milstein, D. *J. Am. Chem. Soc.* **2003**, *125*, 4714.
[38] Fan, L; Parkin, S.; Ozerov, O. V. *J. Am. Chem. Soc.* **2005**, *127*, 16772.
[39] van der Boom, M. E.; Milstein, D. *Chem. Rev.* **2003**, *103*, 1759.
[40] Frech, C. M.; Shimon, L. J. W.; Milstein, D. *Organometallics* **2009**, *28*, 1900.
[41] Adams, J. J.; Lau, A.; Arulsamy, N.; Roddick, D. M. *Inorg. Chem.* **2007**, *46*, 11328.

[42] Gupta, M.; Hagen, C.; Flesher, R. J.; Kaska, W. C.; Jensen, C. M. *Chem. Commun.* **1996**, 2083.
[43] Perry, J. K.; Ohanessian, G.; Goddard, W. A. *Organometallics*, **1994**, *13*, 1870.
[44] Liu, F.; Pak, E. B.; Singh, B.; Jensen, C. M.; Goldman, A. S. *J. Am. Chem. Soc.* **1999**, *121*, 4086.
[45] Xu, W.; Rosini, G. P.; Gupta, M.; Jensen, C. M.; Kaska, W. C.; Krogh-Jespersen, K.; Goldman, A. S. *Chem. Commun.* **1997**, 2273.
[46] Liu, F.; Goldman, A. S. *Chem. Commun.* **1999**, 655.
[47] Renkema, K. B.; Kissin, Y. V.; Goldman, A. S. *J. Am. Chem. Soc.* **2003**, *125*, 7770.
[48] Kanzelberger, M.; Singh, B.; Czerw, M.; Krogh-Jespersen, K.; Goldman, A. S. *J. Am. Chem. Soc.* **2000**, *122*, 11017.
[49] Goldman, A. S.; Roy, A. H.; Huang, Z.; Ahuja, R.; Schinski, W.; Brookhart, M. *Science* **2006**, *312*, 257.
[50] Bailey, B. C.; Schrock, R. R.; Kundu, S.; Goldman, A. S.; Huang, Z.; Brookhart, M. *Organometallics*, **2009**, *28*, 355.
[51] Nawara-Hultzsch, A. J.; Hackenberg, J. D.; Punji, B.; Supplee, C.; Emge, T. J.; Bailey, B. C.; Schrock, R. R.; Brookhart, M.; Goldman, A. S. *ACS Catalysis* **2013**, *3*, 2505.
[52] Soumik, B.; Blessent, M.; Zhou, T.; Wang, D. Y.; Krogh-Jespersen, K.; Goldman, A. S. *J. Am. Chem. Soc.* **2015**, Manuscript Submitted.
[53] Ahuja, R.; Punji, B.; Findlater, M.; Supplee, C.; Schinski, W.; Brookhart, M.; Goldman, A. S. *Nature Chem* **2011**, *3*, 167.

Chapter 2

Synthesis of ($^{i\text{Pr}}$PCOP)Ir(C_2H_4) and Optimization of the Dehydroaromatization Process

Abstract

The synthesis of ($^{i\text{Pr}}$PCOP)Ir(C_2H_4) has been carried out for use in dehydroaromatization reactions and the ligand and subsequent iridium complexes were fully characterized. Other catalysts have proven to be inferior dehydroaromatization catalysts compared to ($^{i\text{Pr}}$PCOP)Ir(C_2H_4). Increased yields for previously reported dehydroaromatization reactions are shown through optimization of the dehydroaromatization process, which has been achieved by increasing the temperature and by adding NaO^{t}Bu as an additive. Dimer formation during the dehydroaromatization process is shown to be limited by increased temperature. Yields for dehydroaromatization of other *n*-alkane starting materials are also reported.

2.1 Introduction

C-H activation and functionalization remains a critical focus for organometallic chemistry research, especially as it applies to catalytic dehydrogenation. The first example of catalytic dehydrogenation with a pincer catalyst was reported by Kaska and Jensen in the mid-1990s using ($^{t\text{Bu}}$PCP)Ir(H_2).[1] In the two decades since that initial report, the Goldman Group, among others, has refined the field of C-H activation by pincer catalysts. A large variety of pincer catalysts have been reported for a wide array of applications depending on the specific sterics or electronics required for each reaction.[2-16] Similarly, the field of C-H activation and functionalization has expanded to multi-step reactions such as dehydroaromatization (Scheme 2.1).[17]

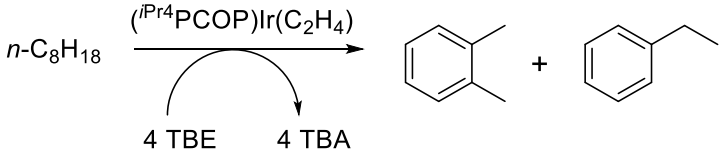

Scheme 2.1: Dehydroaromatization of *n*-octane

Dehydroaromatization is a useful reaction to access valuable alkylbenzenes from cheap *n*-alkane starting materials. Over sixty billion pounds of high molecular weight alkylbenzenes are commercially produced each year for use as detergents or surfactants.[18-20] In fact, 75% of detergents and 25% of surfactants produced each year use

linear alkylbenzene sulfonates (LAS), which are derived directly from linear alkylbenzenes (LABs) (Figure 2.1).[21]

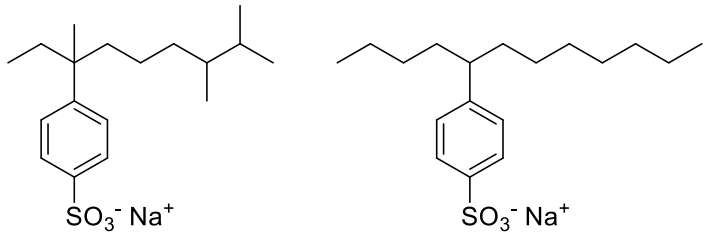

Figure 2.1: Examples of linear alkylbenzene sulfonates

Detergents and surfactants are being investigated for use in enhanced oil recovery and subsequently have drawn further commercial interest as research suggests that LAS are indeed favorable oil displacement agents.[22, 23] These LABs are synthesized via arene-olefin coupling reactions, and benzene alkylation is a prerequisite to produce LABs via commercially viable methods.[18-20, 24-25] The LABs are primarily synthesized through Friedel-Crafts alkylation reactions; however, the products are not exclusively *n*-alkyl derivatives, as an unselective distribution of branched alkylated products are also observed (Scheme 2.2).[26, 27]

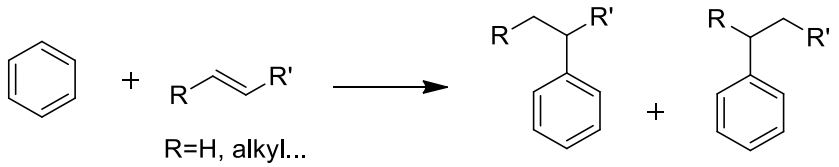

Scheme 2.2: Unselective nature of Friedel-Crafts alkylation reactions

This distribution of products makes these types of reactions less desirable because they lack selectivity for any specific product and for *n*-alkyl arenes in particular. However, LAS products derived from *n*-alkyl arenes may be advantageous over branched arenes, including greater thermal stability due to the benzylic position being less substituted and allowing for better micelle formation properties.[28, 29]

Aromatic compounds are also desirable because they make up three of the seven basic building blocks of the chemical industry: benzene, toluene, and xylene.[30] Inevitably, higher demand for aromatics will result from an increase in the use of the Fischer-Tropsch process as oil supplies diminish and world fuel supplies shift from gasoline to diesel.[31-33] As such, the supply of aromatics and heavy alkylbenzenes will be unable to meet the increasing demand for oil recovery alone.[23] Therefore, developing a new technology to synthesize alkylbenzenes is a pressing need, especially due to the inevitable increase in the cost of oil once LAS are used in larger quantities. Thus, *n*-alkanes offer economically appealing alternatives to the more expensive arenes and olefins as a potential feedstock for accessing linear alkylbenzenes.

Attempts to take advantage of the economically appealing *n*-alkane feedstock have led to catalytic dehydroaromatization of *n*-alkanes to form alkylbenzenes but only via heterogeneous catalysis at high temperatures (500 – 700°C) using metals, metal oxides, and zeolites.[34-38] These reactions are inefficient as they give low yields (≤ 20%) of aromatic compounds with poor selectivity including a variety of aromatics with carbon numbers lower than the alkane feedstock.[39] In addition to the low quantity of aromatics, significant amounts of non-aromatic compounds with fewer than six carbons are formed due to cracking during the reaction; $C_{2\text{-}4}$ alkenes and $C_{1\text{-}4}$ alkanes are primary products.

In 2011, Goldman and coworkers reported the first examples of homogeneous catalytic dehydroaromatization of *n*-alkanes.[17] This paper represents the first use of homogeneous catalysts for the aromatization of acyclic olefins, and although homogeneous catalysts present a separation challenge compared to heterogeneous catalysts, they do have the advantage of being well-defined and tunable based on mechanistic approaches which can affect the activity or selectivity of the catalyst (Figure 2.2).[2]

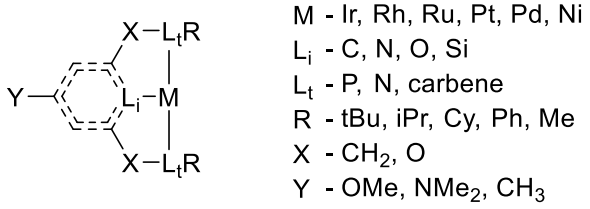

Figure 2.2: Possible modifications for pincer complexes

In that paper, six different catalysts were screened for dehydroaromatization reactions (Figure 2.3).

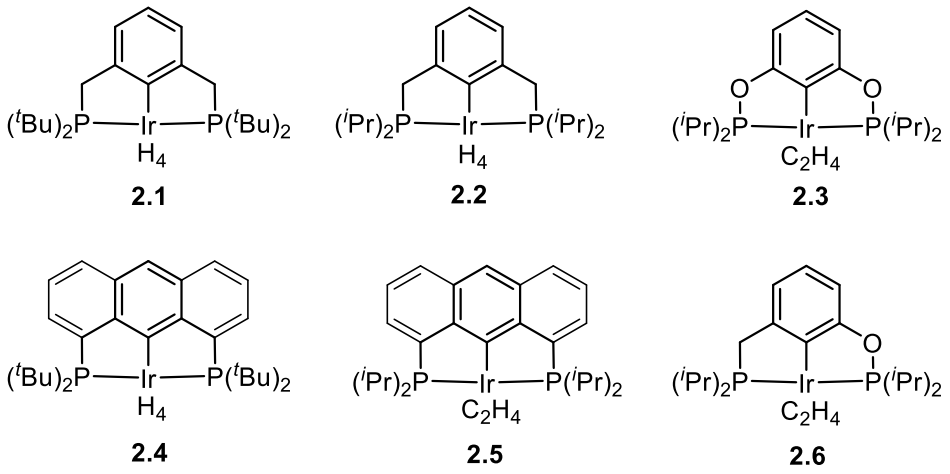

Figure 2.3: Catalysts screened for dehydroaromatization

The ($^{t\text{Bu}}$PCP)Ir(H_4) catalyst (**2.1**) was chosen because it is the most extensively studied pincer catalyst but it was shown to give no aromatic products likely due to the steric bulk of the *tert*-butylphosphines . The ($^{i\text{Pr}}$PCP)Ir(H_4) catalyst (**2.2**) was chosen due to the less bulky *iso*-propyl groups on the phosphines and this catalyst was shown to be highly effective for dehydroaromatization. The ($^{i\text{Pr}}$POCOP)Ir(C_2H_4) catalyst (**2.3**) was chosen due to the oxygen linkers allowing for a larger open coordination sphere around the metal center but the catalyst was shown to be a poor dehydroaromatization catalyst due to poor selectivity and surivivability. Both ($^{t\text{Bu}}$anthrophos)Ir(H_4) (**2.4**) and ($^{i\text{Pr}}$anthrophos)Ir(C_2H_4) (**2.5**) were chosen due to their high thermal stability but neither

catalyst were good dehydroaromatization catalysts. The best catalyst overall by yield was the hybrid ($^{i\text{Pr}}$PCOP)Ir(C_2H_4) catalyst (**2.6**) which sterically falls between ($^{i\text{Pr}}$PCP)Ir(H_4) and ($^{i\text{Pr}}$POCOP)Ir(C_2H_4). The synthesis of this hybrid catalyst is reported below.

As previously detailed, a hydrogen acceptor is required for these dehydrogenation reactions because they are thermally unfavorable reactions (ΔH ≈ 30 kcal/mol).[40] The hydrogen acceptor couples the thermodynamically downhill hydrogenation reaction with a dehydrogenation reaction allowing for catalytic dehydrogenation under lower temperatures. Industrially, ethylene is the best choice for an acceptor due to abundance and low cost, but ethylene binds strongly to pincer catalysts which inhibits dehydrogenation.[41] *Tert*-butylethylene (TBE) is convenient on a laboratory scale because it is a liquid at room temperature and binds weakly to the metal, which allows for a more favorable oxidative addition of the C-H bond of the substrate. Propene has also been shown to be effective for transfer dehydrogenation and dehydroaromatization.[17]

The proposed mechanism for dehydroaromatization, which is heavily supported in a paper by Sunoj and coworkers, consists of three subsequent transfer dehydrogenation reactions, followed by a thermally induced electrocyclization, and a final transfer dehydrogenation reaction to convert the *n*-alkane into alkylbenzene products (Figure 2.4).[42]

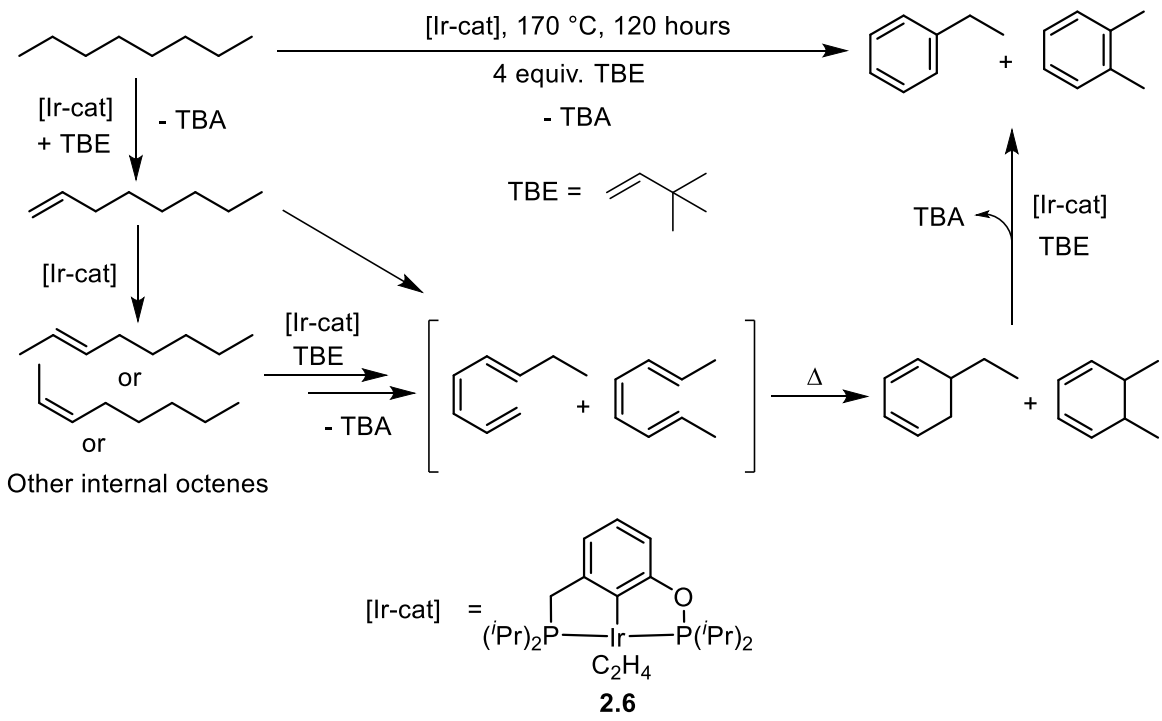

Figure 2.4: Proposed mechanism for dehydroaromatization of *n*-octane

In the case of *n*-octane, the major product is *o*-xylene and the minor product is ethylbenzene. For all *n*-alkanes, the primary C_n product is the *o*-alkyltoluene; the formation of *n*-alkyltoluenes as the major aromatic product is crucial due to the lack of industrial methods for producing *n*-alkylarenes, and the presence of these *n*-alkylarenes is unprecedented for higher *n*-alkanes. This work represents the first examples of dehydroaromatization in which the carbon number of higher (C>9) *n*-alkanes is largely retained in the formation of alkylbenzenes. In addition to the advantage of an inexpensive single feedstock, this represents a unique route to unbranched (*n*-alkyl) arenes that cannot be obtained through alkylation with olefins.

This chapter discusses the synthesis and characterization of ($^{i\text{Pr}}$PCOP)Ir(C_2H_4), which is used for all dehydroaromatization reactions. The previous dehydroaromatization report presents reactions with *n*-octane, *n*-decane, and *n*-dodecane, and this chapter will address improvements to yields of aromatics from those starting materials as well as dehydroaromatization reactions with other *n*-alkanes.

2.2 Synthesis and Characterization of ($^{i\text{Pr}}$PCOP)Ir(η^2 - C_2H_4)

The goal of synthesizing the ($^{i\text{Pr}}$PCOP)Ir catalyst was to find a medium between the ($^{i\text{Pr}}$PCP)Ir and ($^{i\text{Pr}}$POCOP)Ir catalysts. The hypothesis was that one oxygen linker would allow for the phosphine arm around the catalyst to be slightly shortened, which would cause a small increase in the open coordination sphere around the metal center. This is based on the fact that the ($^{i\text{Pr}}$POCOP) ligand allows for a more open coordination sphere compared to the ($^{i\text{Pr}}$PCP) ligand. The open coordination sphere around the ($^{i\text{Pr}}$POCOP) ligand leads to a loss in selectivity, but the ($^{i\text{Pr}}$PCOP) ligand may lead to better reactivity without loss of selectivity.

The synthesis of ($^{i\text{Pr}}$PCOP)Ir(C_2H_4) begins with the commercially available diol, 3-hydroxybenzylalcohol, which was treated with PBr_3 to selectively brominate the benzyl alcohol to give 3-bromomethylphenol in 95 % yield (Scheme 2.3).

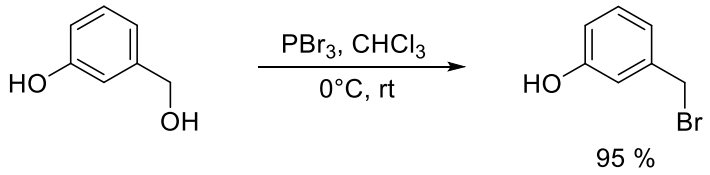

Scheme 2.3: Synthesis of 3-bromomethylphenol

3-Bromomethylphenol was treated with di-*iso*-propylphosphine in an acetone solution at reflux to precipitate a white salt, which was then treated with sodium bicarbonate at 90 °C to give 3-di-*iso*-propylphosphinomethylphenol in 65 % yield after workup (Scheme 2.4).

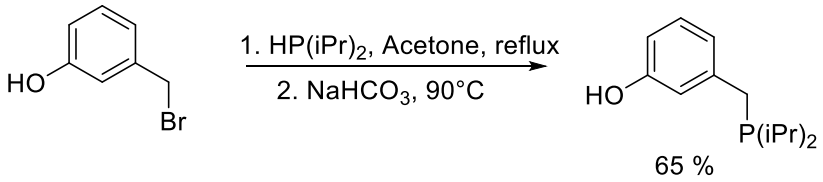

Scheme 2.4: Synthesis of 3-di-*iso*-propylphosphinomethylphenol

3-Di-*iso*-propylphosphinomethylphenol was treated with sodium hydride to deprotonate the phenol, followed by addition of di-*iso*-propylchlorophosphine in THF at reflux to give the hybrid ligand (^{iPr}PCOP) in 84 % yield as a pale white oil (Scheme 2.5).

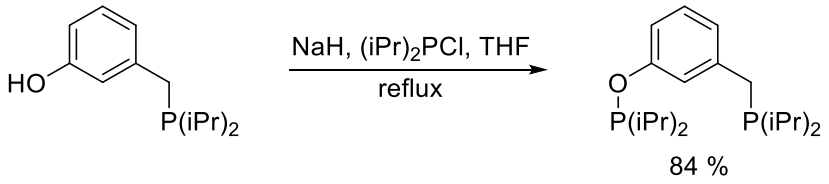

Scheme 2.5: Synthesis of ($^{i\text{Pr}}$PCOP) ligand

The ($^{i\text{Pr}}$PCOP) ligand was treated with $[Ir(COD)Cl]_2$ in refluxing toluene and H_2(g) to give ($^{i\text{Pr}}$PCOP)Ir(HCl) in 79 % yield as an orange powder along with a small amount of ($^{i\text{Pr}}$PCOP)Ir(HBr) (Scheme 2.6).

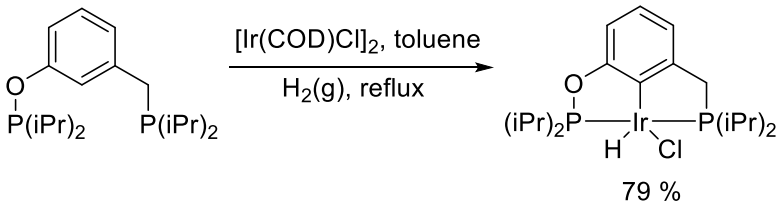

Scheme 2.6: Synthesis of ($^{i\text{Pr}}$PCOP)Ir(HCl)

($^{i\text{Pr}}$PCOP)Ir(HCl) was treated with $LiBEt_3H$ and C_2H_4(g) in pentane to give the final precatalyst ($^{i\text{Pr}}$PCOP)Ir(C_2H_4) in 90 % yield as a dark brown powder (Scheme 2.7).

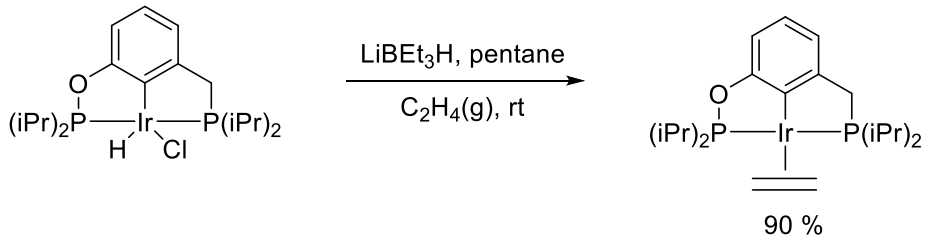

Scheme 2.7: Synthesis of (^{iPr}PCOP)Ir(C_2H_4)

2.3 Dehydroaromatization of *n*-Alkanes

Previous data has been improved upon by increasing the temperature of the reaction from 165 °C to 170 °C and by adding NaO^{t}Bu as an additive for dehydroaromatization reactions.[17] All following reactions are performed with 10 mM of precatalyst (^{iPr}PCOP)Ir(HCl) at 170 °C with four equivalents of hydrogen acceptor relative to the starting *n*-alkane and three equivalents of NaO^{t}Bu relative to the catalyst. The exact role of the NaO^{t}Bu is currently under investigation in the Goldman Group, but the current hypothesis is that it acts as either a co-catalyst in a mechanistically meaningful way or as a means to scrub out lingering impurities.

2.3.1 Dehydroaromatization of n-*Octane*

The dehydroaromatization of *n*-octane yields *o*-xylene and ethylbenzene as the only C_8 products (Scheme 2.8).

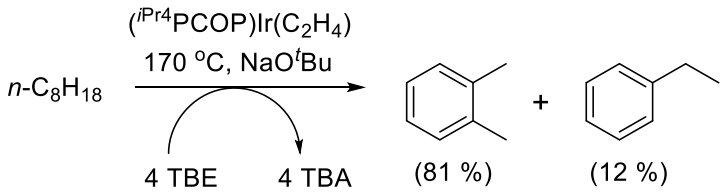

Scheme 2.8: Yields for dehydroaromatization of *n*-octane

Percentages in parenthesis are yields based on the parent *n*-alkane obtained after 120 hours. Kinetics for this reaction are presented below in Table 2.1 and Figure 2.8.

Table 2.1: Kinetics of dehydroaromatization for *n*-octane (mM)

Time	TBE	TBA	Octane	C_8 Olefins	Ethyl Benzene	*o*-Xylene	C_{16} Dimers
0 hr	5190	0	1340	0	0	0	0
2 hr	4243	909	1030	284	2	10	3
4 hr	3520	1441	817	391	9	53	6
7 hr	3050	2021	684	444	22	135	8
24 hr	970	3885	199	212	83	610	20
48 hr	121	4751	28	47	120	884	22
120 hr	19	5740	12	18	160	1082	25

Conditions: [($^{i\text{Pr}}$PCOP)Ir(C_2H_4)] = 10 mM; [*n*-Octane] = 1.34 M; [TBE] = 5.5 M; 170°C, 3 equivalents NaO^tBu relative to catalyst. Dimers are formed via Diels-Alder reactions and iridium-mediated dimerization and are not well resolved on GC. Concentration of dimers are calculated based on missing octane.

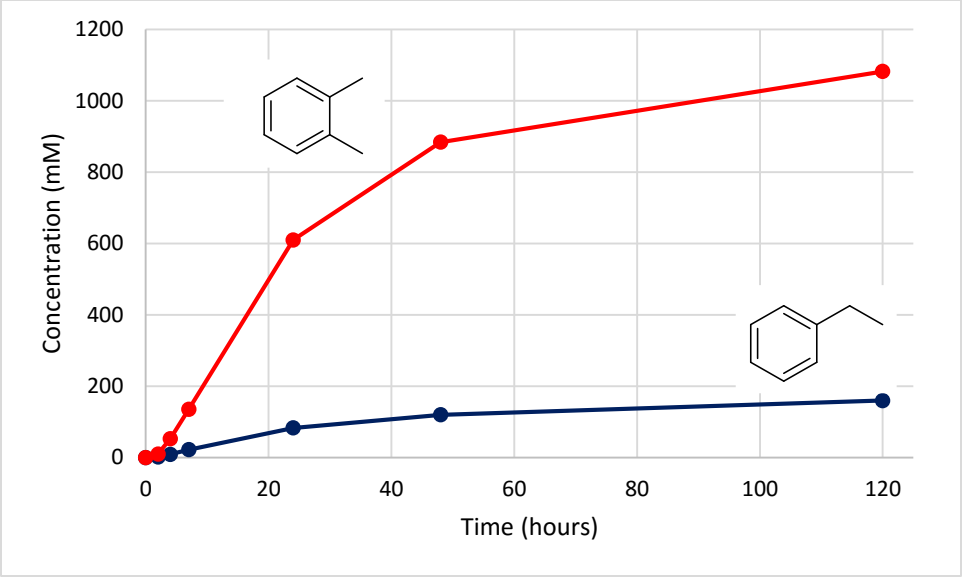

Figure 2.5: Kinetics of product formation for dehydroaromatization of *n*-octane

o-Xylene forms in a six to one ratio to ethylbenzene as the major product, and there is 93 % total conversion of *n*-octane to C_8 aromatics. Small amounts of dimers are formed via Diels-Alder reactions and iridium-mediated dimerization, but they are difficult to accurately quantify due to poor resolution on the GC. Specific concentrations after 120 hours are summarized below in Table 2.2.

Table 2.2: Final concentrations at 120 hours for dehydroaromatization of *n*-octane

Identity	Concentration (mM)
TBE	19
TBA	5740
Octane	12
C_8 olefins	18
C_8 aromatics	1241
C_{16} Dimers	25

Conditions: [(^{iPr}PCOP)Ir(C_2H_4)] = 10 mM; [*n*-Octane] = 1.34 M; [TBE] = 5.5 M; 170°C, 30 mM NaO^{t}Bu. Concentrations obtained after 120 hours.

2.3.2 Dehydroaromatization of n-*Decane*

The dehydroaromatization of *n*-decane yields *o*-propyltoluene, 1,2-diethylbenzene, and *n*-butylbenzene as the C_{10} aromatic products (Scheme 2.9).

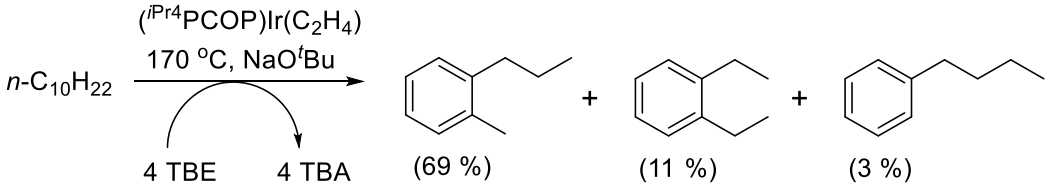

Scheme 2.9: Yields for dehydroaromatization of *n*-decane

Percentages in parenthesis are yields based on the parent *n*-alkane obtained after 120 hours. Kinetics for this reaction are presented below in Table 2.3 and Figure 2.9.

Table 2.3: Kinetics for dehydroaromatization of *n*-decane (mM)

Time	TBE	TBA	Decane	C_{10} Olefins	*o*-propyl toluene	di-ethyl benzene	*n*-butyl benzene	C_{20} Dimers
0 hr	5285	0	1182	0	0	0	0	0
2 hr	4070	1181	929	252	5	7	6	8
24 hr	806	4599	266	195	439	105	5	52
48 hr	20	5366	107	60	673	123	15	71
120 hr	17	5367	27	52	818	135	34	90

Conditions: [(^{iPr}PCOP)Ir(C_2H_4)] = 10 mM; [*n*-decane] = 1.3 M; [TBE] = 5.3 M; 170°C, 3 equivalents NaO^{t}Bu relative to catalyst. Dimers are formed via Diels-Alder reactions and iridium-mediated dimerization and are not well resolved on GC. Concentration of dimers are calculated based on missing decane.

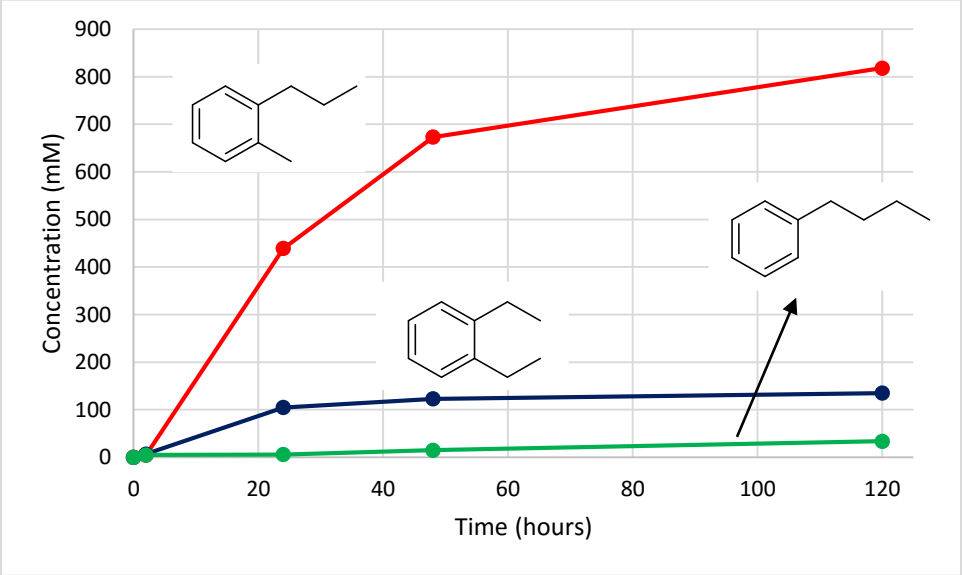

Figure 2.6: Kinetics of product formation for dehydroaromatization of *n*-decane

o-Propyltoluene forms as the major C_{10} aromatic in a six to one ratio to 1,2-diethylbenzene along with a small amount of *n*-butylbenzene, and there is 83% total

conversion to C_{10} aromatic products. Again, a wide variety of Diels-Alder dimers and iridium-mediated dimers are formed, but they are difficult to resolve by GC due to low concentrations. Specific concentrations after 120 hours are summarized below in Table 2.4.

Table 2.4: Final concentrations at 120 hours for dehydroaromatization of *n*-decane

Identity	Concentration (mM)
TBE	17
TBA	5367
Decane	27
C_{10} olefins	52
C_{10} aromatics	987
Dimers	90

Conditions: [($^{i\text{Pr}}$PCOP)Ir(C_2H_4)] = 10 mM; [*n*-decane] = 1.3 M; [TBE] = 5.3 M; 170°C, 30 mM NaO^{t}Bu. Concentrations obtained after 120 hours.

2.3.3 Dehydroaromatization of n-*Undecane*

The dehydroaromatization of *n*-undecane yields *o*-butyltoluene, 1-propyl-2-ethylbenzene, and *n*-pentylbenzene as the C_{11} aromatic products (Scheme 2.10).

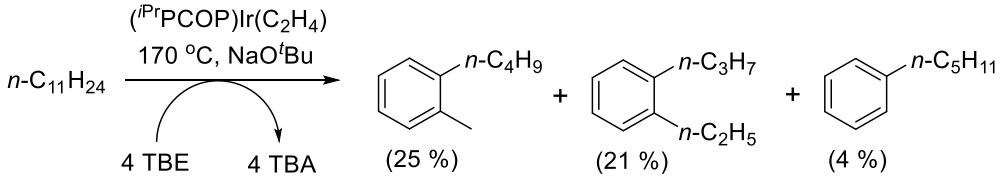

Scheme 2.10: Yields for dehydroaromatization of *n*-undecane

Percentages in parenthesis are yields based on the parent *n*-alkane obtained after 120 hours. Kinetics for this reaction are shown below in Table 2.5 and Figure 2.10.

Table 2.5: Kinetics for dehydroaromatization of *n*-undecane (mM)

Time	TBE	TBA	Undecane	C_{11} Olefins	*o*-Butyl toluene	Propyl ethyl benzene	*n*-Pentyl benzene	C_{22} Dimers
0 hr	4900	0	1256	0	0	0	0	0
2 hr	3777	1020	1045	187	3	17	1	5
24 hr	1017	4058	448	218	55	42	29	70
48 hr	15	5191	185	236	217	190	30	108
120 hr	25	5209	122	79	317	258	54	125

Conditions: [($^{i\text{Pr}}$PCOP)Ir(C_2H_4)] = 10 mM; [*n*-undecane] = 1.3 M; [TBE] = 5.3 M; 170°C, 3 equivalents NaO^{t}Bu relative to catalyst. Dimers are formed via Diels-Alder reactions and iridium-mediated dimerization and are not well resolved on GC. Concentration of dimers are calculated based on missing undecane.

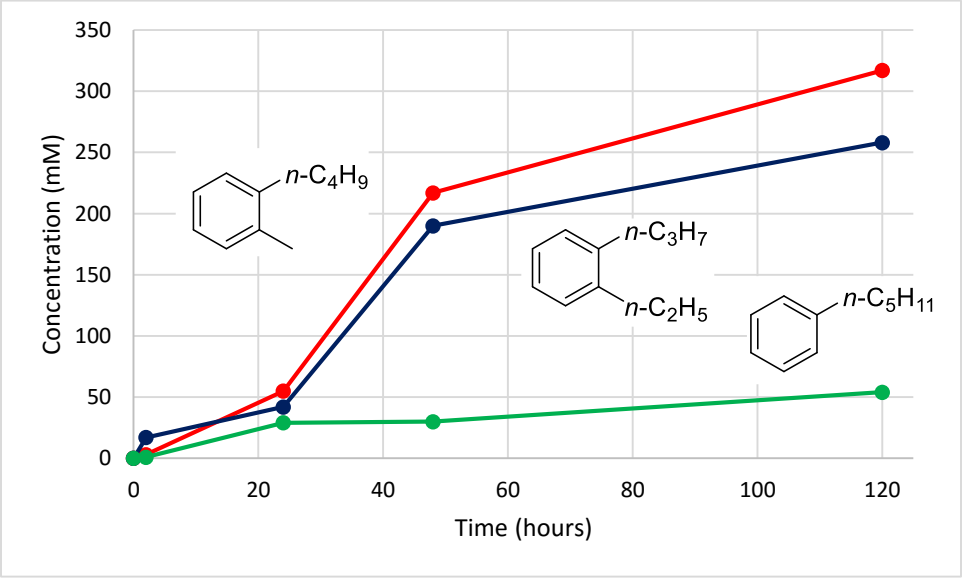

Figure 2.7: Kinetics of product formation for dehydroaromatization of *n*-undecane

o-Butyltoluene forms as the major C_{11} product, but a similar amount of 1-propyl-2-ethylbenzene is formed along with a small amount of *n*-pentylbenzene, and there is 50 % total conversion of *n*-undecane to C_{11} aromatics. The *o*-alkyltoluene remains the major C_n product for dehydroaromatization reactions but in this case, product distribution is different and overall yield is decreased. This will be further addressed in Chapter 3. Again, a wide variety of Diels-Alder dimers and iridium-mediated dimers are formed, but they are difficult to resolve by GC due to low concentrations. Specific concentrations after 120 hours are summarized below in Table 2.6.

Table 2.6: Final concentrations at 120 hours for dehydroaromatization of *n*-undecane

Identity	Concentration (mM)
TBE	25
TBA	5209
Undecane	122
C_{11} olefins	79
C_{11} aromatics	629
Dimers	125

Conditions: [(^{iPr}PCOP)Ir(C_2H_4)] = 10 mM; [*n*-undecane] = 1.3 M; [TBE] = 5.3 M; 170°C, 30 mM NaO^{t}Bu. Concentrations obtained after 120 hours.

2.3.4 Dehydroaromatization of n-*Dodecane*

The dehydroaromatization of *n*-dodecane at 200 °C yields *o*-pentyltoluene, 1-butyl-2-ethylbenzene, 1,2-dipropylbenzene, and *n*-hexylbenzene as the C_{12} aromatic products (Scheme 2.11).

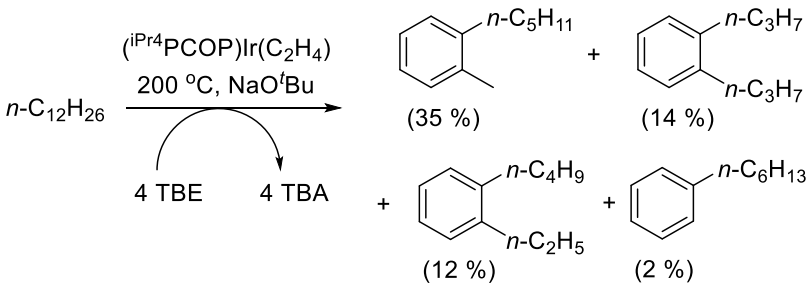

Scheme 2.11: Yields for dehydroaromatization of *n*-dodecane

Percentages in parenthesis are yields based on the parent *n*-alkane obtained after 120 hours. Kinetics for this reaction are shown below in Table 2.7 and Figure 2.11.

Table 2.7: Kinetics for dehydroaromatization of *n*-dodecane (mM)

Time	TBE	TBA	Dodecane	C_{12} Olefins	*o*-Pentyl toluene	Butyl ethyl benzene	Di-propyl benzene	*n*-Hexyl benzene	C_{24} Dimers
0 hr	5348	0	1334	0	0	0	0	0	0
4 hr	33	5372	167	344	199	77	113	20	62
24 hr	17	5294	64	94	435	145	178	27	72
48 hr	17	5304	65	58	437	150	180	28	75
120 hr	13	5220	70	56	462	159	189	30	75

Conditions: [(^{iPr}PCOP)Ir(C_2H_4)] = 10 mM; [*n*-dodecane] = 1.3 M; [TBE] = 5.35 M; 200°C, 3 equivalents NaO^{t}Bu relative to catalyst. Dimers are formed via Diels-Alder reactions and iridium-mediate dimerization and are not well resolved on GC. Concentration of dimers are calculated based on missing dodecane.

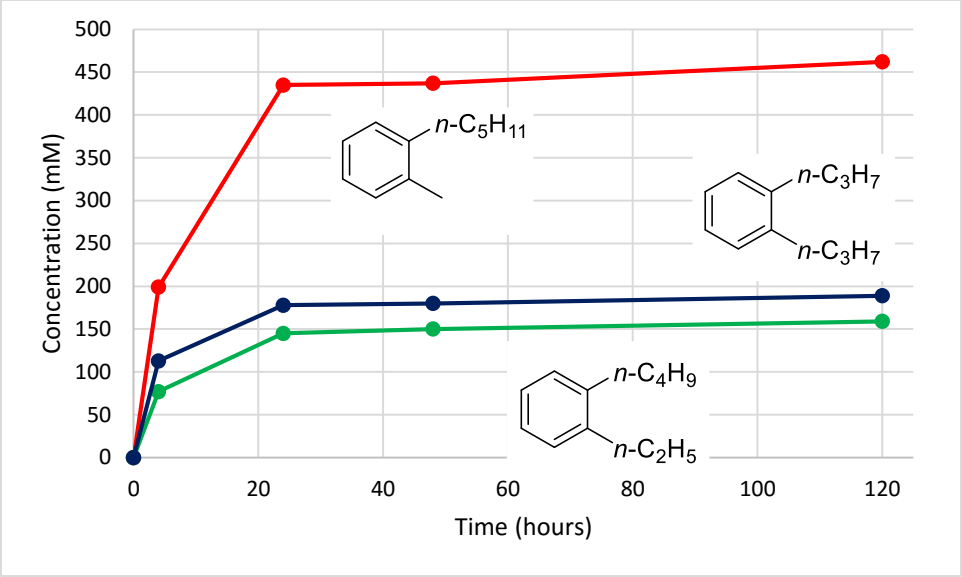

Figure 2.8: Kinetics of major product formation for dehydroaromatization of *n*-dodecane

o-Pentyltoluene is the major C_{12} product, and 1,2-dipropylbenzene and 1-butyl-2-ethylbenzene form in similar amounts along with a small amount of *n*-hexylbenzene. There is 65 % total conversion of *n*-dodecane to C_{12} aromatics. Again, a wide variety of Diels-Alder dimers and iridium-mediated dimers are formed, but they are difficult to resolve by GC due to low concentrations. In this case, the reaction is run at 200 °C which causes less overall dimer formation and increased C_n aromatics compared to other alkane dehydroaromatization reactions. Specific concentrations after 120 hours at 170 °C and 200 °C are summarized below in Table 2.8 to highlight the decrease in dimer formation and necessary increase in C_{12} aromatics.

Table 2.8: Final concentrations at 120 hours for dehydroaromatization of *n*-dodecane

Identity	Concentration at 170 °C (mM)	Concentration at 200 °C (mM)
TBE	20	13
TBA	5440	5220
Dodecane	100	70
C_{12} olefins	40	56
C_{12} aromatics	720	861
Dimers	115	75

Conditions: [(^{iPr}PCOP)Ir(C_2H_4)] = 10 mM; [*n*-dodecane] = 1.3 M; [TBE] = 5.35 M; 200°C or 170°C, 30 mM NaO^tBu. Concentrations obtained after 120 hours.

Increasing the temperature from 170 °C to 200 °C allows for an increase in C_{12} aromatics and a decrease in dimers. Increasing the temperature to 230 °C does not yield any significant difference compared to the results for a reaction at 200 °C.

It should also be noted that attempts to run dehydroaromatization reactions with ethylene as the acceptor instead of TBE have been met with limited success. TBE is convenient on a laboratory scale but is not a commercially viable acceptor, whereas ubiquitous ethylene is a desirable alternative to TBE. In all cases, catalyst decomposition was observed during dehydroaromatization reactions using ethylene as the acceptor and there was a large amount of unreacted starting material. Acceptorless dehydroaromatization was similarly ineffective.

2.3.5 Dehydroaromatization of n-*Tridecane*

The dehydroaromatization of *n*-tridecane yields *o*-hexyltoluene, 1-butyl-2-propylbenzene, 1-pentyl-2-ethylbenzene, and *n*-heptylbenzene (Scheme 2.12).

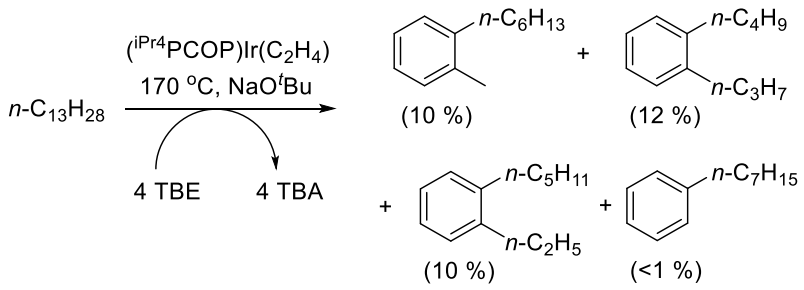

Scheme 2.12: Yields for dehydroaromatization of *n*-tridecane

Percentages in parenthesis are yields based on the parent *n*-alkane obtained after 120 hours. Kinetics for this reaction are shown below in Table 2.9 and Figure 2.12.

Table 2.9: Kinetics for dehydroaromatization of *n*-tridecane (mM)

Time	TBE	TBA	Tridecane	C_{13} Olefins	*o*-Hexyl toluene	Pentyl ethyl benzene	Butyl propyl benzene	*n*-Heptyl benzene	C_{26} Dimers
0 hr	5062	0	1272	0	0	0	0	0	0
2 hr	3579	1360	999	212	6	6	5	1	22
24 hr	19	5257	331	248	45	41	52	4	108
48 hr	6	5308	235	102	112	112	144	5	127
120 hr	12	5255	254	49	130	129	150	6	135

Conditions: [($^{i\text{Pr}}$PCOP)Ir(C_2H_4)] = 10 mM; [*n*-tridecane] = 1.3 M; [TBE] = 5.35 M; 170°C, 3 equivalents NaO^{t}Bu relative to catalyst. Dimers are formed via Diels-Alder reactions and iridium-mediated dimerization and are not well resolved on GC. Concentration of dimers are calculated based on missing tridecane.

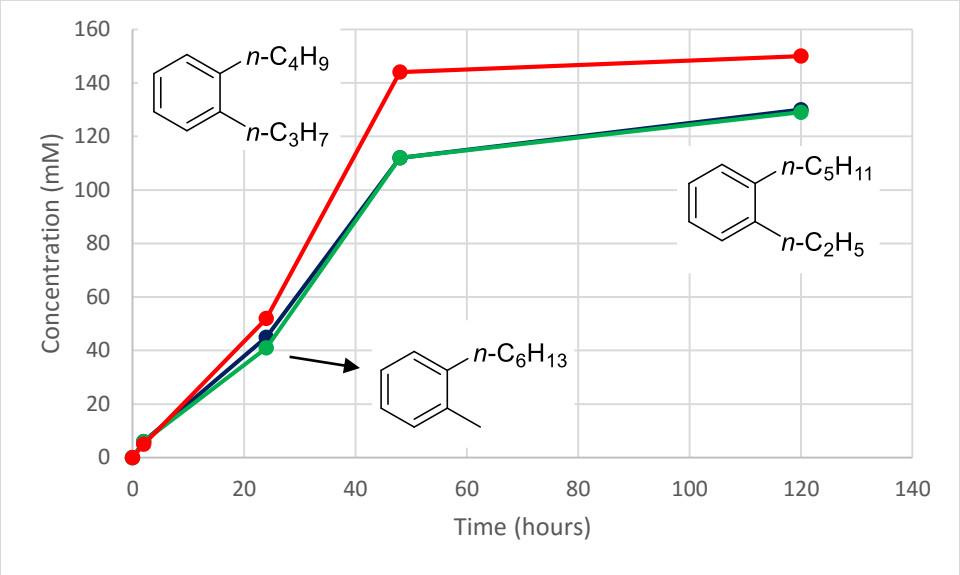

Figure 2.9: Kinetics of major product formation for dehydroaromatization of *n*-tridecane

Surprisingly, *o*-hexyltoluene does not form as the major C_{13} product in this case; 1-butyl-2-propylbenzene forms as the major C_{13} product. This will be addressed in Chapter 4. A similar amount of *o*-hexyltoluene and 1-pentyl-2-ethylbenzene is formed along with a very small amount of *n*-pentylbenzene, and there is 40 % total conversion of *n*-tridecane to C_{13} aromatics. Again, a wide variety of Diels-Alder dimers and iridium-mediated dimers are formed, but they are difficult to resolve by GC due to low concentrations. Specific concentrations after 120 hours are summarized below in Table 2.10.

Table 2.10: Final concentrations at 120 hours for dehydroaromatization of *n*-tridecane

Identity	Concentration (mM)
TBE	12
TBA	5255
Tridecane	254
C_{13} olefins	49
C_{13} aromatics	504
Dimers	135

Conditions: [(^{iPr}PCOP)Ir(C_2H_4)] = 10 mM; [*n*-tridecane] = 1.3 M; [TBE] = 5.35 M; 170°C, 30 mM NaO^{t}Bu. Concentrations obtained after 120 hours.

2.3.6 Dehydroaromatization of n-*Tetradecane*

The dehydroaromatization of *n*-tetradecane yields *o*-heptyltoluene, 1,2-dibutylbenzene, 1-hexyl-2-ethylbenzene, 1-pentyl-2-propylbenzene, and octylbenzene as the C_{14} aromatic products (Scheme 2.13).

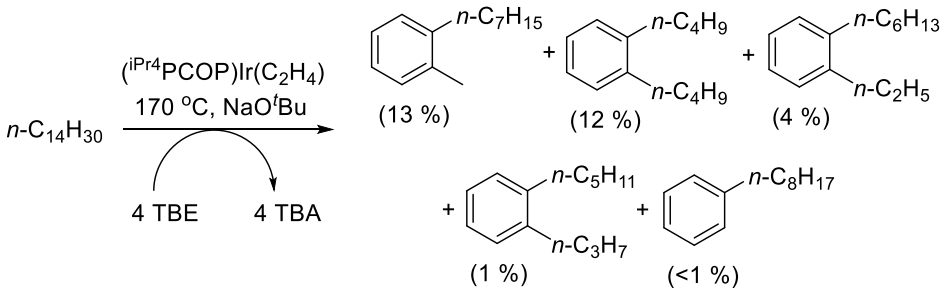

Scheme 2.13: Yields for dehydroaromatization of *n*-tetradecane

Percentages in parenthesis are yields based on the parent *n*-alkane obtained after 120 hours. Kinetics for this reaction are shown below in Table 2.11 and Figure 2.13.

Table 2.11: Kinetics for dehydroaromatization of *n*-tetradecane (mM)

Time	**TBE**	**TBA**	***n*-$C_{14}H_{30}$**	**C_{14} Olefins**	***o*-Heptyl toluene**	**Hexyl ethyl benzene**	**Pentyl propyl benzene**	**Di-butyl benzene**	***n*-Octyl benzene**	**C_{28} Dimers**
0 hr	4739	0	1292	0	0	0	0	0	0	0
2 hr	3162	1654	874	165	54	6	9	10	1	12
24 hr	19	4806	322	218	151	11	51	129	3	78
48 hr	16	4900	325	88	166	12	51	151	4	91
120 hr	12	4959	325	68	169	13	51	154	4	95

Conditions: [(^{iPr}PCOP)Ir(C_2H_4)] = 10 mM; [*n*-tetradecane] = 1.3 M; [TBE] = 5.35 M; 170°C, 3 equivalents NaO^{t}Bu relative to catalyst. Dimers are formed via Diels-Alder reactions and iridium-mediated dimerizations and are not well resolved on GC. Concentration of dimers are calculated based on missing tetradecane.

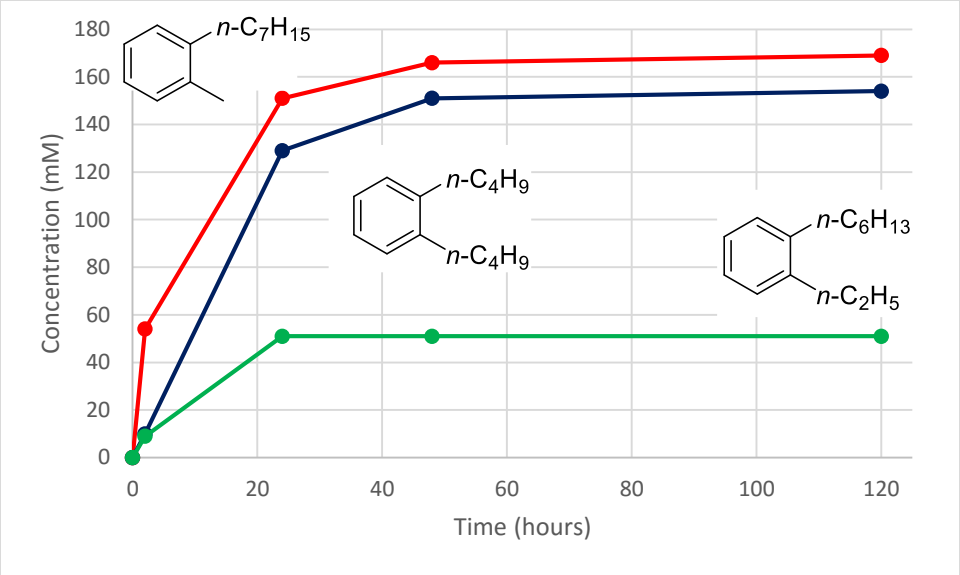

Figure 2.10: Kinetics of major product formation for dehydroaromatization of *n*-tetradecane

o-Heptyltoluene is the major C_{14} product and 1,2-dibutylbenzene forms in a similar amount along with a small amount of 1-hexyl-2-ethylbenzene. 1-Pentyl-2-propylbenzene and *n*-octylbenzene form in very small quantities. There is 33 % total conversion of *n*-tetradecane to C_{14} aromatics. Again, a wide variety of Diels-Alder dimers and iridium-mediated dimers are formed, but they are difficult to resolve by GC due to low concentrations. Specific concentrations after 120 hours are summarized below in Table 2.12.

Table 2.12: Final concentrations at 120 hours for dehydroaromatization of *n*-tetradecane

Identity	Concentration (mM)
TBE	12
TBA	4959
Tetradecane	325
C_{14} olefins	68
C_{14} aromatics	426
Dimers	95

Conditions: [(^{iPr}PCOP)Ir(C_2H_4)] = 10 mM; [*n*-tetradecane] = 1.3 M; [TBE] = 5.35 M; 170°C, 30 mM NaO^{t}Bu. Concentrations obtained after 120 hours.

2.4 Experimental

General

All reactions were performed under an argon atmosphere using standard Schlenk techniques or in an argon-filled glove box. All alkanes, mesitylene, and TBE were distilled under vacuum from Na/K alloy after several freeze-pump-thaw cycles and stored in an argon glove box. ^{1}H and ^{13}P NMR spectra were obtained from either a 400 MHz or 500 MHz Varian NMR instrument. Gas chromatography (GC) measurements were performed on a Varian 430 instrument fitted with a capillary column (30 m length x 0.25 mm inner diameter x 0.5 µm film thickness). Gas chromatography – mass spectrometry (GC-MS) measurements were performed on a Varian 3900 Saturn 2100T instrument fitted with a capillary column (30 m length x 0.25 mm inner diameter x 0.25 µm film thickness).

3-Bromomethylphenol

A solution of 1.5 mL (16.1 mmol) phosphorous tribromide and 20 mL degassed $CHCl_3$ was added dropwise to a solution of 4.0 g (32.2 mmol) of 3-hydroxy benzyl alcohol and 20 mL degassed $CHCl_3$ at 0 °C for one hour. The solution was allowed to stir for two hours at room temperature. The reaction was then quenched in ice and extracted with 2 x 20 mL of $CHCl_3$. The combined organic layers were washed with 80 mL of brine and dried over magnesium sulfate. The solution was filtered and dried by rotary evaporation to give a clear liquid in 95 % yield. ^{1}H NMR (*p*-xylene d_{10}, 400 MHz): 4.47 (s, 2H, CH_2), 6.48 (s, 1H, OH), 6.66 – 7.12 (m, 4H, arene H).

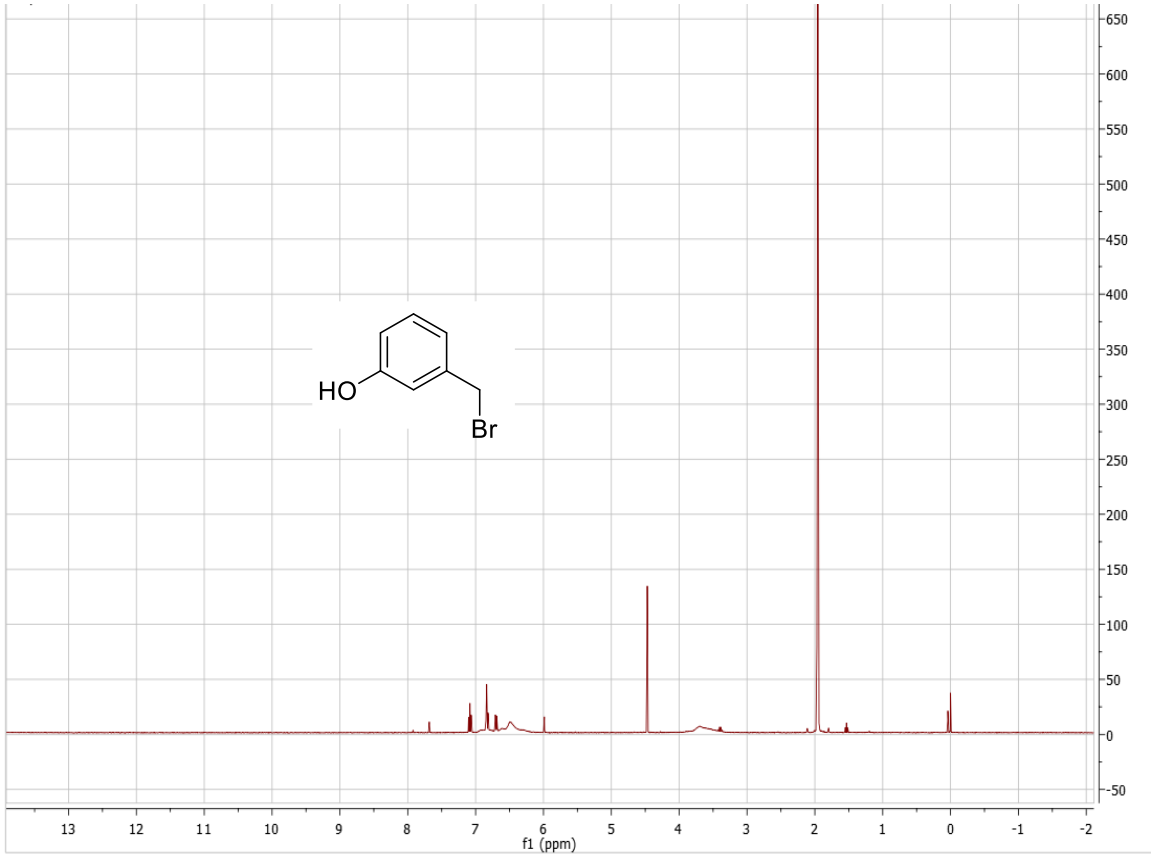

Figure 2.11: ^{1}H NMR spectrum of 3-bromomethylphenol

3-Di-*iso*-propylphosphinomethylphenol

A solution of 4.7 g (25.7 mmol) 3-bromomethylphenol and 3 mL (25.7 mmol) di-*iso*-propylphosphine was refluxed in 55 mL of degassed acetone for two hours. The acetone was cannulated out and the resulting jelly was dried under vacuum. 20 mL of degassed sodium bicarbonate was added and the solution was heated to 90 °C for six hours. The solution was dried under vacuum and the resulting white gel was extracted with 3 x 60 mL of ether via cannula filtration. Solvent was removed under vacuum and the resulting pale yellow oil was left in a 65 % yield. ^{31}P NMR (161.9 MHz, C_6D_6, ppm): δ 10.54

(s, 1P) and ^{1}H NMR (400 MHz, C_6D_6, ppm): δ 0.935 (dd, J = 6.8 Hz, J = 2.4 Hz, 6H, PC(*CH₃)₂*), 0.967 (dd, J = 7.2 Hz, J = 4.4 Hz, 6H, PC(*CH₃)₂*), 1.556 (septet of doublets, J = 7.2 Hz, J = 2 Hz, 2H, P(C*H*$(CH_3)_2)_2$), 2.578 (s, 2H, C*H₂*P), 4.244 (br s, 1H, O*H*), and 6.4 – 7.01 (m, 4H, arene H).

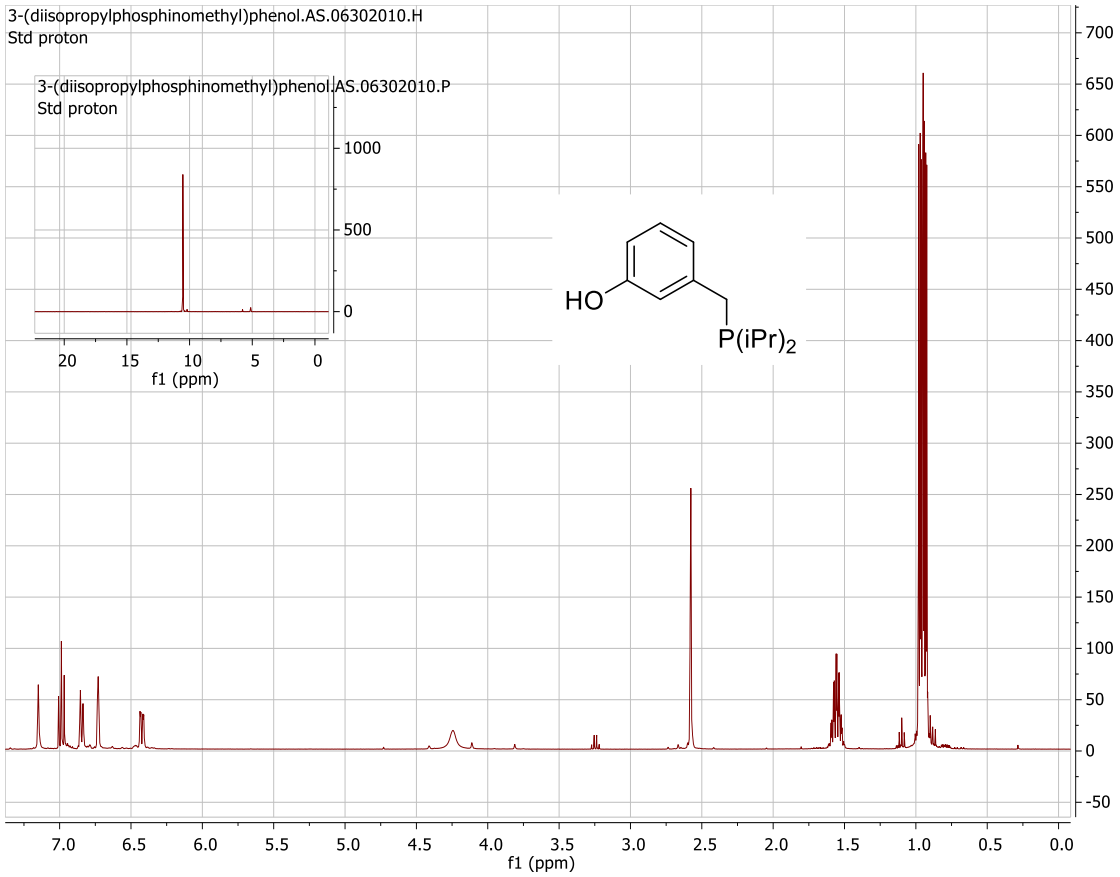

Figure 2.12: ^{31}P and ^{1}H NMR spectra of 3-di-*iso*-propylphosphinomethylphenol

(*i*^{Pr}PCOP) Ligand

A solution of 0.132 g (5.5 mmol) sodium hydride and 15 mL degassed THF was cannulated into a solution of 1.12 g (5.0 mmol) 3-(di-*iso*-propylphosphinomethyl)phenol and 40 mL of degassed THF and the resulting solution was refluxed for 1.5 hours. A solution of 0.79 mL (5.0 mmol) di-*iso*-propylchlorophosphine and 15 mL degassed THF was cannulated into the original solution and the resulting solution was refluxed for two hours. The solvent was removed under vacuum and the resulting oil was extracted with 2 x 35 mL of degassed pentane via cannula filtration. The pentane was removed under vacuum leaving a pale white oil in 84 % yield. ^{31}P NMR (161.9 MHz, C_6D_6, ppm): δ 10.82 (s, 1P) and 147.82 (s, 1P) and ^{1}H NMR (400 MHz, C_6D_6, ppm): δ 0.99 – 0.88 (m, 18H, OPC(C*H*$_3$)$_2$ and CP(C(C*H*$_3$)$_2$)$_2$), 1.12 (dd, J = 10.4 Hz, J = 7.2 Hz, 6H, OPC(C*H*$_3$)$_2$), 1.53 (septet of doublets, 2H, CP(C*H*$(CH_3)_2)_2$), 1.73 (septet of doublets, 2H, OP(C*H*$(CH_3)_2)_2$), 2.60 (s, 2H, C*H*$_2$P), 6.90 – 7.13 (m, 4H, arene H).

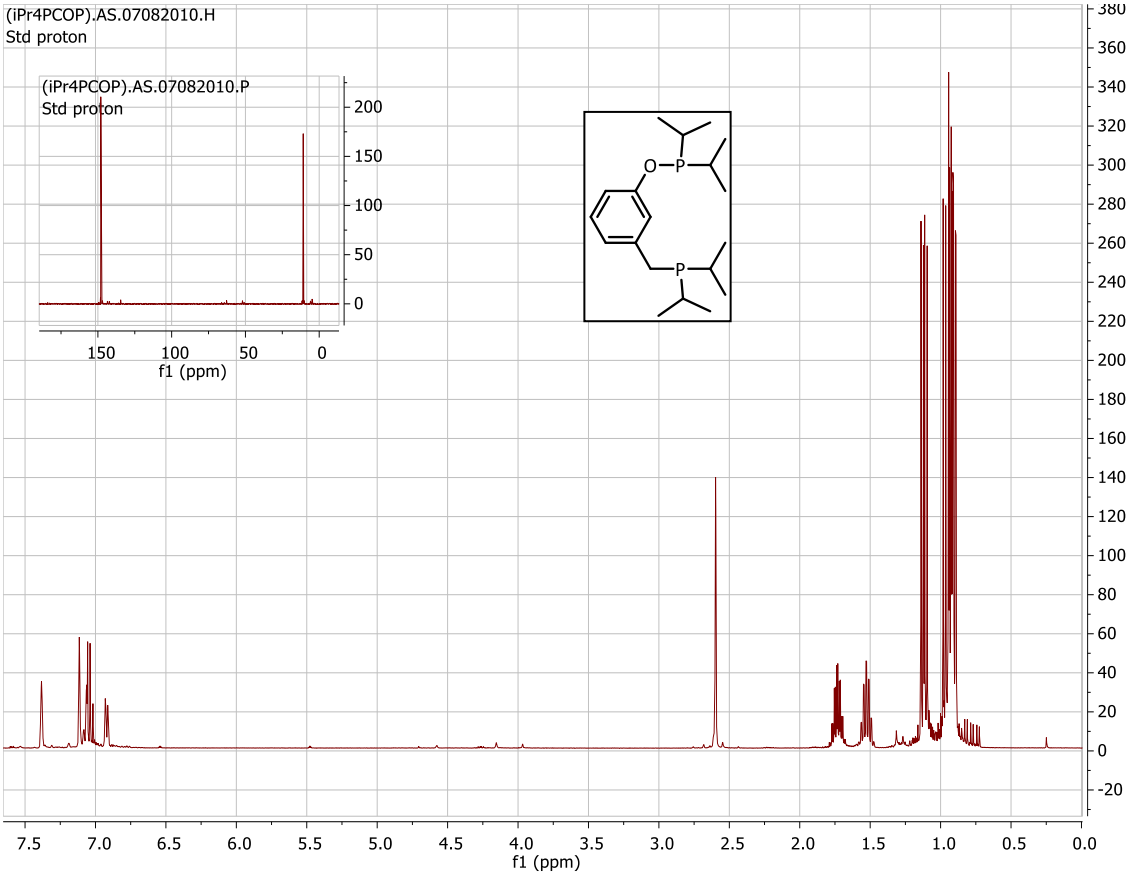

Figure 2.13: ^{31}P and ^{1}H NMR spectra of (^{iPr}PCOP) ligand

(^{iPr}PCOP)Ir(HCl)

A solution of 1.45 g (4.26 mmol) ^{iPr}PCOP and 1.36 g (2.03 mmol) $[Ir(COD)Cl]_2$ was refluxed under hydrogen atmosphere in 45 mL degassed toluene for seven hours. The solvent was removed under vacuum and the resulting solid was extracted with 7 x 30 mL of pentane via cannula filtration leaving a red solid in 79 % yield. ^{31}P NMR (161.9 MHz, *p*-

xylene-d10, ppm): δ 43.34 (d, J = 361.15 Hz, 1P) and 151.29 (d, J = 361.09 Hz, 1P) and ^{1}H NMR (400 MHz, *p*-xylene-d10, ppm): δ -36.54 (t, hydride), 0.82 – 0.87 (m, 6H, CH(C*H*$_3$)$_2$), 1.03 (dd, 6H, CH(C*H*$_3$)$_2$), 1.14 (dd, 6H, CH(C*H*$_3$)$_2$), 1.29 (dd, 6H, CH(C*H*$_3$)$_2$), 1.95 (septet of doublets, 1H, C*H*(CH$_3$)$_2$), 2.05 – 2.08 (m, 1H, C*H*(CH$_3$)$_2$), 2.27 (septet of doublets, 1H, C*H*(CH$_3$)$_2$), 2.66 (septet of doublets, 1H, C*H*(CH$_3$)$_2$), 2.76 (m, 2H, CH$_2$P), 6.78 – 6.89 (m, 3H, arene H).

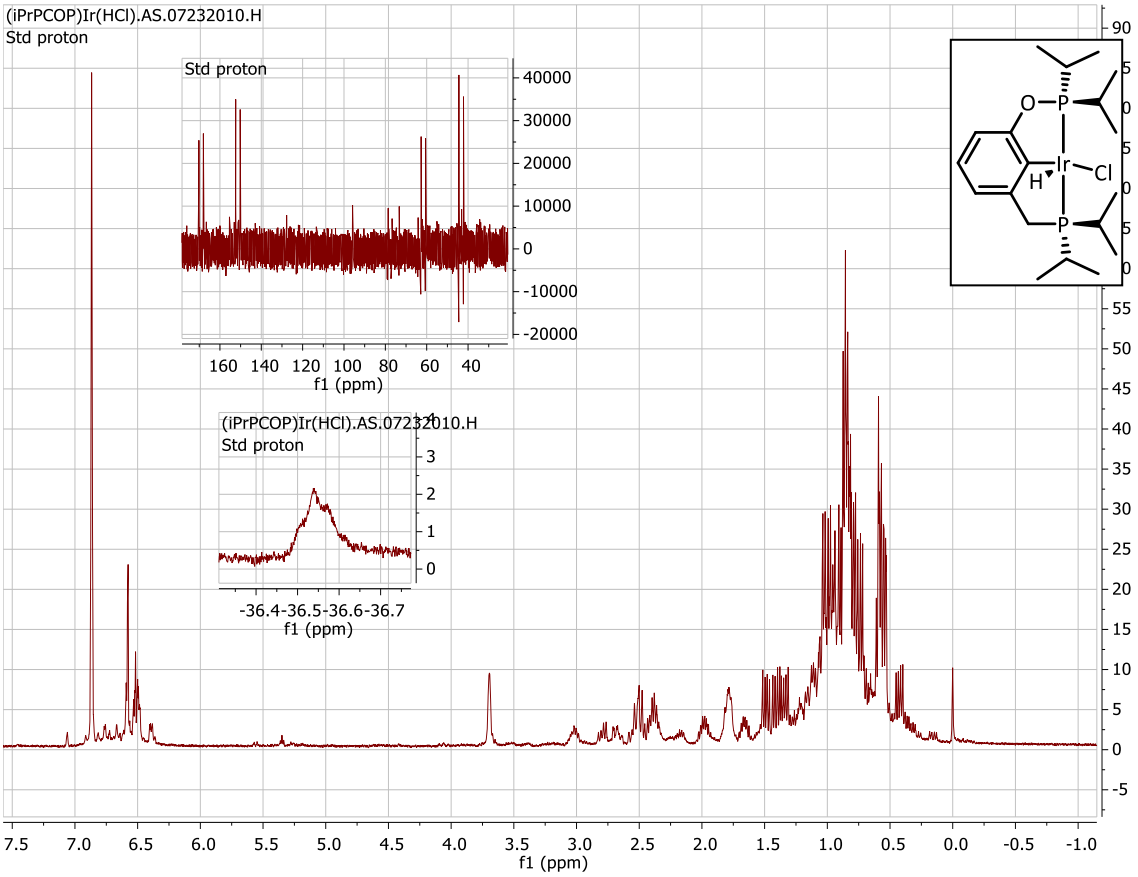

Figure 2.14: ^{31}P and ^{1}H NMR spectra of (^{iPr}PCOP)Ir(HCl)

($^{i\text{Pr}}$PCOP)Ir(C_2H_4)

A solution of 0.3 g (0.53 mmol) ($^{i\text{Pr}}$PCOP)Ir(HCl) and 120 mL degassed pentane was bubbled with ethylene gas. 0.52 mL (0.53 mmol) $LiBEt_3H$ was added dropwise and the resulting solution was allowed to stir at room temperature for thirty minutes. The solution was filtered via cannula filtration and the solvent was removed under vacuum to give a brown solid in 90 % yield. ^{31}P NMR (161.9 MHz, *p*-xylene-d10, ppm): δ 61.50 (d, J = 285.92 Hz, 1P) and 180.86 (d, J = 285.92 Hz, 1P) and ^{1}H NMR (400 MHz, *p*-xylene-d10, ppm): δ 1.01 (dd, J = 12.8 Hz, J = 6.8 Hz, 6H, CPC(C*H*$_3$)$_2$), 1.11 (dd, J = 15.2 Hz, J = 7.2 Hz, 6H, CPC(C*H*$_3$)$_2$), 1.19 (dd, J = 16 Hz, J = 7.2 Hz, 6H, OPC(C*H*$_3$)$_2$), 1.27 (dd, J = 13.2 Hz, J = 6.8 Hz, 6H, OPC(C*H*$_3$)$_2$), 2.12 – 2.23 (m, 2H, CPC*H*(CH$_3$)$_2$), 2.39 – 2.48 (m, 2H, OPC*H*(CH$_3$)$_2$), 2.84 (t, J = 2.8 Hz, 4H, C_2H_4), 3.15 (d, J = 9.2 Hz, 2H, C*H*$_2$P), 7.10 – 7.22 (m, 3H, arene H).

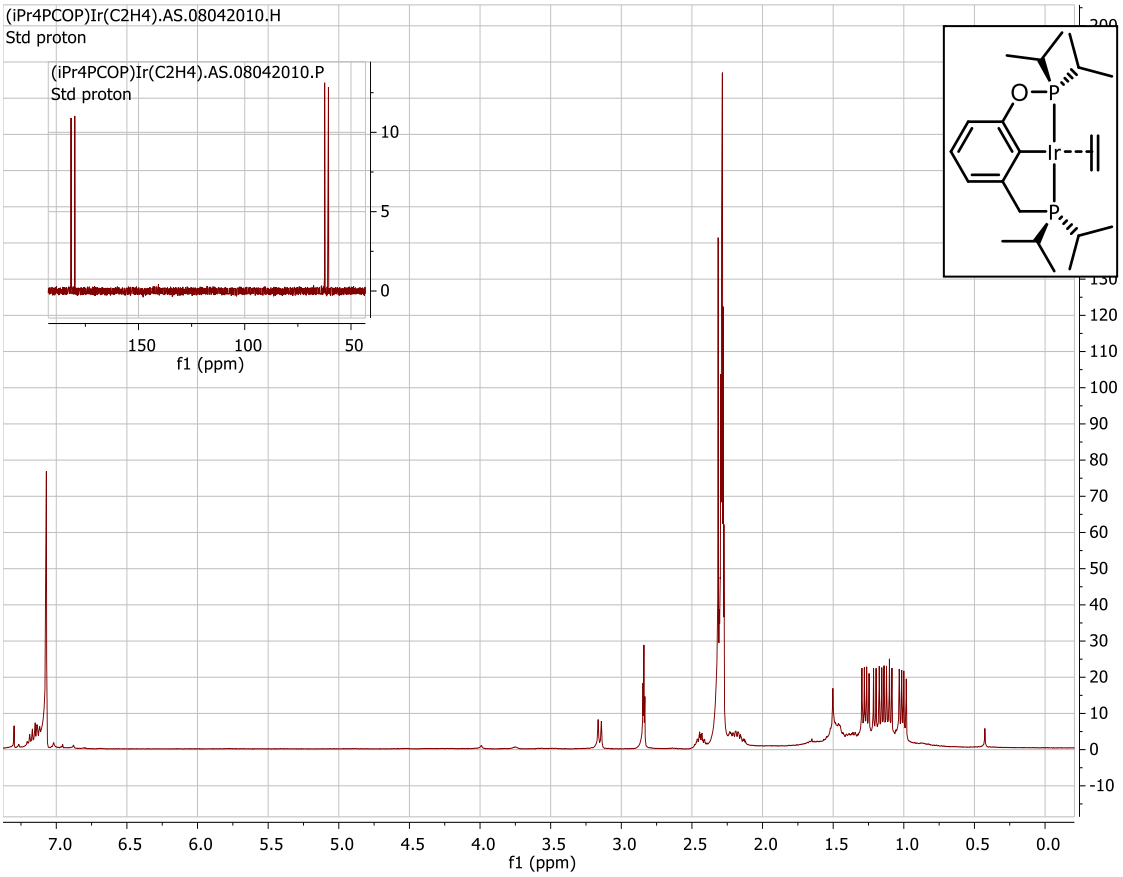

Figure 2.15: ^{31}P and ^{1}H NMR spectra of (^{iPr}PCOP)Ir(C_2H_4)

The representative procedure for dehydroaromatization reactions is as follows: In an argon-filled glove box, (^{iPr}PCOP)Ir(η^2-C_2H_4) (5.6 mg, 0.01 mmol, 10 mM) was dissolved in *n*-alkane (e.g. octane: 0.24 mL, 1.47 mmol, 1.43 M); TBE (4.1 equivalents with respect to octane, 0.78 mL, 6.03 mmol, 5.9 M) and mesitylene (0.01 mL, internal standard) were then added to the solution. Aliquots of this solution (0.1 mL each) were transferred to several 5 mm glass tubes and the contents were cooled under liquid nitrogen and sealed under vacuum. The sealed tubes were heated simultaneously in a preheated oven at 170°C. At regular intervals, a tube was brought to room temperature and the sample was

analyzed by gas chromatography in comparison with authentic products. The major products were confirmed by GC-MS.

The representative procedure for dehydroaromatization using ethylene as the acceptor is as follows: In an argon-filled glove box, ($^{i\text{Pr}}$PCOP)Ir(η^2-C_2H_4) (5.6 mg, 0.01 mmol, 10 mM) was dissolved in *n*-alkane (e.g. dodecane: 1.98 mL, 8.73 mmol, 4.37 M) and mesitylene (0.02 mL, internal standard) in glassware with a bulb and condenser to allow bubbling of excess high purity ethylene through the solution. At regular intervals, an aliquot was removed and the sample was analyzed by GC in comparison with authentic products.

The representative procedure for acceptorless dehydroaromatization is as follows: In an argon-filled glove box, ($^{i\text{Pr}}$PCOP)Ir(η^2-C_2H_4) (5.6 mg, 0.01 mmol, 10 mM) was dissolved in *n*-alkane (e.g. dodecane: 1.98 mL, 8.73 mmol, 4.37 M) and mesitylene (0.02 mL, internal standard) in glassware with a bulb and condenser to allow for release of H_2 gas. At regular intervals, an aliquot was removed and the sample was analyzed by GC in comparison with authentic products.

All alkanes, alkenes, mesitylene, and TBE were distilled under vacuum from Na/K alloy after several freeze-pump-thaw cycles and stored in an argon glove box. Gas chromatography (GC) measurements were performed on a Varian 430 instrument fitted with a capillary column (30 m length x 0.25 mm inner diameter x 0.5 μm film thickness). Gas chromatography – mass spectrometry (GC-MS) measurements were performed on a

Varian 3900 Saturn 2100T instrument fitted with a capillary column (30 m length x 0.25 mm inner diameter x 0.25 µm film thickness).

2.5 Summary

The hybrid phosphine/phosphinite catalyst ($^{i\text{Pr}}$PCOP)Ir(η^2 - C_2H_4) was synthesized and characterized for use in dehydroaromatization reactions based on the previous dehydroaromatization report from the Goldman Group. Dehydroaromatization reactions were performed using the ($^{i\text{Pr}}$PCOP)Ir(η^2 - C_2H_4) catalyst; increased yield was reported for *n*-alkanes that were previously used for dehydroaromatization along with data for several other *n*-alkane starting materials. It is worth noting that as the length of the starting carbon chain increases, the total number of possible products increases, which leads to less selectivity for any one product. Benzene forms as a side product in increasing yield as the length of the starting alkane chain increases, and this will be discussed in Chapter 3. The *o*-alkyltoluene is the major C_n product for all starting *n*-alkanes except *n*-tridecane, which will be further discussed in Chapter 4.

2.6 Appendix

The following figures are GC traces of dehydroaromatization reactions after 120 hours.

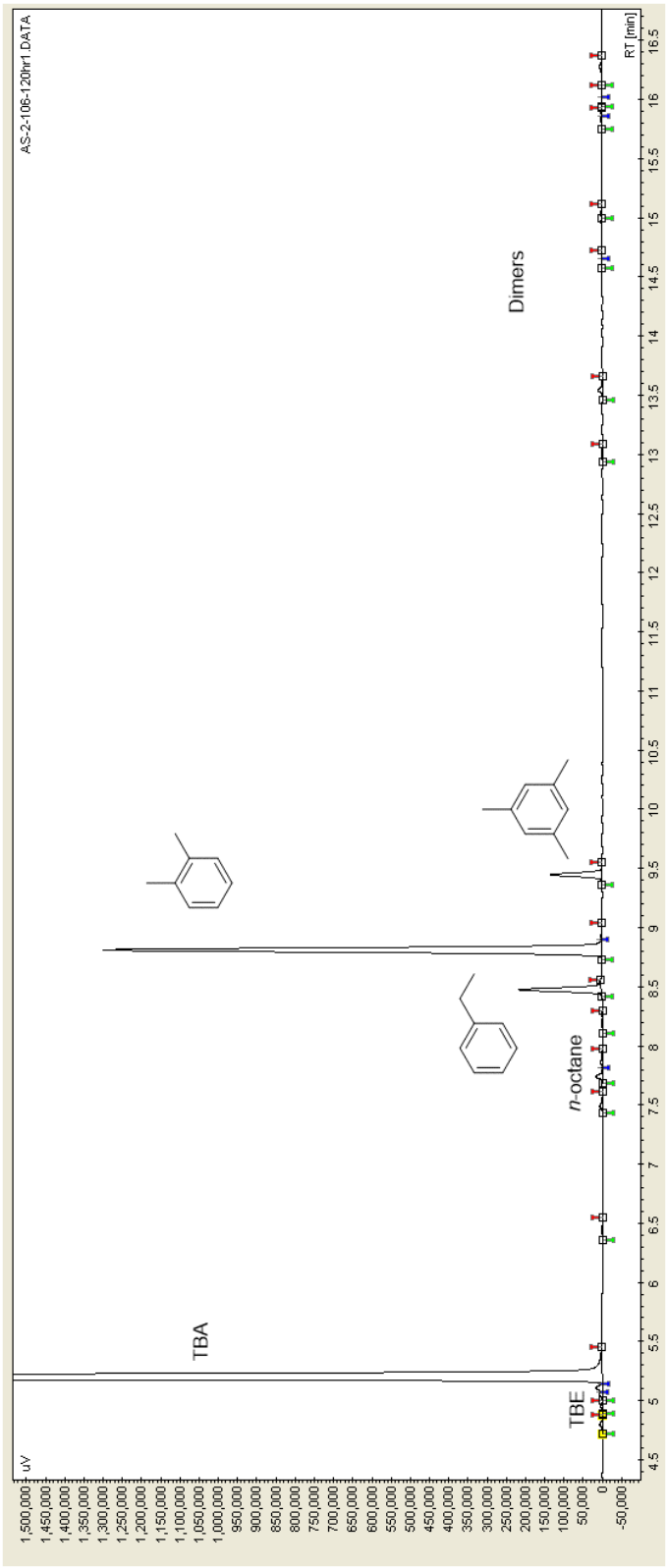

Figure 2.16: GC trace for dehydroaromatization of *n*-octane

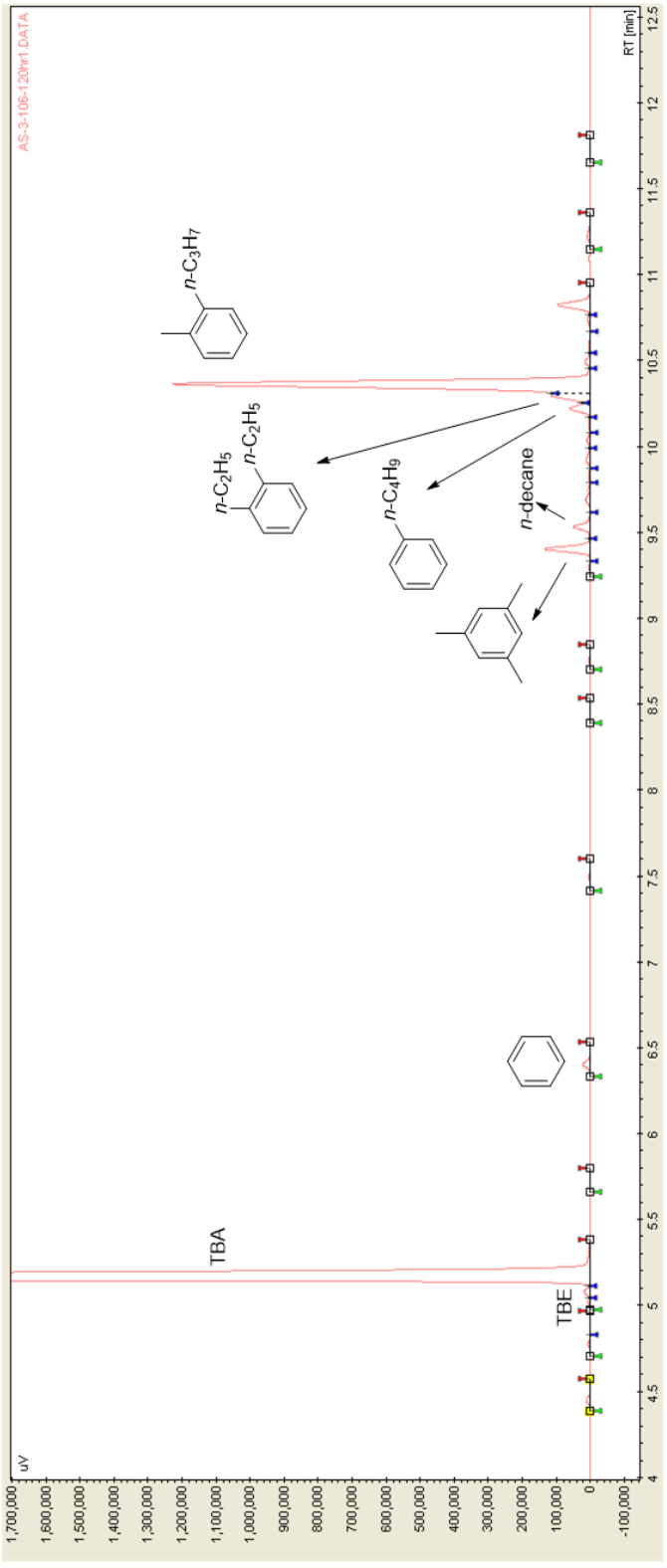

Figure 2.17: GC trace for dehydroaromatization of *n*-decane

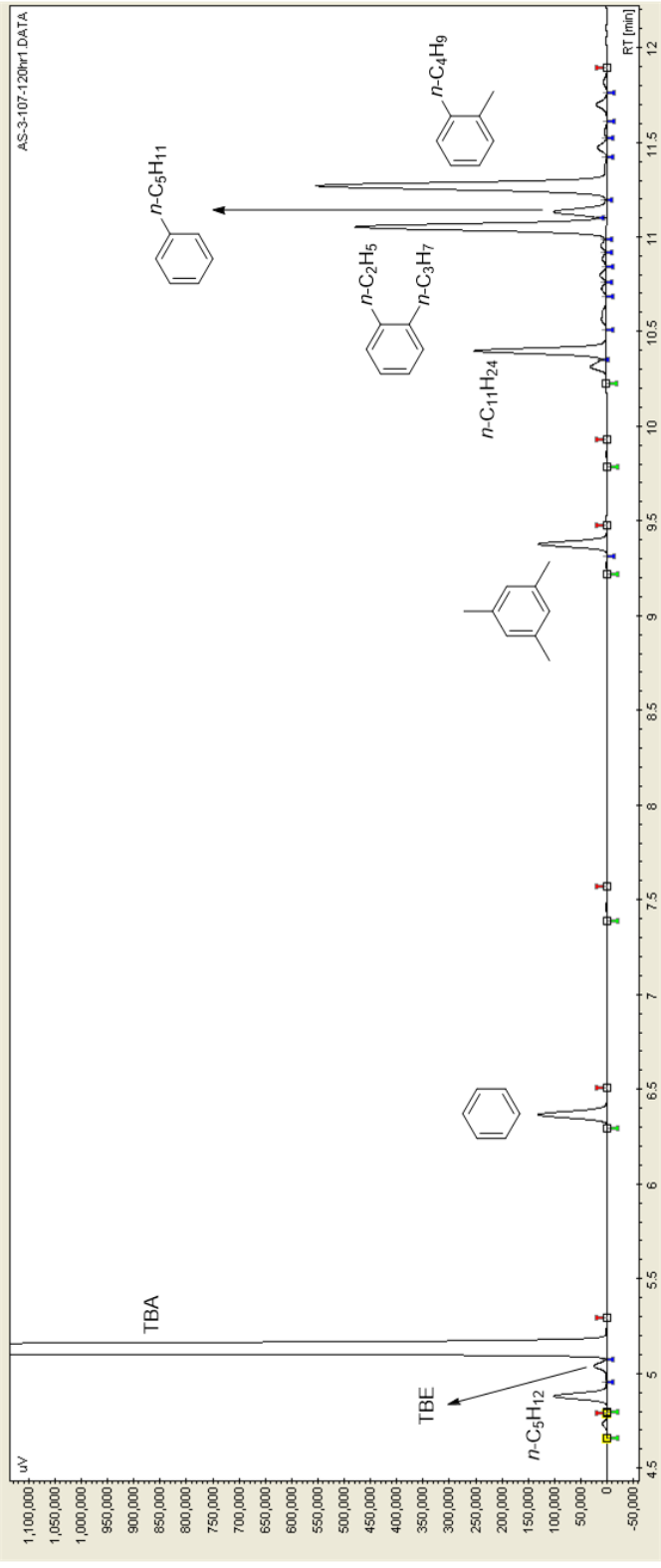

Figure 2.18: GC trace for dehydroaromatization of *n*-undecane

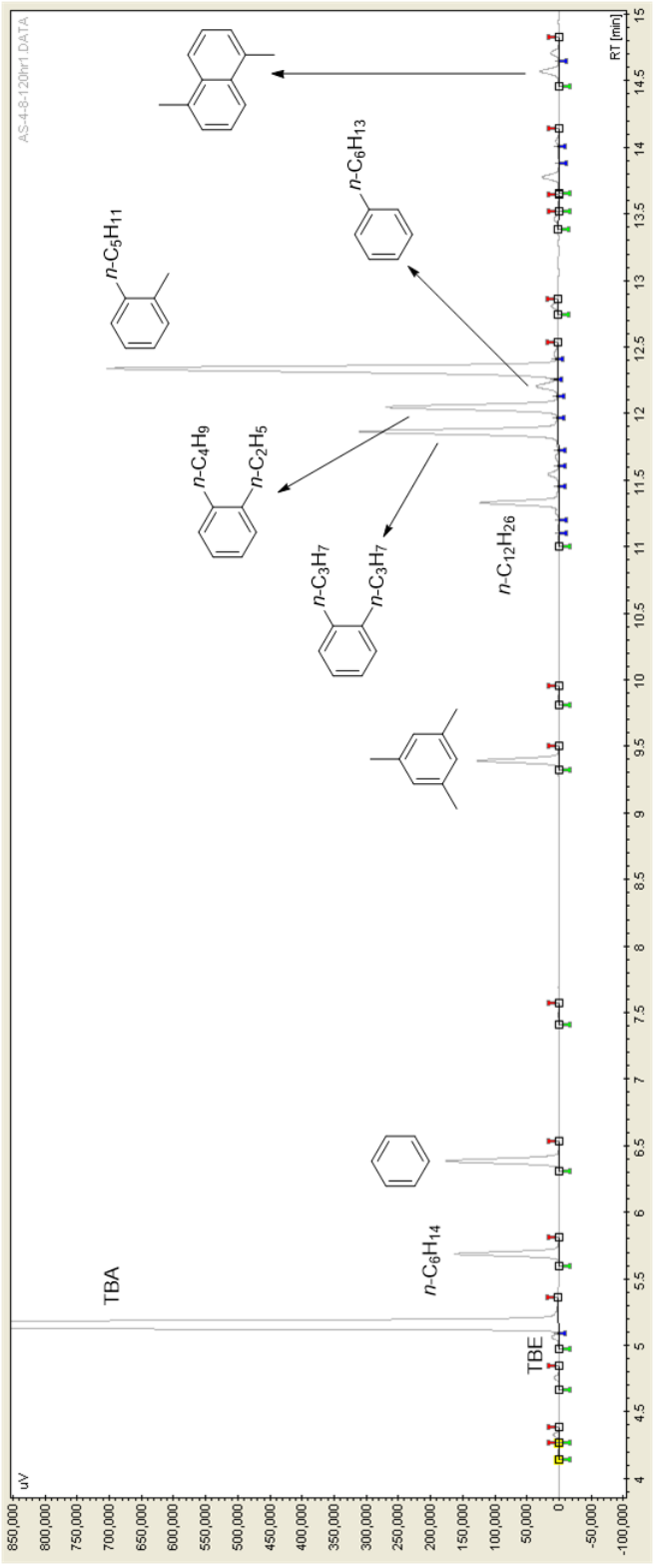

Figure 2.19: GC trace for dehydroaromatization of *n*-dodecane

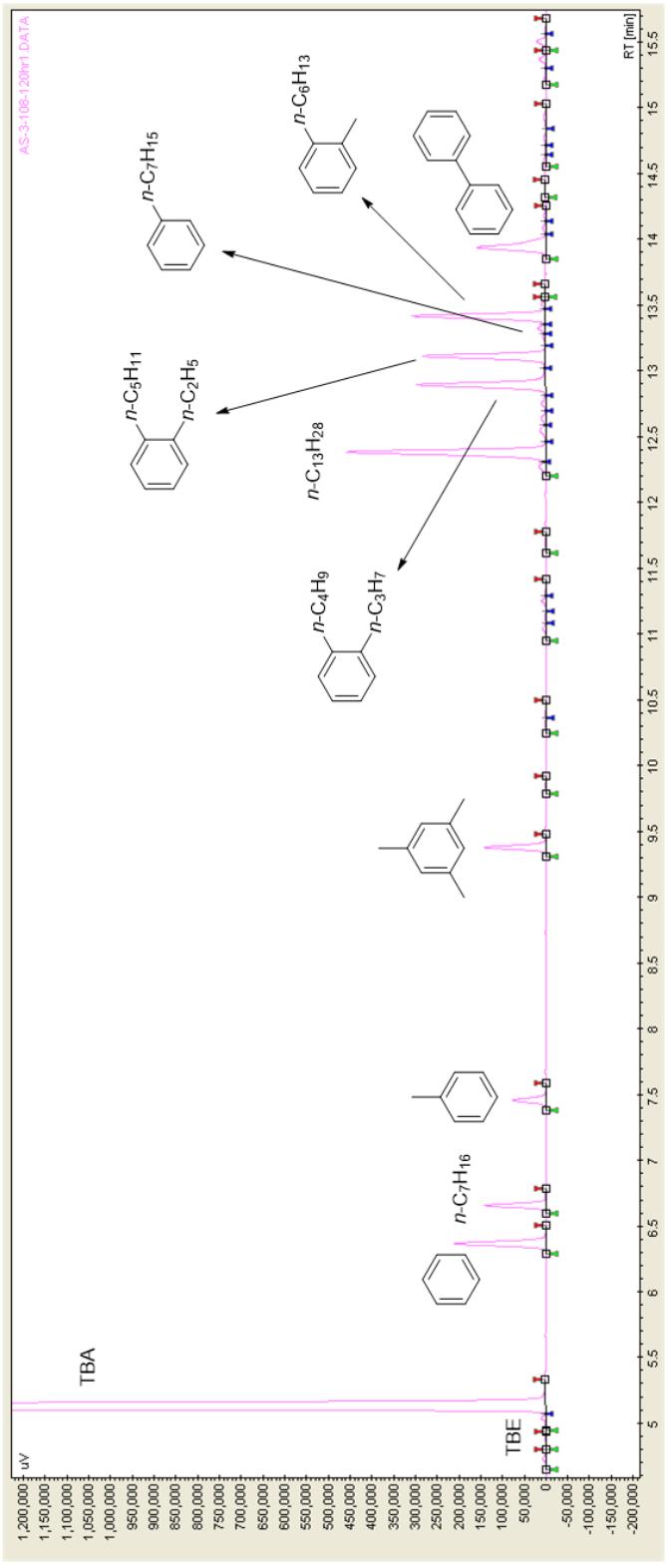

Figure 2.20: GC trace for dehydroaromatization of *n*-tridecane

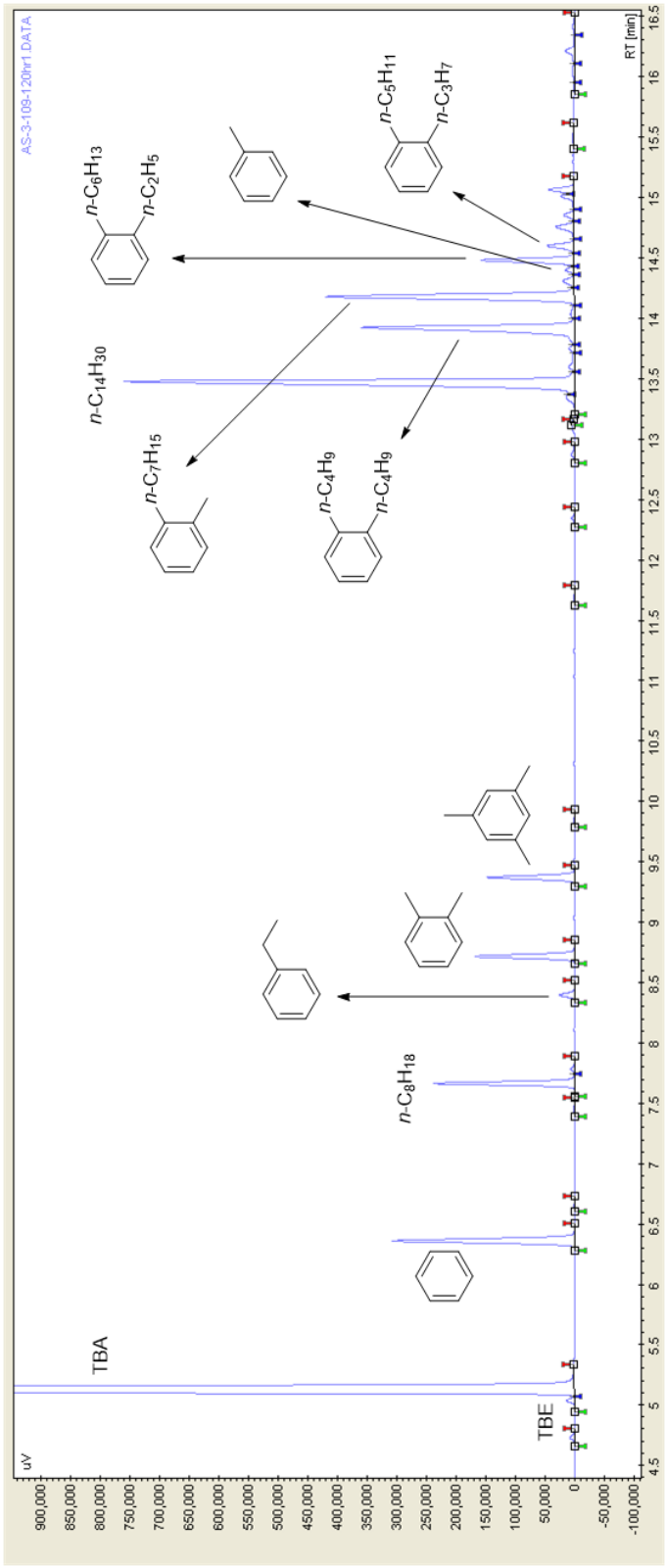

Figure 2.21: GC trace for dehydroaromatization of *n*-tetradecane

2.7 References

[1] Gupta, M.; Hagen, C.; Flesher, R. J.; Kaska, W. C.; Jensen, C. M. *Chem. Commun.* **1996**, 2083.
[2] Choi, J.; MacArthur, A. H. R.; Brookhart, M.; Goldman, A. S. *Chem. Rev.* **2011**, *111*, 1761.
[3] Rybtchinski, B.; Ben-David, Y.; Milstein, D. *Organometallics* **1997**, *16*, 3786.
[4] Punji, B.; Emge, T. J.; Goldman, A. S. *Organometallics*, **2010**, *29*, 2702.
[5] Flores, J. A.; Haibach, M. C.; Goldman, A. S. ACS: 2012, INOR 8.
[6] Nishiyama, H.; Niwa, E.; Inoue, T; Ishima, Y.; Aoki, K. *Organometallics* **2002**, *21*, 2572.
[7] Göttker-Schnetmann, I.; White, P. S.; Brookhart, M. *Organometallics* **2004**, *23*, 1766.
[8] Huang, Z.; Rolfe, E.; Carson, E. C.; Brookhart, M.; Goldman, A. S.; El-Khalafy, S. H.; MacArthur, A. H. R. *Adv. Synth. Catal.* **2010**, *352*, 125.
[9] Krogh-Jespersen, K.; Czerw, M.; Zhu, K.; Singh, B.; Kanzelberger, M.; Darij, N.; Achord, P. D.; Renkema, K. B.; Goldman, A. S. *J. Am. Chem. Soc.* **2002**, *124*, 10797.
[10] Huang, Z.; Brookhart, M.; Goldman, A. S.; Kundu, S.; Ray, A.; Scott, S. L.; Vincente, B. C. *Adv. Synth. Catal.* **2009**, *351*, 188.
[11] Ben-Ari, E.; Gandelman, M.; Rozenberg, H.; Shimon, L. J. W.; Milstein, D. *J. Am. Chem. Soc.* **2003**, *125*, 4714.
[12] Fan, L; Parkin, S.; Ozerov, O. V. *J. Am. Chem. Soc.* **2005**, *127*, 16772.
[13] van der Boom, M. E.; Milstein, D. *Chem. Rev.* **2003**, *103*, 1759.
[14] Frech, C. M.; Shimon, L. J. W.; Milstein, D. *Organometallics* **2009**, *28*, 1900.
[15] Adams, J. J.; Lau, A.; Arulsamy, N.; Roddick, D. M. *Inorg. Chem.* **2007**, *46*, 11328.
[16] Liu, F.; Pak, E. B.; Singh, B.; Jensen, C. M.; Goldman, A. S. *J. Am. Chem. Soc.* **1999**, *121*, 4086.
[17] Ahuja, R.; Punji, B.; Findlater, M.; Supplee, C.; Schinski, W.; Brookhart, M.; Goldman, A. S. *Nature Chem* **2011**, *3*, 167.
[18] Perego, C.; Ingallina, P. *Catalysis Today* **2002**, *73*, 3.
[19] Perego, C.; Ingallina, P. *Green Chemistry* **2004**, *6*, 274.
[20] Kocal, J. A.; Vora, B. V.; Imai, T. *Appl. Catal., A* **2001**, *221*, 295.
[21] He, X.; Guvench, O.; MacKerell Jr., A. D.; Klein, M. L. *J. Phys. Chem. B* **2010**, *114*, 9787.
[22] Yang, J.; Qiao, W.; Li, Z.; Cheng, L. *Fuel* **2005**, *84*, 1607.
[23] Dai, X.; Suo, J.; Duan, X.; Bai, Z.; Zhang, L. *J. Surfact. Deterg.* **2008**, *11*, 111.
[24] Rueping, M.; Nachtsheim, B. J. *Beilstein J. Org. Chem.* **2010**, *6*, No 6.
[25] Nextant 2012; Vol. 2012.
[26] Hartwig, J. F. *Nature Chem.* **2011**, *3*, 99.
[27] Carey, F. A.; Sundberg, R. J. *Advanced Organic Chemistry Part B: Reactions and Synthesis*; 5th ed.; Springer Science + Business Media LLC: Charlottesville, Virginia, 2007.
[28] Peng, Y.; Ma, X.; Schobert, H. H. *Prepr. Am. Chem. Soc. Div. Pet. Chem.* **1988**, *43*, 368.
[29] Eapen, K. C.; Snyder, C. E.; Gschwender, L.; Dua, S. S.; Tamborski, C. *Prepr. Am. Chem. Soc. Div. Pet. Chem.* **1984**, *29*, 1053.
[30] Witcoff, H. A.; Reuben, B. G.; Plotkin, J. S. *Industrial Organic Chemicals* 2nd edn (Wiley-IEEE, 2005).
[31] EIA. Annual Energy Outlook 2012. *Annual Energy Outlook* [Online Early Access]. Published Online: 2012. http://www.eia.gov/forecasts/aeo/er/pdf/0383er(2012).pdf (accessed March 26th 2012).
[32] Dry, M. E. *Catalysis Today* **2002**, *71*, 227.
[33] Dry, M. E. *Applied Catalysis, A: General* **2004**, *276*, 1.
[34] Smiešková, A.; Rojasová, E.; Hudec, P.; Šabo, L. *Applied Catalysis A: General* **2004**, *268*, 235.
[35] Komarewsky, V. I.; Riesz, C. H. *J. Am. Chem. Soc.* **1939**, *61*, 4252.
[36] Meriaudeau, P.; Naccache, C. *Catal. Rev. - Sci. Eng.* **1997**, *39*, 5.
[37] Davis, B. H. *Catal. Today* **2002**, *71*, 227.
[38] Hino, M.; Arata, K. *Appl. Catal. A* **1993**, *100*, 19.
[39] Gairbekov, T. M.; Takaeva, M. I.; Khadzhiev, S. N.; Manovyan, A. K. *J. Appl. Chem. USSR* **1991**, *64*, 2396.
[40] Crabtree, R. H.; Mellea, M. F.; Mihelcic, J. M.; Quirk, J. M. *J. Am. Chem. Soc.* **1982**, *104*, 107.

[41] Haibach, M. C.; Guan, C.; Wang, D. Y.; Li, B.; Lease, N.; Steffens, A. M.; Krogh-Jespersen, K.; Goldman, A. S. *J. Am. Chem. Soc.* **2013**, *135*, 15062.
[42] Thawani, A.; Rajeev, R.; Sunoj, R., B. *Chem.-Eur. J.* **2013**, *19*, 4069.

Chapter 3

Elucidation of the Mechanism for Benzene Formation during Dehydroaromatization Reactions

Abstract

Dehydroaromatization of *n*-alkanes yields a variety of alkylbenzenes along with some interesting side products. Benzene is a surprising side product from dehydroaromatization reactions and the amount of benzene formed increases as the length of the starting *n*-alkane increases. The mechanism for benzene formation during dehydroaromatization reactions is shown to be a retro-ene mechanism. This mechanism is supported by kinetic studies of benzene formation for a variety of different *n*-alkane starting materials, competition reactions between different *n*-alkanes, and through DFT calculations which show that benzene formation increases with increasing carbon number and unsaturation on the alkyl chain. Attempts to limit benzene formation via isomerization or by changing the hydrogen acceptor for dehydrogenation are presented along with attempts to increase benzene formation by favoring terminal olefins.

3.1 Introduction

The elucidation and evaluation of mechanisms of reactions is a key focus for organometallic chemistry because it allows for a more complete understanding of those reactions. Mechanistic understanding of transfer dehydrogenation reactions via C-H activation catalysts has helped to expand the field.[1] Goldman and coworkers reported the mechanism for transfer dehydrogenation of alkanes in a 2003 paper (Figure 3.1).[2, 3]

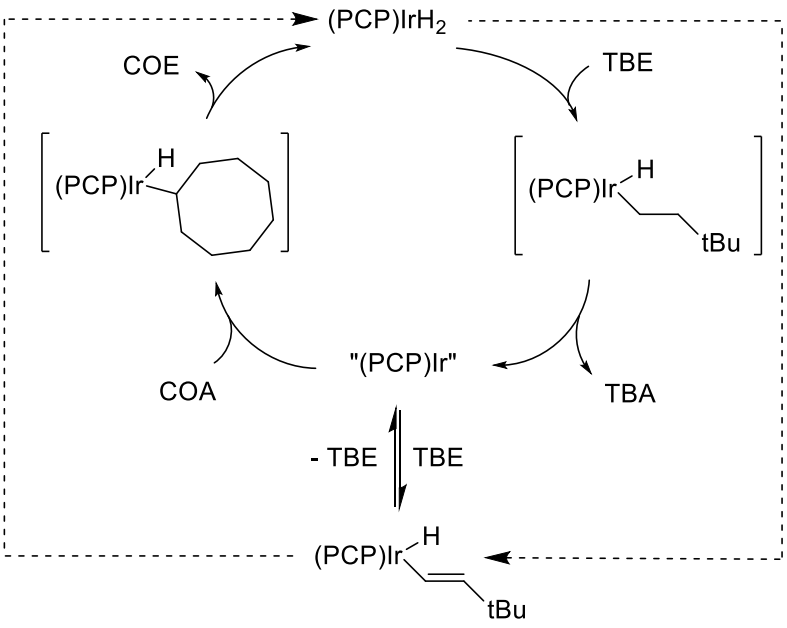

Figure 3.1: Mechanism of transfer dehydrogenation

Transfer dehydrogenation takes place via a 1,2-insertion of the hydrogen acceptor into the metal-hydrogen bond followed by reductive elimination of the hydrogenated acceptor leaving the active $14e^-$ catalyst species. Then, oxidative addition of the alkane

starting material takes place followed by a β-hydride elimination which produces the olefin product. This process has since been expanded to include multiple transfer dehydrogenation reactions, and in 2011 Goldman and coworkers reported the first example of homogeneous dehydroaromatization.[4]

Mechanistic support for this reaction was reported in 2013 by Sunoj and coworkers (Figure 3.2).[4, 5]

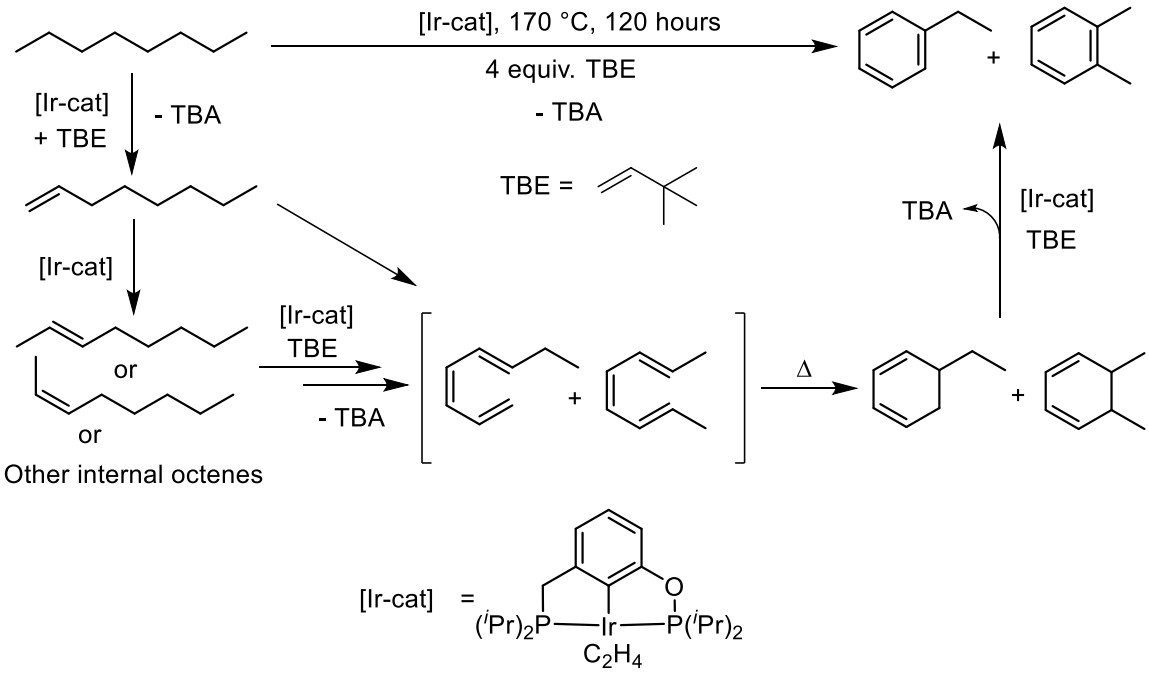

Figure 3.2: Proposed mechanism for dehydroaromatization of *n*-octane

Dehydroaromatization takes place in one pot via transfer dehydrogenation of the starting alkane to give a terminal or internal olefin, followed by transfer dehydrogenation of that olefin to give a terminal or internal diene, followed by a third transfer dehydrogenation of that diene to give a terminal or internal triene. Rapid electrocyclization of that triene gives a monoalkyl or dialkyl cyclic intermediate, and a final transfer dehydrogenation reaction yields the aromatic products with a preference for the *o*-alkyltoluene.

Over the course of studying the dehydroaromatization process, the original researchers noticed that a large amount of benzene formed during the dehydroaromatization of *n*-dodecane.[4] No explanation for the formation of benzene was given in the original dehydroaromatization report, and it is the focus of this chapter to explain the surprising appearance of benzene.

3.2 Results and Discussion

Benzene is a reported side product of the dehydroaromatization reaction with yields typically no more than 3% from reactions using *n*-alkanes with C≤10 after 120 hours. However, for C≥11 the yield of benzene increases dramatically and reaches as much as 32% from heptadecane starting material. Interestingly, no other non-C_n aromatics are observed kinetically alongside benzene (e.g. only C_{12} aromatics and benzene are observed during dehydroaromatization of *n*-dodecane). This indicates that formation of benzene is via a selective cleavage of the C_n starting material. Data from

reactions presented in Chapter 2 are shown again below with particular emphasis on any non-C_n intermediates and products.

3.2.1 Formation of Benzene through Dehydroaromatization of n-*Decane*

A small amount of benzene is formed through the dehydroaromatization of *n*-decane (Scheme 3.1).

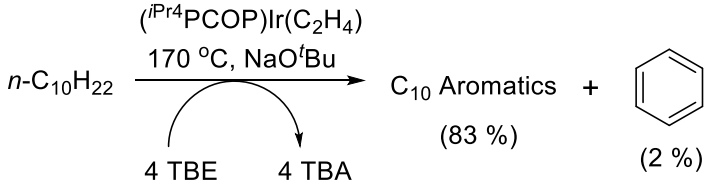

Scheme 3.1: Benzene formation from *n*-decane

Kinetics and concentration for benzene formation are shown below in Table 3.1.

Table 3.1: Kinetics of benzene formation for dehydroaromatization of *n*-decane (mM)

Time	TBE	TBA	Benzene	Decane	C_{10} Aromatics
0 hr	5285	0	0	1182	0
2 hr	4070	1181	3	929	18
24 hr	806	4599	17	266	549
48 hr	20	5366	20	107	811
120 hr	17	5367	21	27	987

Conditions: [(^{iPr}PCOP)Ir(C_2H_4)] = 10 mM; [*n*-decane] = 1.3 M; [TBE] = 5.3 M; 170°C, 30 mM NaO^{t}Bu

Overall, a small amount of benzene is formed and the majority of products are C_{10} aromatics. The amount of benzene differs greatly as the length of the starting *n*-alkane is increased.

3.2.2 Formation of Benzene through Dehydroaromatization of n-*Undecane*

Compared to *n*-decane, the dehydroaromatization of *n*-undecane yields a significantly larger portion of benzene (Scheme 3.2).

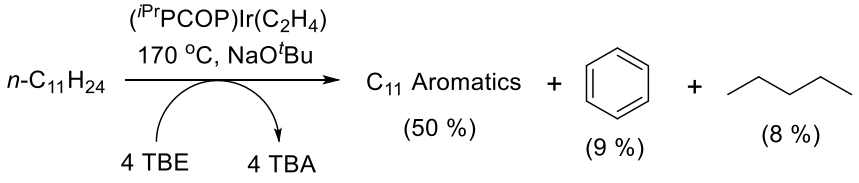

Scheme 3.2: Benzene formation from *n*-undecane

In addition to a significant jump in benzene formation from *n*-undecane compared to *n*-decane, pentane is an observed side product, which indicates that cleavage takes place to give benzene and a C_{n-6} fragment. Presumably, butane was not observed during dehydroaromatization of *n*-decane due to the gaseous nature of butane. Kinetics and

concentration of benzene formation from dehydroaromatization of *n*-undecane are shown in Table 3.2.

Table 3.2: Kinetics of benzene formation from dehydroaromatization of *n*-undecane (mM)

Time	TBE	TBA	Benzene	Pentane	Undecane	C_{11} Aromatics
0 hr	4900	0	0	0	1256	0
2 hr	3777	1020	10	2	1045	21
24 hr	1017	4058	82	16	448	126
48 hr	15	5191	114	91	185	437
120 hr	25	5209	121	98	122	629

Conditions: [(^{iPr}PCOP)Ir(C_2H_4)] = 10 mM; [*n*-undecane] = 1.3 M; [TBE] = 5.3 M; 170°C, 30 mM NaO^tBu

Overall, a significant jump in benzene formation is observed and it is not immediately clear as to the reason for this increase.

3.2.3 Formation of Benzene through Dehydroaromatization of n-*Dodecane*

The dehydroaromatization of *n*-dodecane yields more benzene than the dehydroaromatization of *n*-undecane (Scheme 3.3).

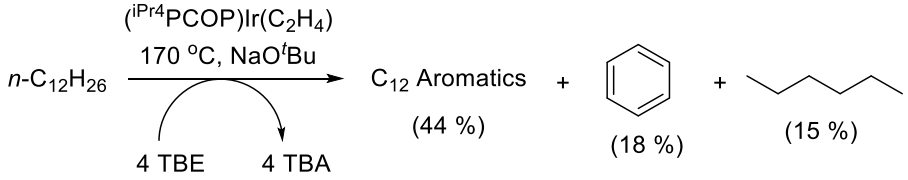

Scheme 3.3: Benzene formation from *n*-dodecane

Again, alongside benzene formation is the formation of a C_{n-6} fragment, namely hexane. The formation of hexane further complicates this reaction because dehydroaromatization of hexane can take place and consume equivalents of acceptor to leave unreacted dodecane. Unreacted dodecane is observed, which is shown in Table 3.3 along with kinetics and concentration of benzene formation.

Table 3.3: Kinetics of benzene formation from dehydroaromatization of *n*-dodecane (mM)

Time	TBE	TBA	Benzene	Hexane	Dodecane	C_{12} Aromatics
0 hr	5303	0	0	0	1354	0
2 hr	3414	2083	36	0	872	23
4 hr	2109	3290	100	0	699	61
24 hr	16	5721	230	181	154	363
48 hr	7	5670	242	197	100	513
120 hr	4	5640	242	199	120	592

Conditions: [(^{iPr}PCOP)Ir(C_2H_4)] = 10 mM; [*n*-dodecane] = 1.3 M; [TBE] = 5.35 M; 170°C, 30 mM NaO^{t}Bu

Benzene formation is further increased starting from *n*-dodecane, but interestingly decreases starting from *n*-tridecane.

3.2.4 Formation of Benzene through Dehydroaromatization of n-*Tridecane*

Benzene formation from dehydroaromatization of *n*-tridecane is decreased compared to *n*-dodecane but still increased compared to *n*-undecane (Scheme 3.4).

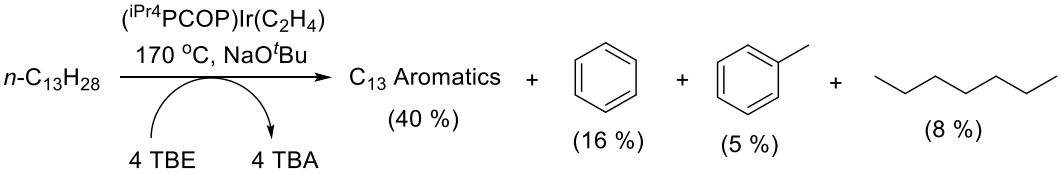

Scheme 3.4: Benzene formation from *n*-tridecane

The decrease in benzene formation compared to *n*-dodecane can be attributed to the formation of toluene and heptane. In the case of *n*-dodecane, fragmentation gives benzene and hexane which can undergo dehydroaromatization to give more benzene. In the case of *n*-tridecane, fragmentation gives benzene and heptane which yields toluene from dehydroaromatization. This is why there is less benzene starting from *n*-tridecane compared to *n*-dodecane. Kinetics and concentration of benzene and fragment formation are shown in Table 3.4.

Table 3.4: Kinetics of benzene formation from dehydroaromatization of *n*-tridecane (mM)

Time	TBE	TBA	Benzene	Heptane	Toluene	Tridecane	C_{13} Aromatics
0 hr	5062	0	0	0	0	1272	0
2 hr	3579	1360	22	0	2	999	22
24 hr	19	5257	171	41	59	331	172

48 hr	6	5308	206	103	61	235	451
120 hr	12	5255	207	107	62	254	504

Conditions: [(^{iPr}PCOP)Ir(C_2H_4)] = 10 mM; [*n*-tridecane] = 1.3 M; [TBE] = 5.35 M; 170°C, 30 mM NaO^tBu

Although benzene formation decreases for *n*-tridecane compared to *n*-dodecane because of the appearance of toluene and heptane, overall fragmentation continues to increase as the length of the starting alkane chain increases. This remains true for *n*-tetradecane.

2.3.5 Formation of Benzene through Dehydroaromatization of n-*Tetradecane*

Dehydroaromatization of *n*-tetradecane yields the largest amount of benzene of all the alkanes presented here (Scheme 3.5).

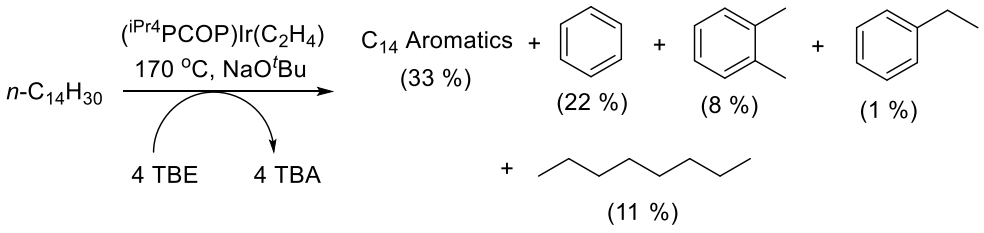

Scheme 3.5: Benzene formation from *n*-tetradecane

Along with the increase in overall benzene formation, there is an increase in other fragmentation products. The C_{n-6} fragments from *n*-tetradecane are octane, ethylbenzene, and *o*-xylene. The fragmentation of tetradecane to give benzene and the

corresponding C_{n-6} fragment allows for dehydroaromatization of the C_{n-6} fragment to give ethylbenzene or *o*-xylene, the same products that are observed from dehydroaromatization of *n*-octane. The lack of toluene or C_9, C_{10}, C_{11}, C_{12}, or C_{13} aromatics at any point during the dehydroaromatization of *n*-tetradecane indicates that fragmentation takes place selectively to give benzene and a C_{n-6} fragment. Kinetics and concentration for benzene formation are shown below in Table 3.5.

Table 3.5: Kinetics of benzene formation from dehydroaromatization of *n*-tetradecane (mM)

Time	TBE	TBA	Benzene	Octane	Ethyl benzene	*o*-Xylene	Tetradecane	C_{14} Aromatics
0 hr	5062	0	0	0	0	0	1266	0
2 hr	3579	1360	37	0	0	2	874	90
24 hr	19	5257	261	120	15	93	322	371
48 hr	6	5308	273	135	17	102	325	417
120 hr	12	5255	278	138	17	103	325	426

Conditions: [(^{iPr}PCOP)Ir(C_2H_4)] = 10 mM; [*n*-tetradecane] = 1.3 M; [TBE] = 5.35 M; 170°C, 30 mM NaO^{t}Bu

Benzene formation increases to 278 mM or 22 % of total products. Alongside the increase in benzene formation is a decrease in total C_{14} aromatics. The mechanism for benzene formation is discussed below.

3.2.6 The Mechanism for Benzene Formation

The surprising appearance of benzene has been addressed for various *n*-alkanes, and this information is summarized below after 7 hours in Table 3.6 with additional *n*-alkane starting materials.

Table 3.6: Concentration and product percent of benzene after 7 hours for various *n*-alkanes

***n*-Alkane**	**[Benzene] (mM)**	**% Benzene**	**% TBE Consumed**	**Total C_n Alkylbenzenes**
Octane	0	0 %	48 %	12 %
Nonane	4	0.3 %	51 %	13 %
Decane	12	0.8 %	55 %	11 %
Undecane	65	5 %	55 %	9 %
Dodecane	95	7 %	57 %	9 %
Tridecane	75	6 %	59 %	8 %
Tetradecane	140	11 %	62 %	8 %
Heptadecane	165	14 %	65 %	7 %

Conditions: [(^{iPr}PCOP)Ir(C_2H_4)] = 10 mM; four equivalents TBE per *n*-alkane; 170°C. Percent and concentration of benzene obtained after seven hours. Percent of benzene based off starting concentration of alkane.

This particular time period was chosen to highlight the lack of benzene for octane; at subsequent time intervals, a small (≤ 0.3%) amount of benzene is present from octane via a different mechanism. The results presented in Table 3.6 suggest a significant correlation between the chain length of the reactant and the yield of benzene because the percent of benzene formed increases as the chain length of the starting alkane increases. For *n*-octane, *n*-nonane, and *n*-decane the amount of benzene is small: 0, 0.3, and 0.8 percent respectively. However, for *n*-undecane the amount of benzene jumps to 5 percent of total

products and this number increases up to 14 percent for *n*-heptadecane. To rationalize this trend, we focused on identifying the number of carbons in each side product alongside benzene so as to ascertain where, and how often, fragmentation was taking place. As previously detailed, fragmentation takes place selectively to give benzene and a corresponding C_{n-6} fragment which can also potentially undergo dehydroaromatization. The amount of TBE consumed increases as the length of the starting alkane chain increases due to the C_{n-6} fragment being dehydroaromatized. It was also determined that cleavage happens before aromatization because a reaction with hexylbenzene under dehydroaromatization reaction conditions yielded no products with C<12 by GC.

The absence of fragmentation from hexylbenzene under the reaction conditions suggested that the fragmentation to give benzene was not catalyzed by iridium. Therefore, benzene formation via the catalytic dehydroaromatization process is proposed to go through a retro-ene type mechanism (Scheme 3.6).[6]

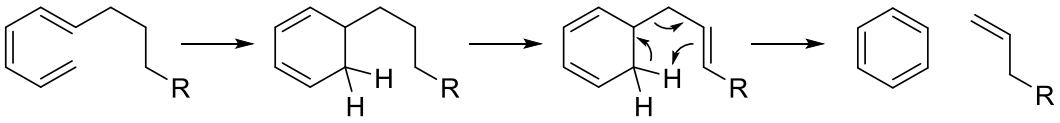

Scheme 3.6: Retro-ene mechanism

This mechanism shows that transfer dehydrogenation can take place on the remaining alkyl chain instead of inside the ring, which would complete aromatization. The double bond on the alkyl chain opens up the possibility for the retro-ene reaction.

3.2.7 Evidence to Support the Retro-ene Mechanism

A retro-ene reaction is a rearrangement akin to a 1,5-hydrogen shift which, in this case, leads to fragmentation to form benzene and a corresponding alkyl fragment. This mechanism accounts for the appearance of benzene and side products which could later react to form aromatics. It also explains the increase in benzene formation with increasing carbon chain length. In addition, the retro-ene mechanism is not possible for octane due to lack of the necessary chain length. For this reason, and due to a difference in kinetics for the formation of benzene between octane and longer *n*-alkanes, the small (≤ 0.3%) amount of benzene present at the end of the octane dehydroaromatization process is proposed to go through an alternate mechanism. Decane should be better for fragmentation than nonane because decane has an internal double bond, which is more favorable for dehydrogenation from the iridium catalyst, and indeed this is the case.[7] However, it is not initially clear from the mechanism why there is such a large jump in benzene production between chains with 10 carbons or less and chains with 11 carbons or more.

Concerning the retro-ene reaction, a specific fragment alongside benzene should be observable via GC. As previously mentioned, there is selective cleavage at the sixth

carbon to give a corresponding C_{n-6} fragment. Based on the retro-ene mechanism, the fragment should be the C_{n-6} terminal olefin. In order to observe the specific fragment and provide more evidence for the retro-ene mechanism, a dehydroaromatization reaction was performed with tridecane and octane in the same solution. The purpose of this was to make a kinetic observation of the C7 fragment that forms from the retro-ene mechanism as benzene is formed while using octane as a kinetic reference. In terms of tridecane, C13 monoenes, dienes, trienes, and cyclic intermediates should form before the retro-ene fragmentation takes place to yield benzene and 1-heptene, and in terms of octane, octenes should form in conjunction with the C13 enes faster than any C7 fragments. As expected, a significant amount of octenes was observed before any C7 fragments, but contrary to expectations, no C7 monoenes were formed at any point during the reaction. Instead, as benzene was formed, 2,4-heptadiene was observed. In fact, the only C7 compounds that are observed are 2,4-heptadiene, heptatriene, 5-methylcyclohexa-1,3-diene, and toluene (Scheme 3.7).

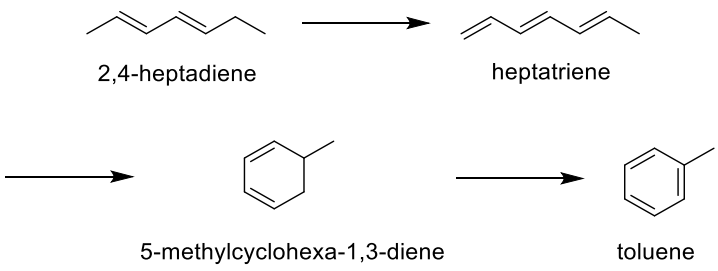

Scheme 3.7: All C_7 fragments formed during dehydroaromatization of *n*-tridecane

These C7 compounds are the same as those observed during the dehydroaromatization of heptane, so the observation of these compounds by GC indicates that the C7 fragment is undergoing dehydroaromatization. This data shows that fragmentation leads to benzene and the corresponding 2,4-diene, and that the 2,4-diene continues to react to form an aromatic product through dehydroaromatization.

The presence of 2,4-heptadiene instead of 1-heptene from the fragmentation reaction went against expectations based on the retro-ene mechanism. However, it was then discovered that the (^{iPr}PCOP)Ir(η^2-C_2H_4) catalyst rapidly isomerizes 1,4-heptadiene to 2,4-heptadiene at room temperature by combining that catalyst with 1,4-heptadiene and examining the contents by GC. The dehydroaromatization reactions are performed at 170 °C, and although 1,4-heptadiene and benzene are the expected products from the retro-ene mechanism, 2,4-heptadiene is actually observed due to rapid isomerization of 1,4-heptadiene (Scheme 3.8).

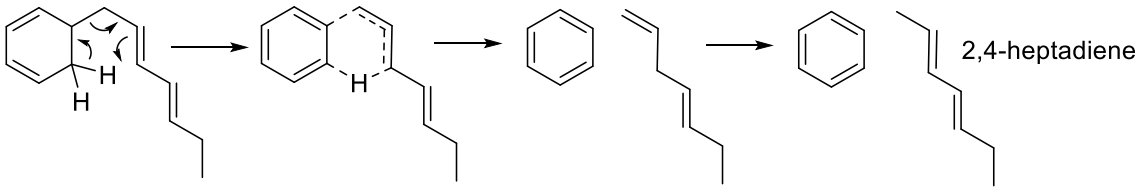

Scheme 3.8: Fragmentation of *n*-tridecane and isomerization of 1,4-heptadiene to 2,4-heptadiene

This explains why 2,4-heptadiene is observed instead of 1,4-heptadiene but does not explain the presence of a diene instead of a monoene.

In order to explain the presence of a diene instead of a monoene, it was hypothesized that increasing degrees of unsaturation on the alkyl chain of the cyclic intermediate during dehydroaromatization favors the retro-ene mechanism. Density Functional Theory (DFT) calculations were performed to test this hypothesis based on the transformation illustrated in Scheme 3.9 (Table 3.7).

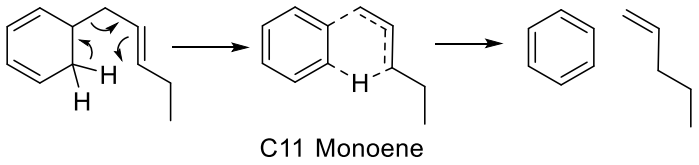

Scheme 3.9: Example of an intermediate used for DFT calculations

Table 3.7: Increasing degrees of unsaturation favor the retro-ene mechanism

Carbon Number	Arm Unsaturation	$\Delta G^{\ddagger}$ (kcal/mol)	Calculated Rate (s^{-1})
C11	Monoene	32.4	9.4E-4
C11	Diene	30.7	6.5E-3
C12	Monoene	32.5	8.4E-4
C12	Diene	30.9	5.2E-3
C14	Monoene	32.3	1.0E-3
C14	Diene	30.9	5.2E-3
C14	Triene	29.9	1.6E-2

The calculations determine that the $\Delta G^{\ddagger}$ and rate of the retro-ene mechanism depend on chain length and arm unsaturation, and show that there is about a 1.5 kcal/mol difference in $\Delta G^{\ddagger}$ and about a factor of 6 difference in rate for the retro-ene mechanism between a single double bond and two double bonds on the alkyl chain. Adding a third double bond to the alkyl chain further decreases the $\Delta G^{\ddagger}$ by 1 kcal/mol and increases the rate by a factor of 3. While this effect is not as pronounced with a third double bond, this data does support the hypothesis that increasing unsaturation on the alkyl chain favors the retro-ene mechanism.

The final data supporting the retro-ene mechanism as the route through which benzene is formed is also presented through DFT calculations. We observe negligible amounts of small aromatics other than benzene that do not form via dehydroaromatization, such as toluene or ethylbenzene, from long chain alkanes. This is because the electrocyclization takes place in a disrotatory fashion according to Woodward-Hoffmann rules which gives an intermediate that places the hydrogen away from the double bond.[8] This makes the retro-ene mechanism extremely unfavorable (Scheme 3.10).

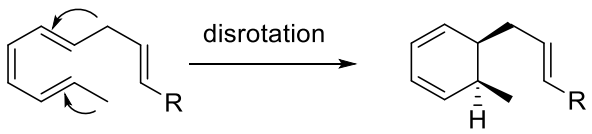

Scheme 3.10: Disrotatory electrocyclization

However, even if there were a rearrangement to place the hydrogen adjacent to the double bond, DFT calculations show that the retro-ene mechanism is still unfavorable towards the formation of ethylbenzene or toluene (Scheme 3.11 and Table 3.8).

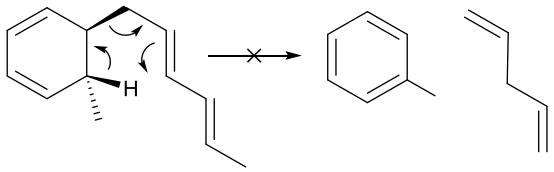

Scheme 3.11: Transformation used for DFT calculations

Table 3.8: DFT calculations show why toluene is not formed

Arene	Arm Unsaturation	$\Delta G^{\ddagger}$ (kcal/mol)	Rate (s^{-1})
Benzene	Monoene	32.5	8.4E-04
Toluene	Monoene	34.4	9.6E-05
Benzene	Diene	30.9	5.2E-03
Toluene	Diene	33.1	4.2E-04

There is an increase in $\Delta G^{\ddagger}$ of about 2 kcal/mol and a decrease of a factor of 9 in rate between the formation of benzene and formation of toluene. The absence of small aromatics such as toluene or ethylbenzene, and the observation that benzene is not formed after aromatization takes place, helps to eliminate homolytic cleavage as a

possible mechanism. The data collected and presented herein is sufficient to accept the retro-ene mechanism as the means through which benzene is formed.

3.2.8 Attempts to Limit Benzene Formation

Understanding the mechanism for benzene formation during dehydroaromatization reactions is the first step towards limiting total benzene production. The fact that the retro-ene mechanism can only take place with a monoalkyl cyclic and not a dialkyl cyclic means that isomerization of double bonds to favor dialkylbenzenes should also prevent benzene formation (Scheme 3.12).

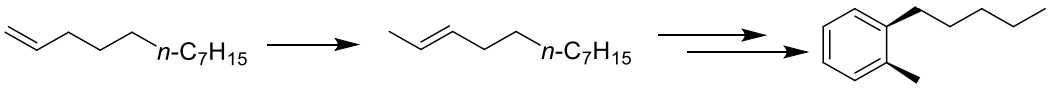

Scheme 3.12: Limiting benzene formation through isomerization of terminal olefins

Isomerizing the terminal double bond to an internal double bond prevents cyclization to monoalkyl intermediates, which prevents benzene formation via the retro-ene mechanism. Similarly, isomerization of the monoalkyl cyclic diene intermediate would prevent benzene formation by moving a double bond to block the retro-ene mechanism (Scheme 3.13).

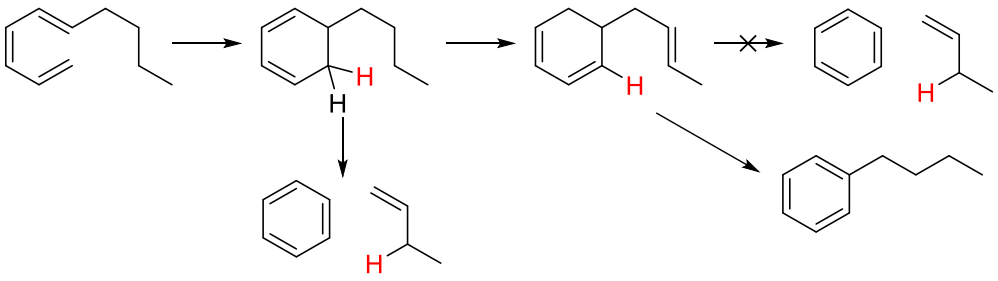

Scheme 3.13: Limiting benzene formation through isomerization of cyclic dienes

Preventing benzene formation by isomerizing double bonds will also have the added benefit of increasing overall yield of alkylaromatics.

Finding a good isomerization catalyst proved to be a significant challenge. Dehydroaromatization reactions are run at 170 °C and homogeneous isomerization catalysts typically decompose at high temperatures. Heterogeneous isomerization catalysts can have negative effects on the iridium pincer catalyst or cause skeletal isomerization of the TBE acceptor. With this in mind, a variety of isomerization catalysts were screened to prevent benzene formation.

The first isomerization catalyst screened was Pd/C, which is typically thought of as a hydrogenation catalyst, but can also be used for isomerization.[9] A rotating oven was used for these reactions to ensure mixing of the Pd/C with the reaction solution. Unfortunately, no decrease in benzene was observed while using Pd/C as an isomerization catalyst despite multiple attempts at different temperatures and catalyst loadings.

In addition to Pd/C, a variety of other pincer catalysts were used as co-catalysts in an attempt to limit benzene formation. It has been established that pincer catalysts are thermally robust and good at isomerization.[10, 11] The ($^{t\text{Bu}}$PCP)Ir catalyst cannot perform dehydroaromatization due to steric hindrance and therefore seems an ideal pincer isomerization catalyst. Unfortunately, a significant change in benzene formation was not observed while using ($^{t\text{Bu}}$PCP)Ir as a co-catalyst with ($^{i\text{Pr}}$PCOP)Ir despite multiple attempts at different temperatures and with different catalyst loadings. In fact, none of the pincer catalysts screened offered any meaningful change in benzene formation (Figure 3.1).

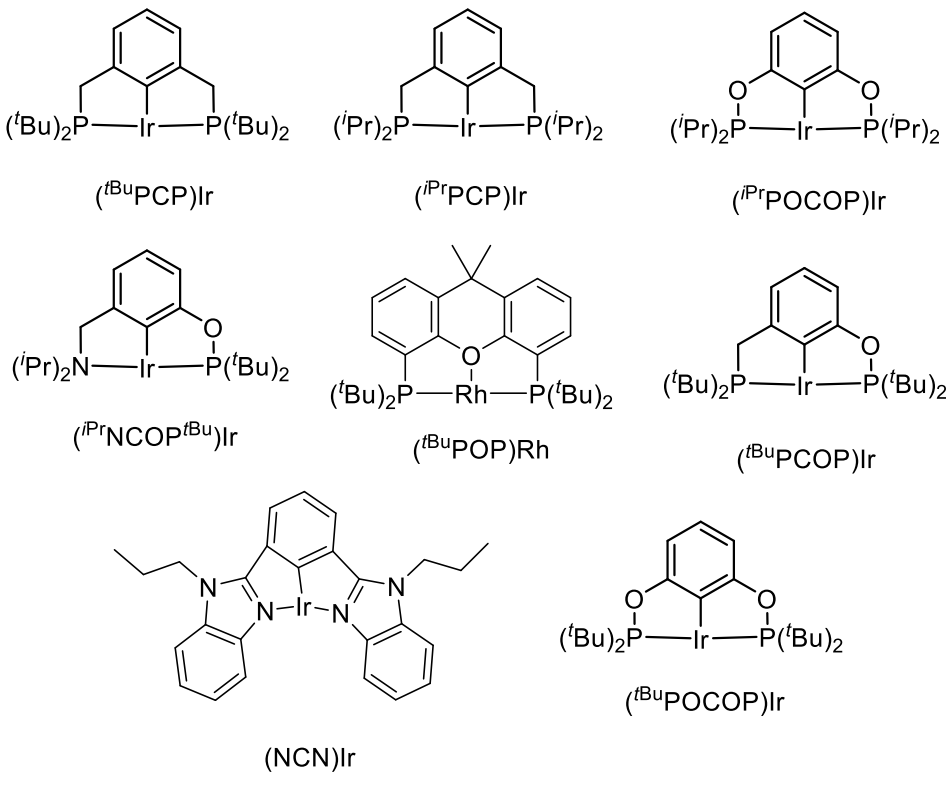

Figure 3.3: Pincer catalysts screened for isomerization

Thus far, the only significant change in total benzene formation through dehydroaromatization reactions has come from changing the hydrogen acceptor. Using 1-pentene instead of TBE as the hydrogen acceptor gives a significant decrease in total benzene formation (Table 3.9).

Table 3.9: Decrease in benzene formation by changing the acceptor

Acceptor	Temperature	Benzene + Hexane	C_{12} Aromatics
TBE[a]	170 °C	18 %	46 %
1-Pentene[b]	170 °C	9 %	56 %

Conditions: a: [(^{iPr}PCOP)Ir(C_2H_4)] = 10 mM; [*n*-dodecane] = 1.3 M; [TBE] = 5.35 M; 30 mM NaO^{t}Bu
b: [(^{iPr}PCOP)Ir(C_2H_4)] = 10 mM; [*n*-dodecane] = 1.47 M; [1-Pentene] = 6 M; 30 mM NaO^{t}Bu

Switching the acceptor causes the total amount of benzene formed to decrease from 17 % to 9 % and total C_{12} aromatics to increase from 46 % to 56 % under the same conditions. The exact nature of this decrease is unknown but the hypothesis is that the 1-pentene adduct is lower in energy which allows for the dehydrogenation reactions to take place faster and leaves less time for retro-ene reactions.

3.2.9 Attempts to Increase Benzene Formation

It should be noted that because the fragmentation intermediates can also undergo dehydroaromatization, more than four equivalents of hydrogen acceptor are required for full conversion of *n*-alkane and the resulting C_{n-6} fragment from the retro-ene reaction. Unfortunately, increasing the equivalents of TBE from four to six or eight causes inhibition of the catalyst by the acceptor resulting from a decrease in concentration of the active $14e^-$ species of the catalyst and resulting yields of aromatics and benzene are both significantly decreased. The reaction rate is also significantly decreased. All attempts to use increased equivalents of acceptor to increase yield of benzene were met with decreased rate and yield of all products.

As previously established, the retro-ene reaction can only take place on a monoalkylbenzene precursor to give benzene and the corresponding fragment. No dialkylbenzene precursors will go through the retro-ene mechanism based on Woodward-Hoffmann rules and DFT calculations. Therefore, attempts to maximize benzene yield revolve around maximizing monoalkylbenzene precursors. This can be done by increasing concentration of terminal olefins in solution because only terminal olefins can lead to the monoalkylbenzene precursors (Scheme 3.14).

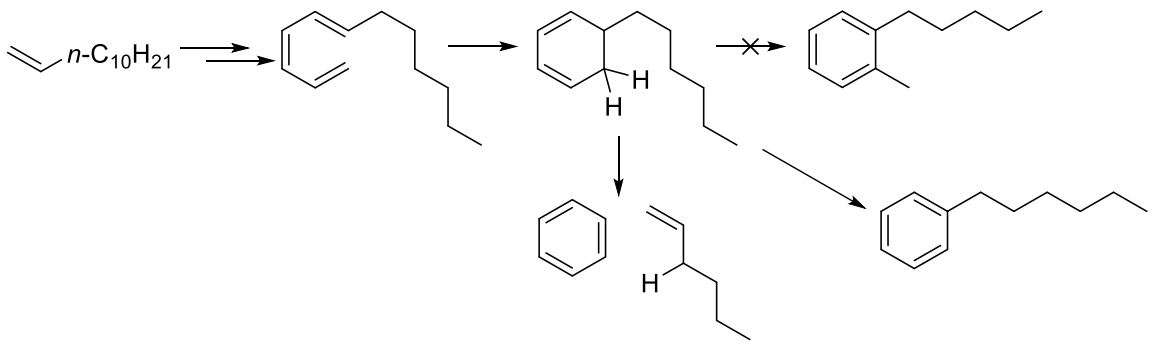

Scheme 3.14: Terminal olefin dehydroaromatization

Using 1-dodecene as a starting material instead of *n*-dodecane should therefore increase yield of benzene. Also, the ($^{i\text{Pr}}$PCP)Ir catalyst is known to be terminally selective for dehydrogenation while the ($^{i\text{Pr}}$PCOP)Ir catalyst is internally selective so using the ($^{i\text{Pr}}$PCP)Ir catalyst should also give more terminal olefins and more benzene. Different dehydroaromatization reactions starting from 1-dodecene are summarized below compared to the dehydroaromatization of *n*-dodecane using both ($^{i\text{Pr}}$PCOP)Ir and ($^{i\text{Pr}}$PCP)Ir catalysts (Table 3.10 and Table 3.11).

Table 3.10: Dehydroaromatization of 1-dodecene compared to *n*-dodecane using ($^{i\text{Pr}}$PCOP)Ir

Reaction	Temperature	Benzene	Hexane	Starting Material	C_{12} Aromatics	Dimers
Dodecane 4:1 TBE ($^{i\text{Pr}}$PCOP)Ir	170 °C	10 %	8 %	9 %	46 %	18 %
Dodecane 4:1 TBE ($^{i\text{Pr}}$PCOP)Ir	200 °C	7 %	6 %	5 %	65 %	12 %
1-Dodecene	170 °C	6 %	6 %	7 %	61 %	14 %

3:1 TBE (^{iPr}PCOP)Ir						
1-Dodecene 3:1 TBE (^{iPr}PCOP)Ir	200 °C	8 %	7 %	7 %	59 %	15 %
1-Dodecene 4:1 TBE (^{iPr}PCOP)Ir	170 °C	8 %	8 %	0 %	65 %	12 %
1-Dodecene 4:1 TBE (^{iPr}PCOP)Ir	200 °C	9 %	8 %	1 %	66 %	10 %

Conditions: [(^{iPr}PCOP)Ir] = 10 mM; [Starting Material] = 1.3 M; 170°C or 200 °C, 30 mM NaO^{t}Bu. Percentages of products calculated from concentration of starting material. Due to dimers being unresolved on GC, dimer concentration is calculated based on missing dodecane.

Interestingly, the amount of benzene and hexane formed using 1-dodecene as the starting material was decreased compared to using *n*-dodecane as the starting material. The amount of dimers also decreased while using 1-dodecene as the starting material, but total C_{12} aromatics were noticeably increased. Surprisingly, increasing the temperature from 170 °C to 200 °C had no significant effect on any reaction starting from 1-dodecene but had a drastic effect on the reactions starting from *n*-dodecane. Overall, the amount of benzene formed is not increased by using 1-dodecene as the starting material for dehydroaromatization.

Table 3.11: Dehydroaromatization of 1-dodecene compared to *n*-dodecane using (^{iPr}PCP)Ir

Reaction	**Temperature**	**Benzene**	**Hexane**	**Starting Material**	**C_{12} Aromatics**	**Dimers**
Dodecane 4:1 TBE	170 °C	12 %	10 %	8 %	36 %	25 %

($^{i\text{Pr}}$PCP)Ir						
Dodecane 4:1 TBE ($^{i\text{Pr}}$PCP)Ir	200 °C	11 %	10 %	6 %	49 %	16 %
1-Dodecene 3:1 TBE ($^{i\text{Pr}}$PCP)Ir	170 °C	11 %	10 %	6 %	34 %	38 %
1-Dodecene 3:1 TBE ($^{i\text{Pr}}$PCP)Ir	200 °C	11 %	10 %	6 %	41 %	30 %

Conditions: [($^{i\text{Pr}}$PCP)Ir] = 10 mM; [Starting Material] = 1.3 M; 170°C or 200 °C, 30 mM NaO^{t}Bu. Percentages of products calculated from concentration of starting material. Due to dimers being unresolved on GC, dimer concentration is calculated based on missing dodecane.

Using ($^{i\text{Pr}}$PCP)Ir as the catalyst for dehydroaromatization showed a small increase in benzene/hexane formed, but overall yield of C_{12} aromatics was drastically decreased while overall yield of dimers was drastically increased. Overall, neither using 1-dodecene as the starting material nor using ($^{i\text{Pr}}$PCP)Ir as the catalyst allowed for an increase in benzene formation.

3.3 Experimental

3.3.1 General Procedure for Dehydroaromatization

The representative procedure for dehydroaromatization reactions is as follows: In an argon-filled glove box, ($^{i\text{Pr}}$PCOP)Ir(η^2-C_2H_4) (5.6 mg, 0.01 mmol, 10 mM) was dissolved in *n*-alkane (e.g. dodecane: 0.3 mL, 1.32 mmol, 1.3 M); TBE (4.1 equivalents with respect to dodecane, 0.7 mL, 5.43 mmol, 5.35 M) and mesitylene (0.01 mL, internal standard)

were then added to the solution. Aliquots of this solution (0.1 mL each) were transferred to several 5 mm glass tubes and the contents were cooled under liquid nitrogen and sealed under vacuum. The sealed tubes were heated simultaneously in a preheated oven. At regular intervals, a tube was brought to room temperature and the sample was analyzed by gas chromatography in comparison with authentic products. The major products were confirmed by GC-MS.

All alkanes, alkenes, mesitylene, and TBE were distilled under vacuum from Na/K alloy after several freeze-pump-thaw cycles and stored in an argon glove box. Gas chromatography (GC) measurements were performed on a Varian 430 instrument fitted with a capillary column (30 m length x 0.25 mm inner diameter x 0.5 μm film thickness). Gas chromatography – mass spectrometry (GC-MS) measurements were performed on a Varian 3900 Saturn 2100T instrument fitted with a capillary column (30 m length x 0.25 mm inner diameter x 0.25 μm film thickness).

3.3.2 DFT Information

All calculations were carried out using the Gaussian 09 suite of quantum chemical programs and the Lee-Yang-Parr correlation functional B3LYP with a 6-311 + (d,g) basis set.[12] Rates were calculated using the Eyring equation.[13] The following tables and figures are DFT coordinates for the calculations presented in Table 3.7 and Table 3.8.

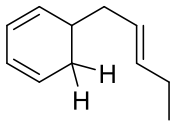

Figure 3.4: C11 monoene

Table 3.12: DFT coordinates for C11 monoene

C	0	2.1371672072	0.9755687054	-1.3348721769
C	0	0.9832871701	0.3281949797	-1.009906185
C	0	0.9377182571	-0.7240585804	0.0448035348
C	0	2.2087707943	-0.8007068305	0.8382676731
C	0	3.3775978425	-0.1638359789	0.4060975441
C	0	3.3566788726	0.7338693447	-0.6446510831
H	0	2.1285303499	1.6877663053	-2.1536933168
H	0	1.294659909	0.1004899365	2.1403879912
H	0	2.2906672472	-1.6154793834	1.5499178024
H	0	4.3027668971	-0.3510820823	0.9413041088
H	0	4.2595796782	1.2511448499	-0.9456133172
H	0	0.099104087	0.4940137405	-1.6080406242
H	0	0.8649650122	-1.6922777561	-0.5175865648
C	0	-0.2894712044	-0.9540975882	0.8950279935
H	0	-0.1968976282	-1.8766063408	1.4666666706

H	0	0.4686817941	-0.0506155723	2.0892870457
C	0	-1.650713258	-0.5579636069	0.676822224
H	0	-2.3503391927	-1.0649845747	1.3422180525
C	0	-2.1950485227	0.3827035701	-0.1359910737
H	0	-1.5825384299	0.929577037	-0.8426672818
C	0	-3.650440682	0.7458040264	-0.1272728131
H	0	-4.1674476023	0.1831041156	0.6570175171
H	0	-3.7525360643	1.8083279788	0.1347835148
C	0	-4.3457041882	0.5121568529	-1.4807369697
H	0	-4.3143795101	-0.5446971889	-1.7589079013
H	0	-5.3933988885	0.8239808595	-1.4410276341
H	0	-3.8583126571	1.0815624211	-2.2778615412

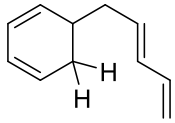

Figure 3.5: C11 diene

Table 3.13: DFT coordinates for C11 diene

C	0	1.0227464197	-1.8936430038	0.1791887536
C	0	0.5634235251	-0.7012524186	0.9064237921
C	0	1.4418456755	0.4717305578	0.8283451927
C	0	2.6260886092	0.4190646318	0.0590270696
C	0	2.9469786792	-0.6952965544	-0.6790756524
C	0	2.1254887368	-1.8633371705	-0.6154722281
H	0	0.433891675	-2.8009448085	0.2654785528
H	0	-0.5005590211	-0.380426516	0.4239208992
H	0	3.2878361849	1.2789761462	0.0566539154
H	0	3.8515389004	-0.7112124999	-1.2762072607
H	0	2.4186888214	-2.7473653692	-1.1716150098
H	0	0.1908486597	-0.9143037052	1.9148876452
H	0	1.3456034857	1.2403950687	1.5822404304
C	0	0.1725796067	2.0100285833	-0.6107342247
H	0	0.6371990038	2.9487340538	-0.3350063851
H	0	0.595614954	1.4989921852	-1.4663600535

C	0	-1.0757139221	1.6739698949	-0.1412045095
H	0	-1.5143247506	2.2869293941	0.645173263
C	0	-1.6996965829	0.4492333136	-0.4238177194
H	0	-1.3729758985	-0.0955206022	-1.3084105009
C	0	-2.9761518354	0.0598518761	0.141973752
H	0	-3.3414521917	0.6723331706	0.9652471844
C	0	-3.7155364927	-0.9893361374	-0.2556243974
H	0	-3.4003603409	-1.627583632	-1.0751782625
H	0	-4.6564825613	-1.2321932484	0.2225812535

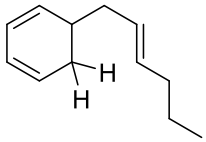

Figure 3.6: C12 monoene

Table 3.14: DFT coordinates for C12 monoene

C	0	0.9906780983	-1.7877534347	-0.0314219188
C	0	0.5654569596	-0.6764313901	0.8189846717
C	0	1.4196712727	0.5149679638	0.8129869674
C	0	2.6374074173	0.4908279133	0.0565837457
C	0	2.933827888	-0.5445220629	-0.7821217065
C	0	2.0811920434	-1.6957626999	-0.8375011051
H	0	0.395468875	-2.6956403715	-0.0221398173
H	0	-0.5724304794	-0.2842008071	0.3785097455
H	0	3.316711895	1.3330131582	0.1431178436
H	0	3.8420222535	-0.5254120912	-1.37418706
H	0	2.3495966788	-2.5231730763	-1.4857511057
H	0	0.1905918845	-0.9724852077	1.8024835232
H	0	1.3982873138	1.1487915352	1.6902816369
C	0	0.3175559229	2.0298266616	-0.359889375
H	0	0.8295554695	2.9299840962	-0.0396354884
H	0	0.657953729	1.6160637586	-1.3016880554
C	0	-0.9813192225	1.7775941478	0.0622616272

H	0	-1.3659879808	2.341244416	0.9117606583
C	0	-1.6430280142	0.5990206595	-0.2887160741
H	0	-1.3820063748	0.1586476446	-1.2530645494
C	0	-3.0236007925	0.2501997737	0.2198378752
H	0	-3.1681508898	0.6853764727	1.2161521168
H	0	-3.7741361363	0.7252518985	-0.4287125938
C	0	-3.3149563295	-1.2570984329	0.2699575801
H	0	-2.6041893286	-1.7421598665	0.9484715657
H	0	-3.1349681047	-1.6905048927	-0.7211110875
C	0	-4.7451178268	-1.5746336419	0.7143979091
H	0	-5.4785602297	-1.1345491869	0.0313728538
H	0	-4.9238921061	-2.6529479532	0.7434988873
H	0	-4.9460224657	-1.1776561139	1.7145821897

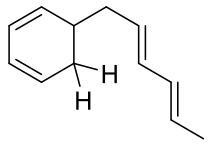

Figure 3.7: C12 diene

Table 3.15: DFT coordinates for C12 diene

C	0	1.4252576077	-1.7118751498	0.1722753018
C	0	0.8398675354	-0.5917793075	0.9231365856
C	0	1.5282995114	0.6964435003	0.7839876651
C	0	2.6601615424	0.8082429386	-0.0545372546
C	0	3.0976238537	-0.2552894747	-0.8079514317
C	0	2.4615862016	-1.5296247245	-0.6894082269
H	0	0.9850663966	-2.6956808915	0.2988897105
H	0	-0.2922286327	-0.4355727743	0.5096187975
H	0	3.1861986998	1.7563251024	-0.1001517416
H	0	3.9571409218	-0.1457143487	-1.4592756143
H	0	2.8472534668	-2.3684883848	-1.259175976
H	0	0.5654568521	-0.844799412	1.9537550356
H	0	1.3623399082	1.4551866502	1.5360476146
C	0	-0.0418715197	1.9893002585	-0.5979744434
H	0	0.2944520357	2.9935935289	-0.3715495392
H	0	0.4017741983	1.5194272776	-1.466665648
C	0	-1.197349422	1.4884830634	-0.0453158186
H	0	-1.6747200877	2.0532133902	0.7545421946

C	0	-1.6464293859	0.1757413023	-0.2619303415
H	0	-1.2969221342	-0.3366348622	-1.1572623991
C	0	-2.819601947	-0.3802035065	0.3843684583
H	0	-3.2239557551	0.1881363639	1.2222682788
C	0	-3.4233114549	-1.5317641391	0.0401749188
H	0	-3.0230813983	-2.0968447083	-0.8007225124
C	0	-4.626198306	-2.1106486011	0.7197955761
H	0	-4.9630656547	-1.4799931253	1.5463448828
H	0	-5.4620115112	-2.2261442252	0.0195305022
H	0	-4.416702672	-3.1100162805	1.1199144552

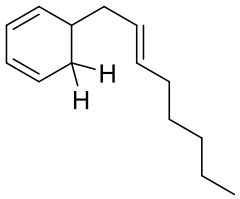

Figure 3.8: C14 monoene

Table 3.16: DFT coordinates for C14 monoene

C	0	1.1339039053	-1.7981887001	-0.3141195977
C	0	0.8516102087	-0.7518587748	0.6681445626
C	0	1.8868047757	0.2696907201	0.8517881305
C	0	3.1197245488	0.1436161572	0.1305607906
C	0	3.2861654011	-0.8076197328	-0.8342116742
C	0	2.2634232499	-1.7843157829	-1.0698315087
H	0	0.4000318355	-2.5872626714	-0.4459540154
H	0	-0.1823586149	-0.120239519	0.2516529216
H	0	3.9210743059	0.8421303532	0.3500116169
H	0	4.2133409004	-0.8618254952	-1.3938244542
H	0	2.4267948544	-2.552583393	-1.8181185824
H	0	0.3827344105	-1.1067217006	1.5898978636
H	0	1.9274208034	0.7723458204	1.8096472278
C	0	1.1024236806	2.0962277831	-0.1141925182
H	0	1.7315701497	2.8457255225	0.3522374415
H	0	1.4235699927	1.7732100988	-1.0972823919
C	0	-0.2409550296	2.0033945594	0.226577762
H	0	-0.5759331747	2.496769759	1.1386275644
C	0	-1.0610834025	1.0105902028	-0.3131938931
H	0	-0.8215040605	0.6717989106	-1.3230689782
C	0	-2.505204514	0.8258846669	0.0957296712
H	0	-2.631348749	1.1278420378	1.1423512997
H	0	-3.1324640282	1.5103125487	-0.4936641916
C	0	-3.0360166471	-0.6024738356	-0.0968136815
H	0	-2.4546192849	-1.2947916345	0.5241765322
H	0	-2.8682286747	-0.9114197513	-1.136498756
C	0	-4.5240420545	-0.7464493131	0.2387974107

H	0	-5.1039341056	-0.0525954056	-0.3837677395
H	0	-4.6938287514	-0.4347512544	1.2778305041
C	0	-5.0641765941	-2.1679138282	0.0446085856
H	0	-4.8927351658	-2.4796205877	-0.993044125
H	0	-4.4877210214	-2.8616277065	0.6688209056
C	0	-6.5532890324	-2.3012611069	0.3762808675
H	0	-7.159392332	-1.6432806515	-0.254559426
H	0	-6.9064015462	-3.3248567639	0.2231433386
H	0	-6.7525874393	-2.0340293914	1.4188906468

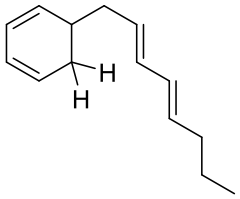

Figure 3.9: C14 diene

Table 3.17: DFT coordinates for C14 diene

C	0	1.0227464197	-1.8936430038	0.1791887536
C	0	0.5634235251	-0.7012524186	0.9064237921
C	0	1.4418456755	0.4717305578	0.8283451927
C	0	2.6260886092	0.4190646318	0.0590270696
C	0	2.9469786792	-0.6952965544	-0.6790756524
C	0	2.1254887368	-1.8633371705	-0.6154722281
H	0	0.433891675	-2.8009448085	0.2654785528
H	0	-0.5005590211	-0.380426516	0.4239208992
H	0	3.2878361849	1.2789761462	0.0566539154
H	0	3.8515389004	-0.7112124999	-1.2762072607
H	0	2.4186888214	-2.7473653692	-1.1716150098
H	0	0.1908486597	-0.9143037052	1.9148876452
H	0	1.3456034857	1.2403950687	1.5822404304
C	0	0.1725796067	2.0100285833	-0.6107342247
H	0	0.6371990038	2.9487340538	-0.3350063851
H	0	0.595614954	1.4989921852	-1.4663600535
C	0	-1.0757139221	1.6739698949	-0.1412045095
H	0	-1.5143247506	2.2869293941	0.645173263

C	0	-1.6996965829	0.4492333136	-0.4238177194
H	0	-1.3729758985	-0.0955206022	-1.3084105009
C	0	-2.9761518354	0.0598518761	0.141973752
H	0	-3.3414521917	0.6723331706	0.9652471844
C	0	-3.7155364927	-0.9893361374	-0.2556243974
H	0	-3.4003603409	-1.627583632	-1.0751782625
H	0	-4.6564825613	-1.2321932484	0.2225812535

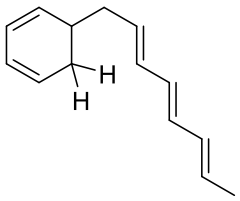

Figure 3.10: C14 triene

Table 3.18: DFT coordinates for C14 triene

C	0	1.7613959857	-1.9639638184	0.2567517458
C	0	1.6471298578	-0.6576425338	0.9274844211
C	0	2.8460893195	0.1893031754	0.8682708815
C	0	3.9810329478	-0.2323376359	0.1535116939
C	0	3.9868323555	-1.4248557891	-0.5391025441
C	0	2.8564644531	-2.2945085373	-0.4797575835
H	0	0.9255827741	-2.6514080602	0.3350872653
H	0	0.7600530293	-0.0590091457	0.3943662842
H	0	4.8664028647	0.3950182742	0.1557242481
H	0	4.867108932	-1.7287475862	-1.0936316563
H	0	2.8956318421	-3.2485441997	-0.9948317454
H	0	1.1970587005	-0.7168927551	1.9262798618
H	0	2.9377150676	1.0095247641	1.5661805652
C	0	2.092347216	2.0251010756	-0.7354014418
H	0	2.7994790361	2.8020026221	-0.4724405849
H	0	2.387486968	1.3526361938	-1.5308903911
C	0	0.7955831557	2.068645793	-0.2935405418
H	0	0.5260837524	2.8230742879	0.4444586352
C	0	-0.1569003132	1.0668227887	-0.562261688
H	0	0.0351912441	0.3975536303	-1.3993183764

C	0	-1.4925274253	1.081367819	-0.0354322093
H	0	-1.7018053704	1.815088566	0.7427719561
C	0	-3.8247141174	0.2630192166	0.1436789135
H	0	-4.0141975412	0.9973649146	0.9264237884
C	0	-4.8278428577	-0.5518139558	-0.2319798131
H	0	-4.6359900158	-1.2843225952	-1.0149016926
C	0	-6.2100086106	-0.5382689971	0.3434509012
H	0	-6.3141362221	0.2215651992	1.1219840481
H	0	-6.9610668113	-0.3367516109	-0.4297826089
H	0	-6.4689214001	-1.5099748926	0.7808147611
C	0	-2.4946738518	0.2468394227	-0.4155277844
H	0	-2.298115815	-0.4846176103	-1.1980801787

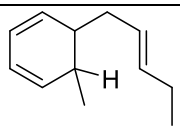

Figure 3.11: C12 monoene methyl

Table 3.19: DFT coordinates for C12 monoene methyl

C	0	0.8070388958	-1.71043863	-0.1113520972
C	0	0.5747864287	-0.5932472338	0.8075872368
C	0	1.6852838225	0.3634171195	0.92718102
C	0	2.922409796	0.0975386164	0.2519546241
C	0	3.0398427126	-0.9264249765	-0.6419781189
C	0	1.9487566241	-1.8340658704	-0.838568303
H	0	0.0149542366	-2.446812502	-0.2160971579
H	0	-0.3703679968	0.0832218664	0.2536642159
H	0	3.768755897	0.7480114038	0.4498011553
H	0	3.9718181591	-1.0881459298	-1.1720178467
H	0	2.0621195551	-2.6580261503	-1.5351822694
H	0	1.7508364499	0.9161493139	1.8575024514
C	0	1.0710548589	2.177589412	-0.1381422192
H	0	1.732038301	2.9052159326	0.3189268099
H	0	1.4054701355	1.7897356714	-1.0928702852
C	0	-0.2902348683	2.1983898164	0.1411313711
H	0	-0.634614416	2.7612982143	1.0079747342
C	0	-1.1449640599	1.2306010131	-0.3929218963
H	0	-0.8769863497	0.8327503188	-1.3743364313
C	0	-0.1452410326	-0.9370060521	2.11928633
H	0	-0.4991033115	-0.0289197137	2.617138636
H	0	-1.0101367092	-1.5807183282	1.9358051506

H	0	0.5235044074	-1.4611166775	2.8083672551
C	0	-2.6224674571	1.1741279178	-0.0711070643
H	0	-3.1458034387	1.9082448052	-0.6992211267
H	0	-2.7849688948	1.4934260199	0.9642907226
C	0	-3.2602746803	-0.2014310219	-0.2988116448
H	0	-4.3355314654	-0.1722077152	-0.1032709258
H	0	-3.1203132984	-0.5347047272	-1.3317461744
H	0	-2.8218745012	-0.9586027526	0.356808698

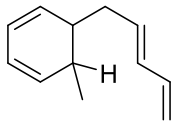

Figure 3.12: C12 diene methyl

Table 3.20: DFT coordinates for C12 diene methyl

C	0	0.9295576547	-1.8571525426	0.034182856
C	0	0.6619335835	-0.6793502581	0.8787778162
C	0	1.7650980744	0.2935975339	0.9384799303
C	0	2.9620760829	0.0751630711	0.2197676087
C	0	3.1036177007	-1.0061892649	-0.6160074042
C	0	2.0617887661	-1.9793491834	-0.7085329713
H	0	0.1643082771	-2.6266883901	-0.0066732772
H	0	-0.2452411652	-0.1057514444	0.3189658411
H	0	3.7793825054	0.7793066808	0.3380222877
H	0	4.0221541448	-1.1502700484	-1.1732573335
H	0	2.2009853789	-2.8457550028	-1.3464887336
H	0	1.7831025237	0.9871695238	1.7692012291
C	0	0.9257993868	2.1975395914	-0.3488973817
H	0	1.5378238417	2.989123987	0.0656297822
H	0	1.3070439346	1.7122848782	-1.2382438171
C	0	-0.3980516399	2.0671069176	0.0028893133
H	0	-0.7774916561	2.6642903144	0.8308416769
C	0	-1.2128214763	1.0257302996	-0.4672808491
H	0	-0.9208318091	0.5324129413	-1.3934132597
C	0	-2.5863203086	0.8379274226	-0.0415256775
H	0	-2.8988782483	1.4101739284	0.8309118551

C	0	-0.0176069282	-0.9784796255	2.2294165231
H	0	-0.3417815353	-0.0503557195	2.7083099964
H	0	-0.898828682	-1.6091432196	2.0881348161
H	0	0.6685687033	-1.4924913696	2.9075972315
C	0	-3.4767073716	0.0194397116	-0.6265268401
H	0	-4.4867913275	-0.0804164473	-0.2484810596
H	0	-3.2188020005	-0.5678440457	-1.5022734493

3.4 Summary

Benzene formation during dehydroaromatization reactions increases as the length of the starting *n*-alkane increases. This has been attributed to a retro-ene reaction which yields benzene and a corresponding C_{n-6} fragment. Kinetic studies and DFT calculations provide support for this claim and show that increasing degrees of unsaturation on the alkyl chain of the cyclic intermediate favors the retro-ene mechanism. Attempts to limit benzene formation by isomerization has been met by limited success, while changing the hydrogen acceptor from TBE to 1-pentene yields a significant decrease in benzene formation. Neither using 1-dodecene as a starting material instead of *n*-dodecane nor using ($^{i\text{Pr}}$PCP)Ir instead of ($^{i\text{Pr}}$PCOP)Ir led to an increase in benzene formation.

3.5 Acknowledgements

We thank Dr. Charles Casey for discussions leading to the retro-ene mechanism.

3.6 References

[1] Golberg, K. I.; Goldman, A. S. *Activation and Functionalization of C-H Bonds*; Oxford University Press, 2004.
[2] Renkema, K. B.; Kissin, Y. V.; Goldman, A. S. *J. Am. Chem. Soc.* **2003**, *125*, 7770.
[3] Kanzelberger, M.; Singh, B.; Czerw, M.; Krogh-Jespersen, K.; Goldman, A. S. *J. Am. Chem. Soc.* **2000**, *122*, 11017.
[4] Ahuja, R.; Punji, B.; Findlater, M.; Supplee, C.; Schinski, W.; Brookhart, M.; Goldman, A. S. *Nature Chem* **2011**, *3*, 167.
[5] Thawani, A.; Rajeev, R.; Sunoj, R., B. *Chem.-Eur. J.* **2013**, *19*, 4069.
[6] Krantz, A.; Lin, C. Y. *Journal of the Chemical Society D: Chemical Communications* **1971**, 2.
[7] Liu, F.; Pak, E. B.; Singh, B.; Jensen, C. M.; Goldman, A. S. *J. Am. Chem. Soc.* **1999**, *121*, 4086.
[8] Woodward, R. B.; Hoffmann, R. *J. Am. Chem. Soc.* **1965**, *87*, 395.
[9] Hu, J.; Wang, X.; Guo, L.; Hu, Y.; Liu, X.; Liang, Y. *Catal. Commun.* **2010**, *11*, 346.
[10] Göttker-Schnetmann, I.; White, P. S.; Brookhart, M. *Organometallics* **2004**, *23*, 1766.
[11] Huang, Z.; Brookhart, M.; Goldman, A. S.; Kundu, S.; Ray, A.; Scott, S. L.; Vincente, B. C. *Adv. Synth. Catal.* **2009**, *351*, 188.
[12] Lee, C.; Yang, W.; Parr, R. G. *Phys. Rev. B* **1988**, *37*, 785.
[13] Eyring, H. *J. Chem. Phys.* **1935**, *3*, 9.

Chapter 4

Dehydroaromatization of *n*-Alkanes to Yield Polyethylene Naphthalate Precursors

Abstract

Polyethylene naphthalate is a highly desirable polymer that could replace polyethylene terephthalate, which is used commercially in containers for foods and liquids, fibers for clothing, and packing materials, among many other uses. Dehydroaromatization reactions starting from *n*-dodecane can yield 1,5-dimethylnaphthalene, which can be isomerized with zeolites to a precursor to polyethylene naphthalate, 2,6-dimethylnapthalene. Similarly, dehydroaromatization reactions from *n*-dodecane yield *o*-pentyltoluene, which can be cyclized using zeolites to give 1,5-dimethylnaphthalene. Dehydroaromatization reactions were performed starting from *n*-dodecane and *n*-tridecane in attempts to maximize potential precursors to polyethylene naphthalate. The mechanism for formation of 1,5-dimethylnaphthalene via dehydroaromatization is discussed.

4.1 Introduction

The original goal for dehydroaromatization was to synthesize alkylbenzenes from *n*-alkane starting materials.[1] Expansion of the dehydroaromatization process has been underway since this goal has been achieved. Synthesizing biaromatic compounds through multiple dehydroaromatization reactions on the same starting material would be both interesting and commercially viable. Specifically, two dehydroaromatization reactions starting from *n*-dodecane could yield 1,5-dimethylnaphthalene (Scheme 4.1).

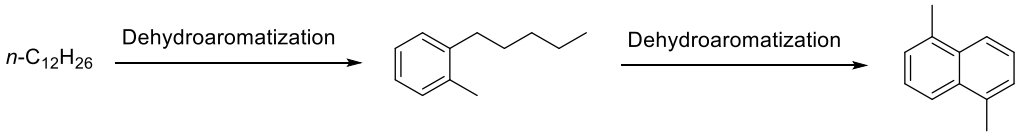

Scheme 4.1: Dehydroaromatization of *n*-dodecane to yield 1,5-dimethylnaphthalene

1,5-Dimethylnaphthalene is useful because it can be easily converted into monomers of polyethylene naphthalate (PEN), which is a highly desirable polymer (Scheme 4.2).[2-8]

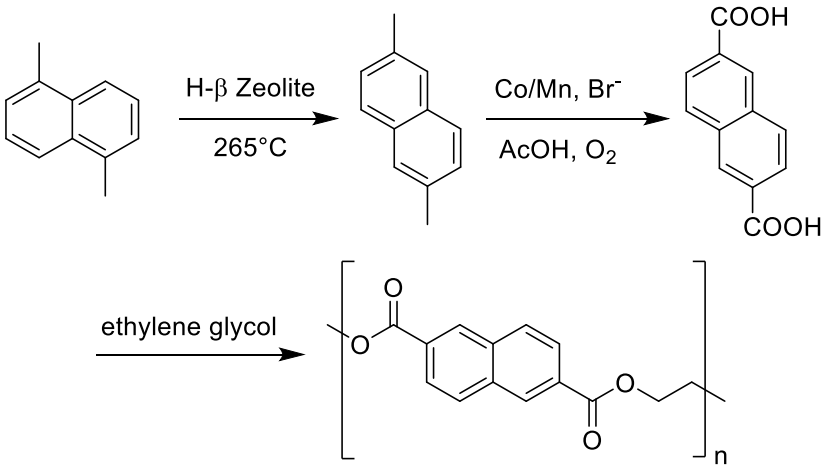

Scheme 4.2: Synthesis of polyethylene naphthalate from 1,5-dimethylnaphthalene

The methyl shift reaction to convert 1,5-dimethylnaphthalene to 2,6-dimethylnaphthalene is known to be effective using zeolites, conversion of 2,6-dimethylnaphthalene to naphthalene-2,6-dicarboxylic acid goes through the industrialized AMOCO process, and polymerization to PEN takes place using condensation polymerization with ethylene glycol. PEN is an extremely useful polymer that has been used sparingly in commercial applications. It can most closely be associated to the ubiquitous polymer polyethylene terephthalate (PET) (Figure 4.1).

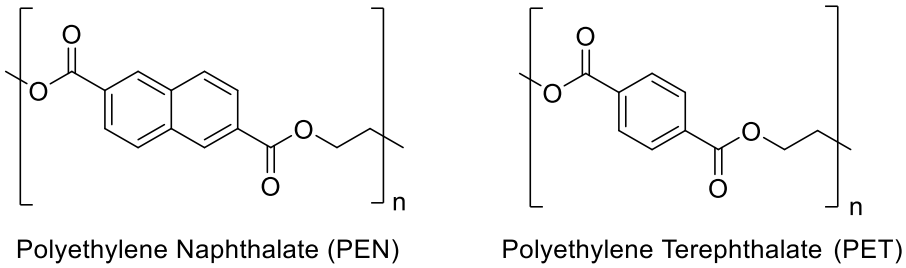

Figure 4.1: Structures of PEN and PET

PEN has better properties than PET in most important categories. For instance, PEN has better thermal stability, a less permeable gas barrier, higher mechanical strength, and a better UV light barrier.[7] PET is used commercially for water bottles, peanut butter jars, fibers for clothing, and video packing films among many others and replacing PET would be a massive undertaking because PET is produced on a scale of forty million tonnes per year with a growth factor of seven percent.[9, 10] Unfortunately, the cost of producing PEN in large quantities is prohibitively high due to the cost of producing 2,6-dimethylnaphthalene.

The two major methods for synthesizing 2,6-dimethylnaphthalene are through isolation of side products from naphthalene manufacturing and through condensation of *o*-xylene and butadiene. Access to 2,6-dimethylnaphthalene via isolation of monomethylnaphthalenes from feedstock used for naphthalene manufacture has proved to be too inefficient due to availability of the feedstock.[11, 12] Condensation of *o*-xylene and butadiene is also a commercially undesirable process due to the chemicals required for condensation. (Scheme 4.3).[13 - 18, 19, 20]

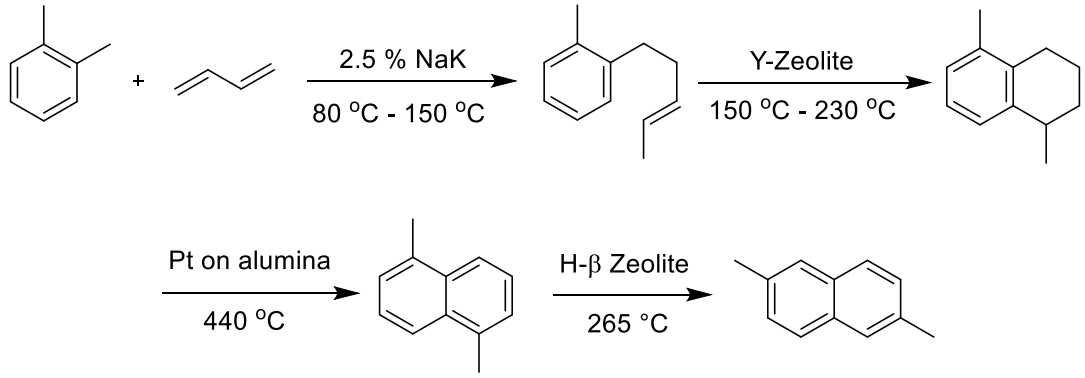

Scheme 4.3: Condensation of *o*-xylene and butadiene to yield 2,6-dimethylnaphthalene

This process is extremely harsh, requiring the dangerous use of sodium and potassium metal at elevated temperatures for the condensation reaction. However, the methyl shift reaction to convert 1,5-dimethylnaphthalene to 2,6-dimethylnaphthalene has been shown to be effective. [7]

A provisional patent from the Goldman Group has shown that dehydrogenation and aromatization using a pincer iridium catalyst and zeolites as a co-catalyst can give 1,5-dimethylnaphthalene from *o*-pentyltoluene (Scheme 4.4).[21]

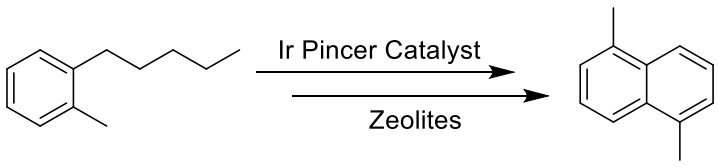

Scheme 4.4: Synthesis of 1,5-dimethylnaphthalene from *o*-pentyltoluene

Access to *o*-pentyltoluene was not trivial, but the advent of homogeneous dehydroaromatization with a pincer catalyst shows that *o*-pentyltoluene is the major C_{12} product from dehydroaromatization of *n*-dodecane. Therefore, both accessing 1,5-dimethylnaphthalene via dehydroaromatization or increasing yields of *o*-pentyltoluene for use in aromatization with pincer catalysts and zeolites are of great interest.

4.2 Results and Discussion

Over the course of studying the dehydroaromatization reaction, better GC methods were developed to identify more intermediates and products from these reactions. Through these new methods it was discovered that 1,5-dimethylnaphthalene was a product starting from *n*-dodecane in addition to the previously discussed alkylbenzenes. Dehydroaromatization reactions with *n*-dodecane as the starting material yield a small amount of 1,5-dimethylnaphthalene (Scheme 4.5 and Table 4.1).

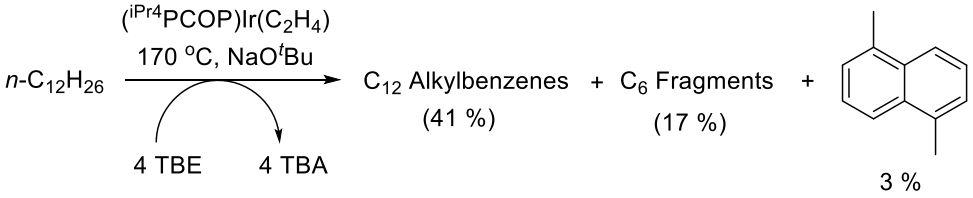

Scheme 4.5: Dehydroaromatization of *n*-dodecane yields 1,5-dimethylnaphthalene

Table 4.1: Yields from a representative dehydroaromatization reaction with *n*-dodecane

Identity	Concentration (mM)
TBE	20
TBA	5440
Hexane	199
Benzene	235
Dodecane	100
C_{12} olefins	40
C_{12} alkylbenzenes	680
1,5-dimethylnaphthalene	40
Dimers	115

Conditions: [(^{iPr}PCOP)Ir(C_2H_4)] = 10 mM; [*n*-dodecane] = 1.3 M; [TBE] = 5.35 M; 170°C, 30 mM NaO^{t}Bu

A three percent overall yield for 1,5-dimethylnaphthalene is very low but it was promising that any 1,5-dimethylnaphthalene is observed via dehydroaromatization starting from *n*-dodecane. It is important to note that for this reaction, four equivalents of TBE are used and because a total of seven equivalents of TBE are required to go from *n*-dodecane to 1,5-dimethylnaphthalene, it is unsurprising that total yield of 1,5-dimethylnaphthalene is low.

4.2.1 Mechanistic Study for Formation of 1,5-Dimethylnaphthalene

Before trying to maximize 1,5-dimethylnaphthalene formation from dehydroaromatization of *n*-dodecane, effort was made to understand the mechanism

through which this product was being formed. The initial hypothesis was that dehydroaromatization took place to give *o*-pentyltoluene as an intermediate and then a second dehydroaromatization took place to give 1,5-dimethylnaphthalene (Scheme 4.6).

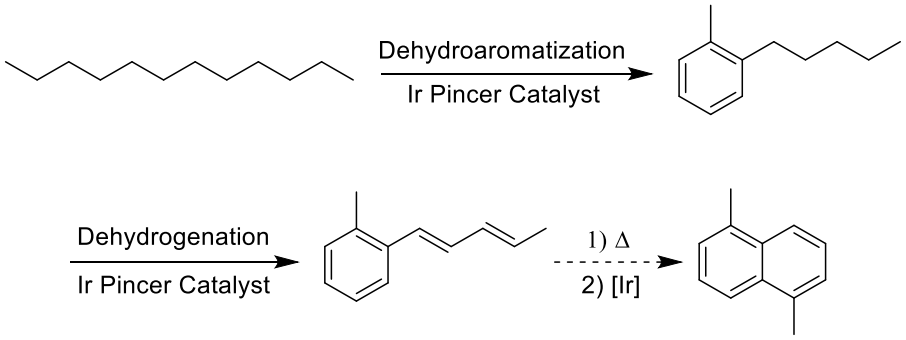

Scheme 4.6: Initial hypothesis for the mechanism of formation of 1,5-dimethylnaphthalene

o-Pentyltoluene was synthesized to test this hypothesis. Surprisingly, a reaction with *o*-pentyltoluene as the starting material under dehydroaromatization reaction conditions gave no biaromatic or bicyclic compounds of any kind. The only products observed were dehydrogenated *o*-pentyltoluene compounds (Scheme 4.7).

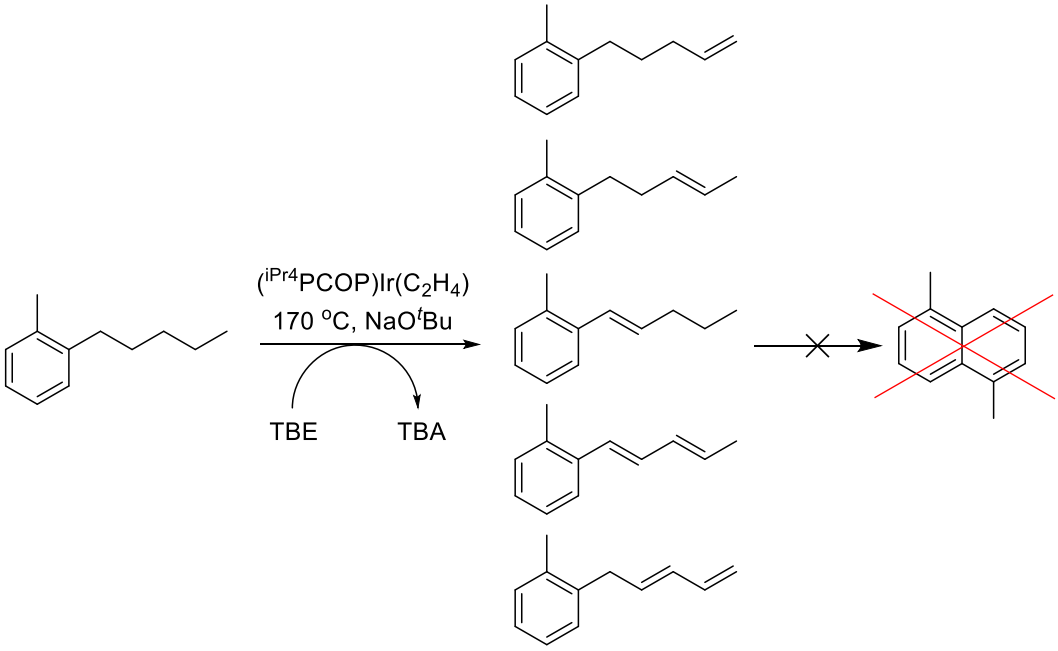

Scheme 4.7: Reaction with *o*-pentyltoluene under dehydroaromatization reaction conditions

This data rules out the initial hypothesis that 1,5-dimethylnaphthalene is formed via dehydroaromatization of *o*-pentyltoluene.

A second hypothesis for the formation of 1,5-dimethylnaphthalene is that a cyclic diene precursor can undergo a second cyclization before aromatization takes place to give a partially dehydrogenated fused ring intermediate which can then be dehydrogenated to give 1,5-dimethylnaphthalene (Scheme 4.8).

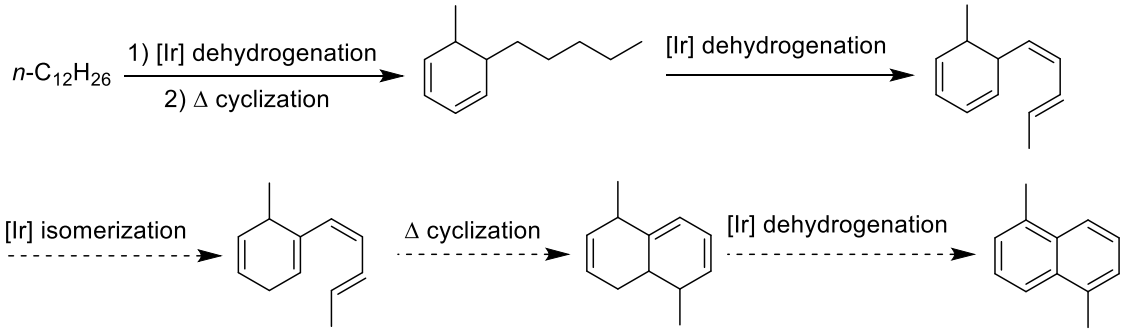

Scheme 4.8: Second hypothesis for the mechanism of formation of 1,5-dimethylnaphthalene

This hypothesis is based on an iridium-mediated isomerization of the double bonds inside the initial ring which allows for a second electrocyclization and dehydrogenation to give 1,5-dimethylnaphthalene. This idea is similar in nature to the retro-ene mechanism presented in Chapter 3, where dehydrogenation takes place on the alkyl chain instead of inside the ring to complete aromatization. Based on the mechanism for dehydroaromatization, a second electrocyclization seems entirely plausible (Scheme 4.9).[1,22]

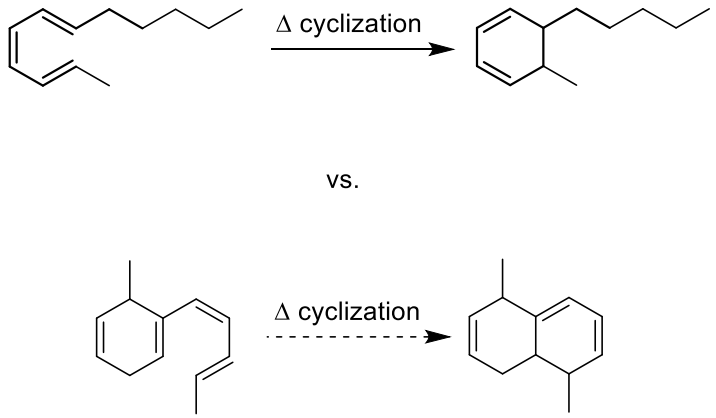

Scheme 4.9: Electrocyclization based on the mechanism for dehydroaromatization

The final step of the proposed mechanism can be tested by using 1,5-dimethyltetralin as a starting material to see if that can be dehydrogenated to give 1,5-dimethylnaphthalene. A reaction with 1,5-dimethyltetralin as the starting material under dehydroaromatization reaction conditions gives full conversion of the 1,5-dimethyltetralin to 1,5-dimethylnaphthalene (Scheme 4.10).

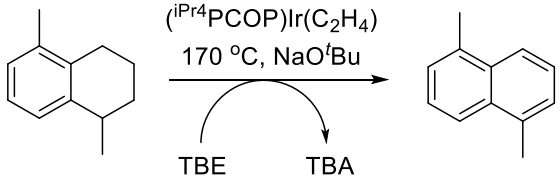

Scheme 4.10: Reaction with 1,5-dimethyltetralin under dehydroaromatization reaction conditions

Unfortunately, the iridium-mediated isomerization is difficult to test independently. No comparable cyclic dienes are commercially available and it would extremely difficult to synthesize a cyclic diene to test if this iridium-mediated isomerization is possible. However, it is well established that these iridium pincer catalysts are good isomerization catalysts and the most favorable position for the double bond to be on the molecule is in the tertiary position.[23, 24] Therefore, the iridium-mediated isomerization for this mechanism is plausible. The previous information allows for this mechanism to be accepted as the mechanism for formation of 1,5-dimethylnaphthalene.

4.2.2 Attempts to Increase 1,5-Dimethylnaphthalene

As previously discussed, seven equivalents of TBE are required to convert *n*-dodecane into 1,5-dimethylnaphthalene. Unfortunately, increasing the number of equivalents of TBE from four to seven had a negative impact on the reaction. Overall yield of all products decreased significantly along with the rate of the reaction. This is an established effect on pincer catalysis when using TBE as the acceptor, but a similar trend is observed while using 1-pentene as the acceptor.[25] The decrease in reactivity and yield is likely due to a reduced concentration of the active $14e^-$ species in solution because more olefin is in solution to bind to the $14e^-$ species.

One way to circumvent the problem of having a decreased concentration of $14e^-$ species is to increase the olefin to alkane ratio while maintaining a constant concentration of olefin. This can be achieved by diluting the reaction in a solvent. However, diluting the

reaction in unreactive *p*-xylene to allow for an increase in equivalents of acceptor without increasing total volume of acceptor was shown to be ineffective. Therefore, increasing the amount of acceptor relative to the starting alkane is not an option.

Although there is a mechanism to explain the formation of 1,5-dimethylnapthalene, it is difficult to take advantage of that information to maximize formation of 1,5-dimethylnapthalene due to the complex mixture of dehydrogenated intermediates. Using a co-catalyst to promote the isomerization step of the mechanism should allow for an increase in yield of 1,5-dimethylnaphthalene because this can decrease formation of alkylaromatics which cannot go on to form 1,5-dimethylnaphthalene under dehydroaromatization conditions (Scheme 4.11).

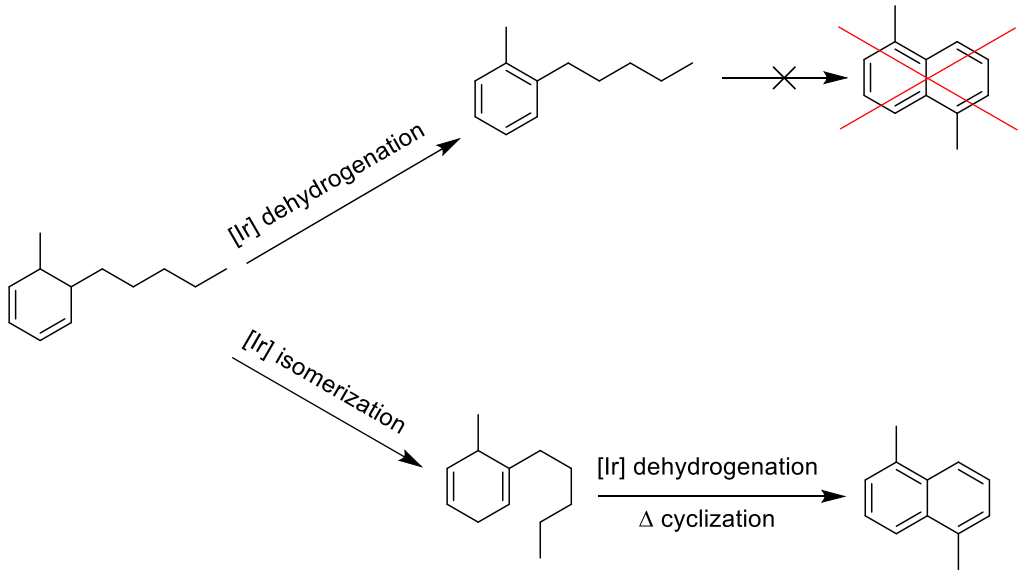

Scheme 4.11: Isomerization can favor formation of 1,5-dimethylnaphthalene

Conventional isomerization catalysts do not work for these reactions: most homogeneous isomerization catalysts do not survive at 170 °C and most heterogeneous catalysts cause skeletal isomerization of the hydrogen acceptor. Pincer catalysts are known isomerization catalysts and therefore a large number of pincer catalysts were screened as co-catalysts (Figure 4.2).

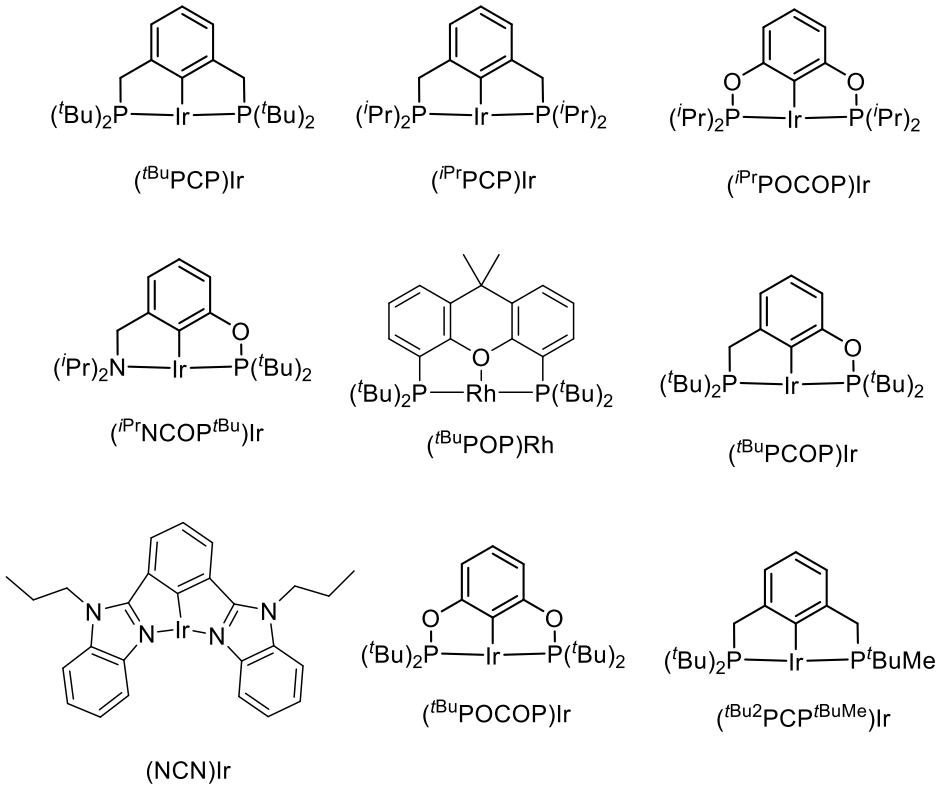

Figure 4.2: Catalysts screened to increase 1,5-dimethylnaphthalene concentration

These reactions were carried out under dehydroaromatization reaction conditions while maintaining a total catalyst concentration of 10 mM in solution. In all cases, ratios of one to one and two to one of the ($^{i\text{Pr}}$PCOP)Ir catalyst to the isomerization co-catalyst were tested. No meaningful change in 1,5-dimethylnaphthalene concentration was observed for any of the co-catalysts screened and yields of other products were not increased in any significant way.

4.2.3 Attempts to Increase o-*Pentyltoluene*

As previously detailed, the Goldman Group has established that pincer catalysts and zeolites can convert *o*-pentyltoluene to 1,5-dimethylnaphthalene (Scheme 4.12).[21]

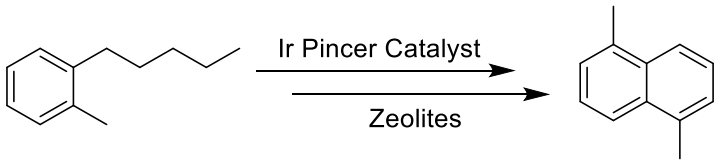

Scheme 4.12: Conversion of o-pentyltoluene to 1,5-dimethylnaphthalene

Attempts to maximize *o*-pentyltoluene formation would therefore be of interest because *o*-pentyltoluene is a potential precursor to polyethylene naphthalene monomers. Based on the original report from the Goldman Group, β-zeolite and HSZ-25 zeolite were used as co-catalysts for dehydroaromatization reactions to convert any *o*-pentyltoluene

formed to 1,5-dimethylnaphthalene. Under dehydroaromatization conditions, both zeolites caused deactivation of the catalyst and overall yield was significantly decreased regardless of concentration of zeolite. Also, all of the co-catalysts used in Figure 4.2 caused no appreciable difference in *o*-pentyltoluene concentration due to lack of control over product distribution of C_n aromatics.

The only instances where *o*-pentyltoluene concentration was changed was related to either decreasing dimer formation or decreasing benzene formation, which is further detailed in Chapters 2 and 3. Adding NaO^tBu, increasing the temperature, and changing the acceptor from TBE to 1-pentene all give increased yields of *o*-pentyltoluene (Table 4.2).

Table 4.2: Attempts to change the yield of *o*-pentyltoluene

Reaction	Benzene + Hexane	Dodecane	*o*-Pentyl Toluene	1,5-Dimethyl Naphthalene	Other C_{12} Aromatics	Dimers
170 °C TBE	16 %	15 %	16 %	2 %	12 %	22 %
170 °C with 30 mM NaO^{t}Bu TBE	17 %	9 %	26 %	3 %	17 %	18 %
200 °C with 30 mM NaO^{t}Bu TBE	13 %	5 %	36 %	3 %	30 %	11 %
170 °C with 30 mM NaO^{t}Bu 1-Pentene	9 %	29 %	29 %	1 %	27 %	2 %

Conditions: [(^{iPr}PCOP)Ir(C_2H_4)] = 10 mM; [*n*-dodecane] = 1.3 M. Dimers are formed via Diels-Alder reactions and iridium-mediated dimerizations and are not well resolved on GC. Concentration of dimers are calculated based on missing dodecane.

There are significant changes in *o*-pentyltoluene concentration for these reactions. Without NaO^{t}Bu at 170 °C the total *o*-pentyltoluene yield is at 16 %, but this can be increased up to 36 % by increasing the temperature and adding base. Adding 1-pentene as an acceptor instead of TBE causes a huge drop in dimer and benzene formation but there is a large amount of unreacted *n*-dodecane due to dimerization of the acceptor. By increasing the yield of *o*-pentyltoluene, the tandem pincer/zeolite catalyst reaction to synthesize 1,5-dimethylnaphthalene becomes more viable and overall there is an increase from 18 % to 39 % of PEN precursors.

4.2.4 Attempts to Access 1,5-Dimethylnaphthalene from n-*Tridecane*

As previously detailed, dehydroaromatization of *n*-dodecane can give 1,5-dimethylnaphthalene as a biaromatic product. However, only one of the C_{12} alkylaromatics can be further used towards formation of 1,5-dimethylnaphthalene (Scheme 4.13).

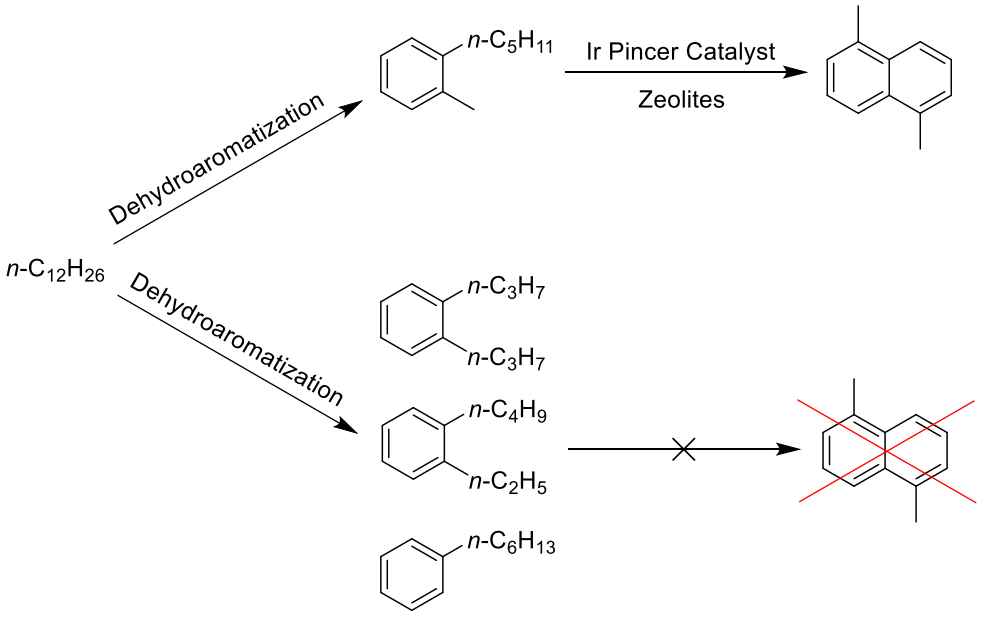

Scheme 4.13: One C_{12} alkylaromatic can form 1,5-dimethylnaphthalene

n-Tridecane was thought to be a good alternative because two of the C_{13} alkylaromatic products are potential PEN precursors as opposed to just one alkylaromatic from *n*-dodecane (Scheme 4.14).[26]

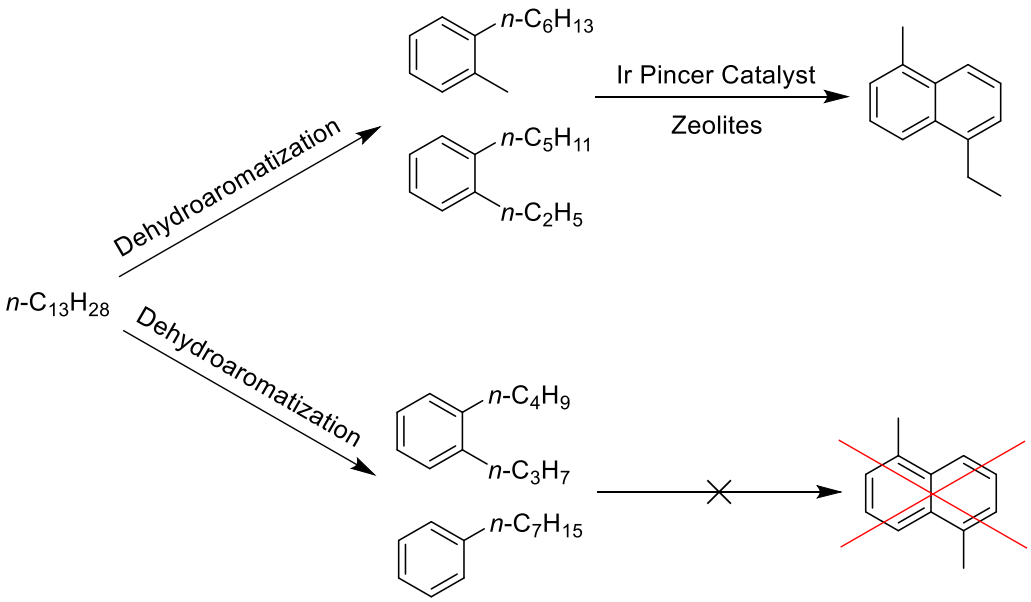

Scheme 4.14: PEN precursors from *n*-tridecane

The 1-ethyl-5-methylnaphthalene can undergo scission of the ethyl group to give 1,5-dimethylnaphthalene via a known process (Scheme 4.15).[27]

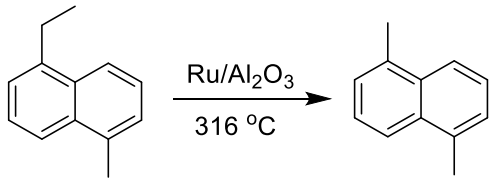

Scheme 4.15: Scission of 1-ethyl-5-methylnaphthalene to give 1,5-dimethylnaphthalene

Interestingly, dehydroaromatization of tridecane does not give a fused biaromatic but instead give 2-methylbiphenyl as the only biaromatic product (Scheme 4.16 and Table 4.3).

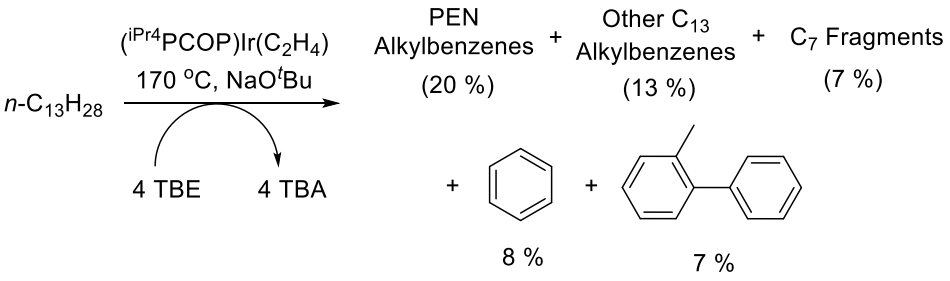

Scheme 4.16: Dehydroaromatization of *n*-tridecane yields 2-methylbiphenyl

Table 4.3: Yields from a representative dehydroaromatization with *n*-tridecane

Identity	Concentration (mM)
TBE	12
TBA	5255
Benzene	207
Heptane	107
Toluene	62
Tridecane	254
C_{13} olefins	49
Other C_{13} alkylbenzenes	176
PEN alkylbenzenes	259
2-methylbiphenyl	89
Dimers	135

Conditions: [(^{iPr}PCOP)Ir(C_2H_4)] = 10 mM; [*n*-tridecane] = 1.3 M; [TBE] = 5.35 M; 170°C, 30 mM NaO^{t}Bu. Dimers are formed via Diels-Alder reactions and iridium-mediated dimerizations and are not well resolved on GC. Concentration of dimers are calculated based on missing tetradecane.

2-Methylbiphenyl is an undesirable product because it is not a PEN precursor and it is synthesized directly from *o*-hexyltoluene, which is a PEN precursor. Similar to the attempts to optimize 1,5-dimethylnaphthalene from *n*-dodecane, optimization of PEN precursors from *n*-tridecane was met with limited success despite multiple attempts with a variety of catalysts (see Figure 4.3).

4.3 Experimental

The representative procedure for dehydroaromatization reactions is as follows: In an argon-filled glove box, ($^{i\text{Pr}}$PCOP)Ir(η^2-C_2H_4) (5.6 mg, 0.01 mmol, 10 mM) was dissolved in *n*-alkane (e.g. dodecane: 0.3 mL, 1.32 mmol, 1.3 M); TBE (4.1 equivalents with respect to dodecane, 0.7 mL, 5.43 mmol, 5.35 M) and mesitylene (0.01 mL, internal standard) were then added to the solution. Aliquots of this solution (0.1 mL each) were transferred to several 5 mm glass tubes and the contents were cooled under liquid nitrogen and sealed under vacuum. The sealed tubes were heated simultaneously in a preheated oven. At regular intervals, a tube was brought to room temperature and the sample was analyzed by gas chromatography in comparison with authentic products. The major products were confirmed by GC-MS.

All alkanes, mesitylene, and TBE were distilled under vacuum from Na/K alloy after several freeze-pump-thaw cycles and stored in an argon glove box. Gas chromatography (GC) measurements were performed on a Varian 430 instrument fitted with a capillary column (30 m length x 0.25 mm inner diameter x 0.5 μm film thickness). Gas

chromatography – mass spectrometry (GC-MS) measurements were performed on a Varian 3900 Saturn 2100T instrument fitted with a capillary column (30 m length x 0.25 mm inner diameter x 0.25 µm film thickness).

4.4 Summary

Dehydroaromatization reactions can yield precursors to the highly desirable polymer, polyethylene naphthalate. Dehydroaromatization of *n*-dodecane can give 1,5-dimethylnaphthalene or *o*-pentyltoluene, which can be converted to 1,5-dimethylnaphthalene in a known process using a pincer catalyst and zeolites. Yields of 1,5-dimethylnaphthalene from dehydroaromatization are low despite multiple attempts to increase those yields. Yields of PEN precursors from *n*-dodecane can be increased from 18 % to 39 %, but are still low. Dehydroaromatization of *n*-tridecane can give two alkylaromatics which can be converted to 1,5-dimethylnaphthalene. Attempts to increase yields of those two alkylaromatics were met with limited success due to the presence of 2-methylbiphenyl, which is the only biaromatic product present from dehydroaromatization of *n*-tridecane.

4.5 References

[1] Ahuja, R.; Punji, B.; Findlater, M.; Supplee, C.; Schinski, W.; Brookhart, M.; Goldman, A. S. *Nature Chem* **2011**, *3*, 167.
[2] Saffer, A.; Barker, R. S. U. S. Patent 2833816, May 6th, 1958
[3] Saffer, A.; Barker, R. S. GB Patent 807091, January 7th, 1959
[4] Saffer, A.; Barker, R. S. U.S. Patent 3089906, May 14th, 1963
[5] Landau, R.; Saffer, A. *Chem. Eng. Prog.* **1968**, *64*, 20.
[6] Tomás, R. A. F.; Bordado, J. C. M.; Gomes, J. F. P. *Chem. Rev.* **2013**, *113*, 7421.
[7] Kumsapaya, C.; Bobuatong, K.; Khongpracha, P.; Tantirungrotechai, Y.; Limtrakul, J. *J. Phys. Chem. C*. **2009**, *113*, 16128-16137.
[8] Sebelist, F. J.; Weir, R. H. U. S. Patent 3057909, October 9th 1962.
[9] PETRA: PET Resin Association. An Introduction to PET. http://www.petresin.org/news_introtoPET.asp (accessed Sept. 29th, 2015).
[10] The Essential Chemical Industry Online. Polyesters. http://www.essentialchemicalindustry.org/polymers/polyesters.html (accessed Sept. 29th, 2015).
[11] Allen, J.; Malmberg, E. US 3235615, **1966** to Sun Oil
[12] Ogata, K.; Shimosato, K. US 3671578, **1972** to Teijin Ltd.
[13] Eberhardt, G. C.; Peterson, H. J. *J. Org. Chem.* **1965**, *30*, 82.
[14] Suld, G.; Stuart, A. P. *J. Org. Chem.* **1964**, *29*, 2939.
[15] Eberhardt, G. US 3244758, **1966** to Sun Oil.
[16] Harad, T.; Kurozumi, S.; Nagahama, S.; Nishikawa, T.; Shimada, K.; Takeuchi, Y. US 3798280, **1974** to Teijin Ltd.
[17] Ogasawara, M.; Oka, I.; Shima, T.; Urasaki, T. US 3851002, **1974** to Teijin Ltd.
[18] Yamamoto, K.; Yamashita, G. US 3870754, **1975** to Teijin Ltd.
[19] Sikkenga, D. L.; Lamb, J. D.; Zaenger, I. C.; Williams, G. S. U. S. 4950825 to Amoco Corporation
[20] Amelse, J. A. U. S. 5189234 to Amoco Corporation
[21] Goldman, A. S.; Dinh, L. V.; Schinski, W., Preparation of Alkyl Aromatic Compounds. U. S. Provisional Patent 70205.0254US01 T-8617, Nov. 8th 2011.
[22] Thawani, A.; Rajeev, R.; Sunoj, R., B. *Chem.-Eur. J.* **2013**, *19*, 4069.
[23] Liu, F.; Goldman, A. S. *Chem. Commun.* **1999**, *7*, 655.
[24] Anslyn, E. V.; Dougherty, D. A. *Modern Physical Organic Chemistry*; University Science Books: Sausalito, CA, 2006.
[25] Goldman Group, unpublished results.
[26] Chen, Q.; Froment, G. *J. Anal. Appl. Pyr.* **1991**, *21*, 51.
[27] Feinstein, A. I.; Bertolacini, R. J.; Kim, D. K. U. S. 4177219 to Standard Oil Company, Dec. 4th, 1979.

Chapter 5

Dehydroaromatization of Branched Starting Materials to Form Xylenes

Abstract

Dehydroaromatization reactions of *n*-alkanes can yield benzene, toluene, and *o*-xylene from *n*-hexane, *n*-heptane, and *n*-octane, respectively. *p*-Xylene or *m*-xylene are not observed at any point from dehydroaromatization of linear alkanes. Dehydroaromatization reactions of branched starting materials are presented to allow for formation of *p*-xylene and *m*-xylene. Specifically, 2-ethyl-1-hexene can yield mostly *p*-xylene and is a convenient starting material because it can be synthesized from ethylene using known procedures. Attempts to maximize *p*-xylene formation and minimize dimer formation are discussed.

5.1 Introduction

Benzene, toluene and xylene, the so-called BTX family, are three of the seven basic building blocks of the chemical industry and *p*-xylene is the most desirable of the three xylenes and of the entire BTX family.[1] Several million tons of *p*-xylene are produced each year with a six to eight percent increase every year.[2 - 4] *p*-Xylene is used primarily as a precursor to terephthalic acid, which is used to synthesize polyethylene terephthalate (PET). PET is a highly versatile polymer that is used in a wide variety of commercial products, including bottles, containers, fabrics, films, and packaging materials.[5]

Almost all industrially produced *p*-xylene comes from catalytic reforming of naphtha.[6] This process is an unselective process that produces all three xylene isomers, as well as benzene, toluene and other aromatics. Xylenes are separated from other aromatics through fractional crystallization or adsorption, but separation of xylene isomers is a difficult and energy intensive process due to similar boiling points.[7] Therefore, alternative methods to access *p*-xylene are highly desirable.

Other ways to produce *p*-xylene are through toluene disproportionation or methylation of benzene or toluene. Toluene disproportionation allows for two molecules of toluene to react and form xylenes and benzene (Scheme 5.1).[8]

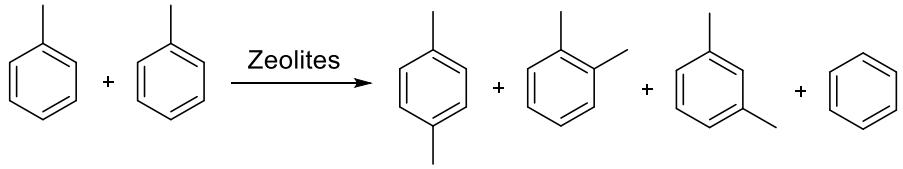

Scheme 5.1: Toluene disproportionation

This is a useful process because toluene is the least desirable of the BTX family and allows for conversion of toluene to xylenes. New processes allow for up to ninety percent selectivity for *p*-xylene during toluene disproportionation reactions.[9] The downside of this reaction is that toluene is used for a variety of other purposes and using toluene to synthesize the *p*-xylene decreases overall stock of toluene. Also, the reaction necessarily allows for a theoretical maximum yield of fifty percent for *p*-xylene due to concurrent production of benzene.

Unlike toluene disproportionation reactions, methylation of benzene or toluene does not have the same limitations on maximum yield of *p*-xylene. This process usually requires methanol and a zeolite catalyst, giving xylenes and water as a byproduct (Scheme 5.2).[10]

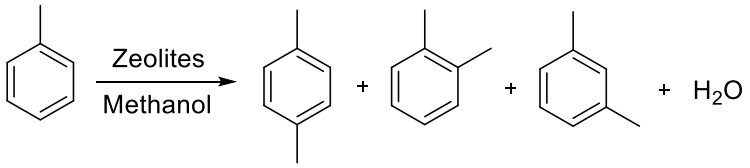

Scheme 5.2: Methylation of toluene

This process typically yields an unfavorable composition of xylenes due to the thermodynamic equilibrium of the reaction (52 % *m*-xylene, 24 % *o*-xylene and 24 % *p*-xylene).[4, 11, 12] Again, these isomers are difficult to separate due to similar boiling points.[7] However, the zeolites used for the reaction can be tuned to allow for isomerization of *m*-xylene and *o*-xylene to *p*-xylene.[13 - 19] This can be achieved by decreasing the pore size or removing the surface acid sites on the zeolites. Decreasing the pore size allows for increased diffusion of *p*-xylene compared to *o*-xylene or *m*-xylene, which leads to an increase in isomerization of both *o*-xylene and *m*-xylene while leaving *p*-xylene unchanged. The surface acid sites of zeolites can also isomerize xylenes and neutralizing the acid sites on the exterior of the zeolites prevents unselective acid-catalyzed isomerization of *p*-xylene by those surface sites. In some cases, zeolite modification can allow for close to 100 percent selectivity for *p*-xylene.[11, 20] While these reactions can be highly selective, the use of toluene or benzene as a starting material is undesirable due to the variety of other useful applications for those molecules. An alternative method for producing *p*-xylene from less valuable starting materials would be highly useful.

Accessing *p*-xylene via dehydroaromatization is a worthwhile goal because the reaction would allow for conversion of an alkane to *p*-xylene. Dehydroaromatization of linear alkanes can give benzene, toluene, and *o*-xylene but cannot yield any *m*-xylene or *p*-xylene due to the mechanism for aromatic formation (Scheme 5.3 and Figure 5.1).[21]

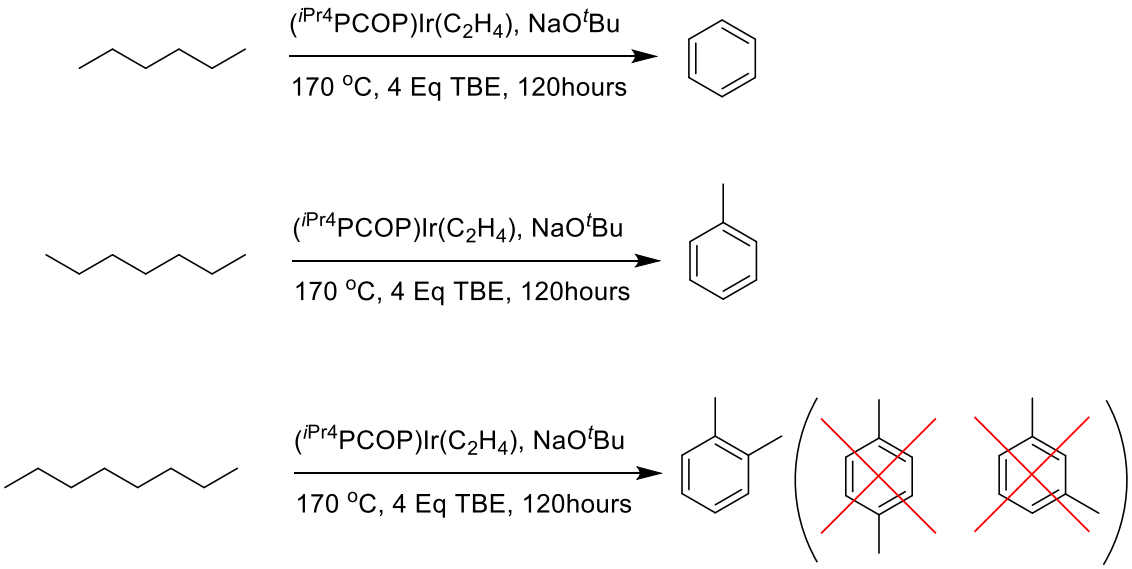

Scheme 5.3: Formation of BTX aromatics via dehydroaromatization

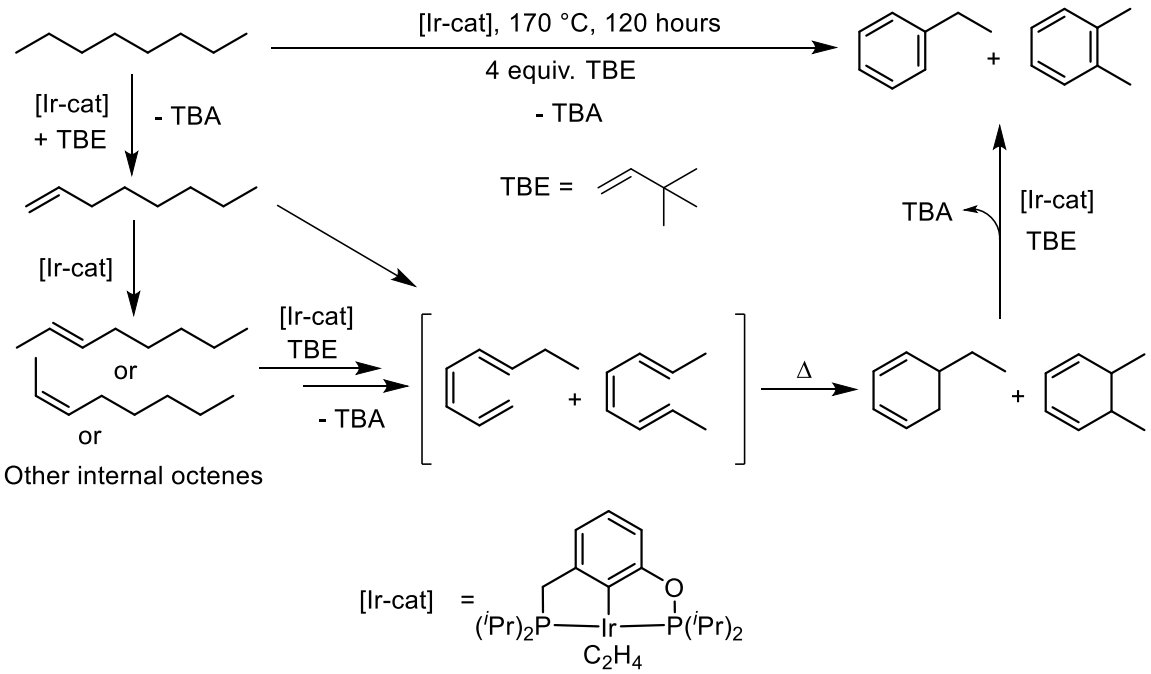

Figure 5.1: Dehydroaromatization of *n*-octane yields *o*-xylene and ethylbenzene

Dehydroaromatization of *n*-alkanes allows for access to members of all three aromatics of the BTX family but dehydroaromatization of *n*-octane can only yield *o*-xylene of the different xylene isomers. It would be desirable to find a way to use dehydroaromatization reactions to give *p*-xylene, and that goal is the focus of this chapter.

5.2 Results and Discussion

5.2.1 Dehydroaromatization of 3-Methylheptane

One possible alkane that can be used as a starting material for dehydroaromatization to form *p*-xylene is 3-methylheptane (Scheme 5.4).

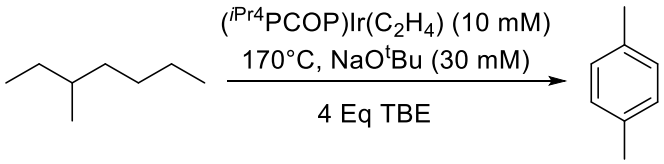

Scheme 5.4: Formation of *p*-xylene via dehydroaromatization of 3-methylheptane

Dehydroaromatization of 3-methylheptane can yield multiple aromatic products depending on the manner in which cyclization occurs (Scheme 5.5).

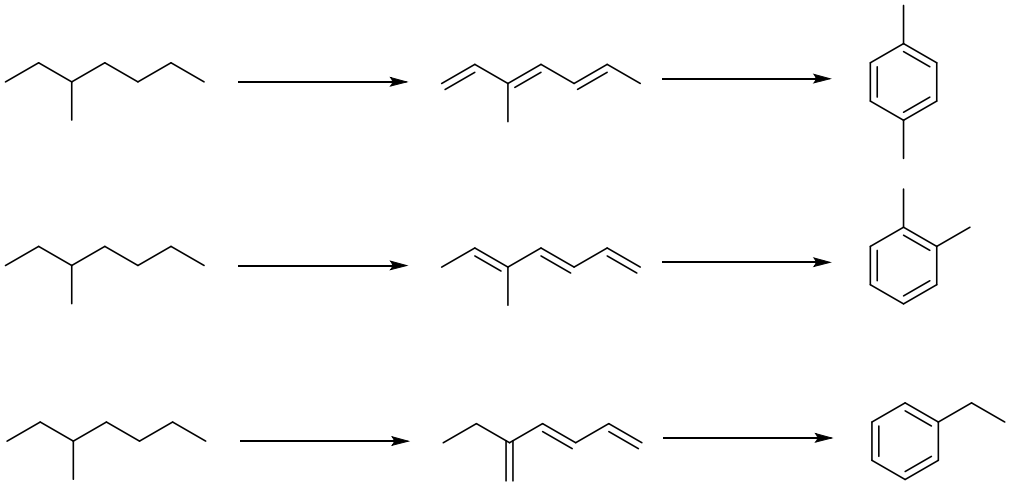

Scheme 5.5: Potential products formed from dehydroaromatization of 3-methylheptane

Cyclization can take place from three different trienes, which yields three different C_8 aromatic products. The potential for multiple C_8 aromatic products from 3-methylheptane starting material is not ideal, but this would be an interesting reaction nonetheless.

Data for dehydroaromatization of 3-methylheptane are shown below in Scheme 5.6, Figure 5.2, and Table 5.1.

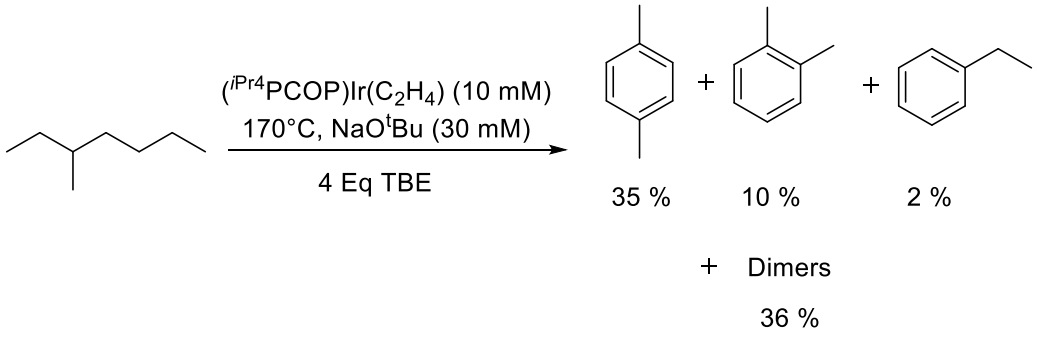

Scheme 5.6: Dehydroaromatization of 3-methylheptane

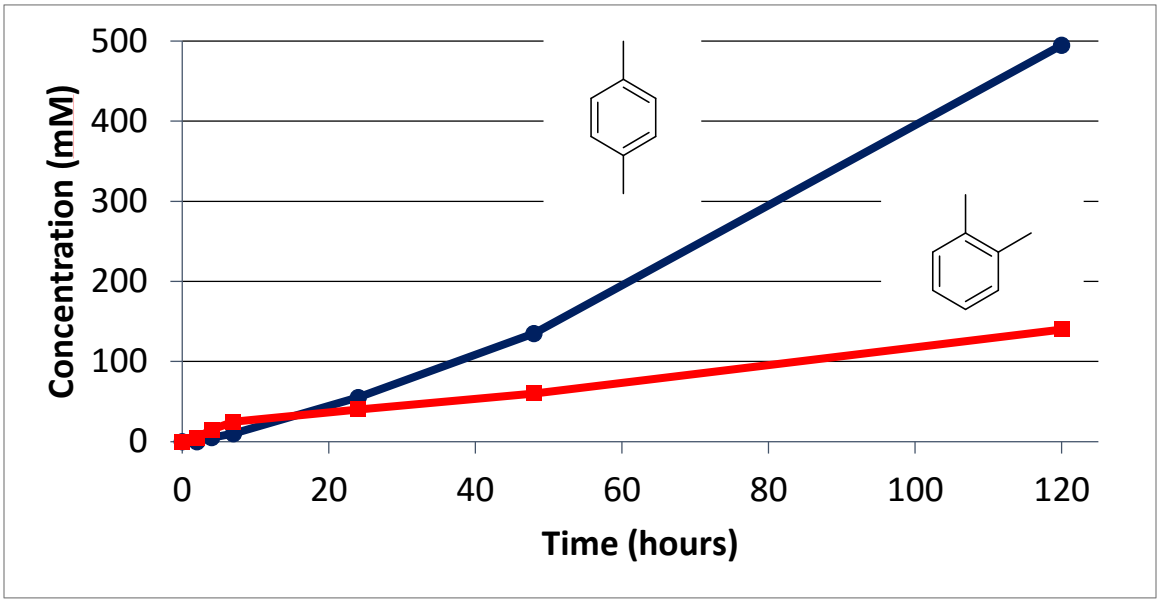

Figure 5.2: Dehydroaromatization of 3-methylheptane

Table 5.1: Dehydroaromatization of 3-methylheptane (mM)

Time	TBE	TBA	3-Methyl heptane	C_8 Olefins	Ethyl benzene	*o*-Xylene	*p*-Xylene	C_{16} Dimers
0 hr	5549	0	1376	0	0	0	0	0
2 hr	4855	645	1006	352	2	7	4	0
4 hr	4711	932	912	455	9	17	6	0
7 hr	4447	1077	822	500	12	25	13	5
24 hr	3696	1882	568	573	21	53	70	55
48 hr	2767	2555	366	480	24	72	151	150
120 hr	954	4335	101	175	29	132	474	245

Conditions: [(^{iPr}PCOP)Ir(C_2H_4)] = 10 mM; [3-methylheptane] = 1.4 M; [TBE] = 5.6 M; 170°C, 3 equivalents NaO^{t}Bu relative to catalyst. Dimers are formed via Diels-Alder reactions and iridium-mediated dimerization and are not well resolved on GC. Concentration of dimers are calculated based on missing 3-methylheptane.

Interestingly, the major C_8 product is *p*-xylene by a factor of about 3.5:1 relative to *o*-xylene and about 18:1 relative to ethylbenzene. This is a positive result towards the goal of synthesizing *p*-xylene from an alkane starting material, but there are some disadvantages with this reaction.

Dehydroaromatization of 3-methylheptane yields a significant amount of dimers so that the overall reaction is inefficient, but the main issue with this reaction is the use of 3-methylheptane as a starting material. 3-Methylheptane is not an economically viable starting material because access to 3-methylheptane is not trivial. 3-Methylheptane is available through gas streams but is not easily separated, and synthesis of 3-methylheptane would be cost prohibitive. Therefore, another method for synthesizing *p*-xylene is required.

5.2.2 Dehydroaromatization of 2-Ethyl-1-hexene

Although the dehydroaromatization of 3-methylheptane offered promising results for formation of *p*-xylene, the cost prohibitive nature of the starting material was undesirable. Attempts to find a suitable alternative led to using 2-ethyl-1-hexene for dehydroaromatization, which should form the same products as dehydroaromatization of 3-methylheptane (Scheme 5.7).

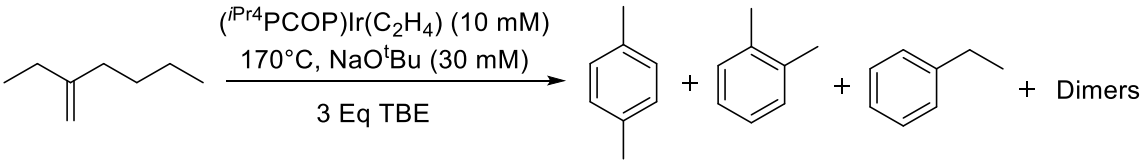

Scheme 5.7: Products formed by dehydroaromatization of 2-ethyl-1-hexene

2-Ethyl-1-hexene is a desirable starting material for dehydroaromatization reactions because it can be synthesized in an economically attractive fashion. Dimerization of ubiquitous ethylene is a known reaction to form 1-butene and dimerization of 1-butene is a known reaction to form 2-ethyl-1-hexene (Scheme 5.8).[22-26]

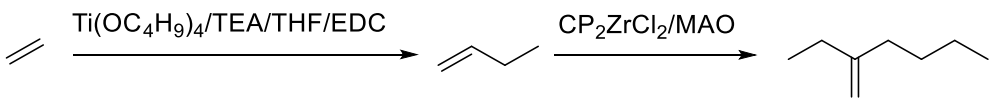

Scheme 5.8: Synthesis of 2-ethyl-1-hexene

These two known reactions show that 2-ethyl-1-hexene can be synthesized from ethylene. Combining the synthesis shown in Scheme 5.8 with dehydroaromatization of 2-ethyl-1-hexene means that *p*-xylene can be accessed from ethylene as the starting material. This is highly desirable due to the massive amount of ethylene supply across the world.

Data for the dehydroaromatization of 2-ethyl-1-hexene are shown below in Scheme 5.9, Figure 5.3, and Table 5.2.

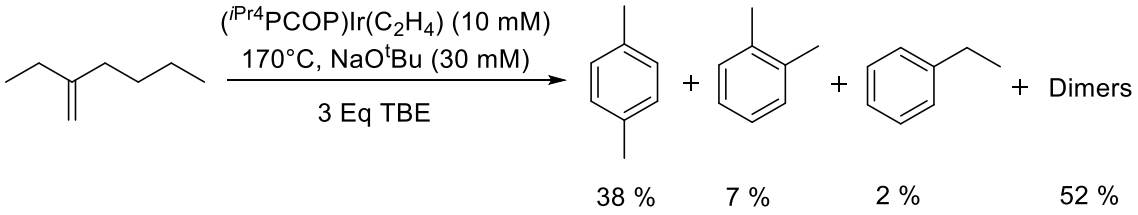

Scheme 5.9: Dehydroaromatization of 2-ethyl-1-hexene

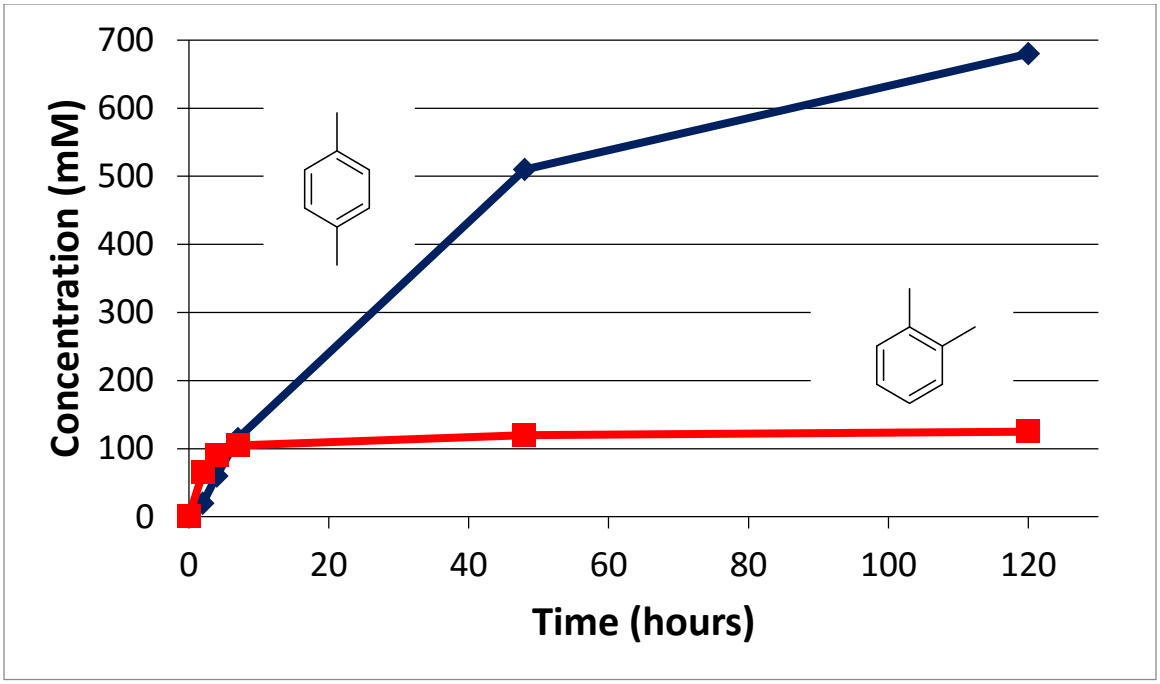

Figure 5.3: Dehydroaromatization of 2-ethyl-1-hexene

Table 5.2: Dehydroaromatization of 2-ethyl-1-hexene (mM)

Time	TBE	TBA	2-Ethyl-1-hexene	C_8 Olefins	Ethyl benzene	*o*-Xylene	*p*-Xylene	C_{16} Dimers
0 hr	5540	0	1179	557	0	0	0	0
2 hr	4748	852	598	961	19	61	21	70
4 hr	4403	1215	482	987	24	80	53	85
7 hr	4247	1715	315	849	31	81	90	215
48 hr	1184	4762	16	225	36	126	535	420
120 hr	108	6153	0	8	37	128	687	470

Conditions: [(^{iPr}PCOP)Ir(C_2H_4)] = 10 mM; [2-ethyl-1-hexene] = 1.8 M; [TBE] = 5.6 M; 170°C, 3 equivalents NaO^{t}Bu relative to catalyst. Dimers are formed via Diels-Alder reactions and iridium-mediated dimerization and are not well resolved on GC. Concentration of dimers are calculated based on missing 2-ethyl-1-hexene.

Compared to 3-methylheptane, dehydroaromatization of 2-ethyl-1-hexene gives a slightly higher percentage of *p*-xylene (38 % vs 35 %), but the biggest difference is the ratio of *p*-xylene to *o*-xylene (5.4:1 vs 3.5:1). Another advantage to using 2-ethyl-1-hexene as a starting material is that the dehydroaromatization process in this case only requires three equivalents of hydrogen acceptor. This further decreases the overall cost of the reaction due to the cost of using TBE as an acceptor.

Two other issues that need to be addressed are the interesting kinetics of formation for *o*-xylene and the significant formation of dimers from this reaction. The kinetics of formation for *o*-xylene show that a large amount of *o*-xylene is formed during the first several hours of reaction but the total *o*-xylene concentration levels off after seven hours while *p*-xylene is still forming for the full length of the reaction (see Figure 5.3). In order to understand this observation, analysis of the pathways of *o*-xylene and *p*-xylene must be performed.

The pathways for formation of *o*-xylene and *p*-xylene show why *o*-xylene formation levels off after a couple hours (Scheme 5.10).

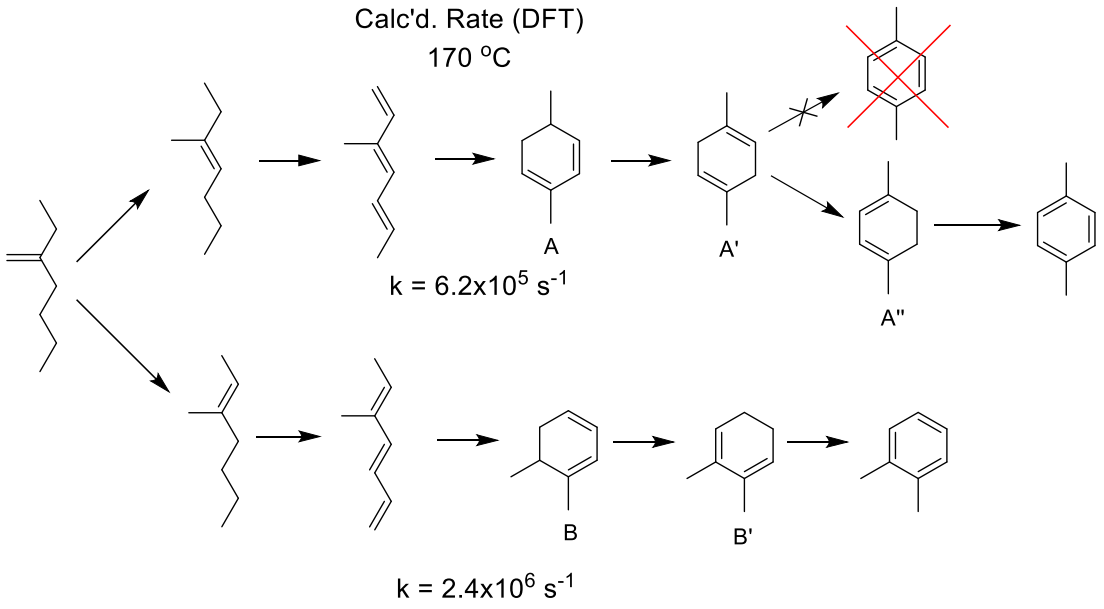

Scheme 5.10: Pathway of formation for *p*-xylene and *o*-xylene

In order for either *o*-xylene or *p*-xylene to form from 2-ethyl-1-hexene, isomerization of the initial double bond needs to take place. That double bond can isomerize to the right, which will ultimately lead to formation of *p*-xylene, or it can isomerize to the left, which will ultimately lead to formation of *o*-xylene. Isomerization across the methyl group is higher in energy than either isomerization between primary and secondary carbon or isomerization between two secondary carbons and a second dehydrogenation reaction will be favorable due to the presence of a diene which is stabilized by hyperconjugation, so isomerization across the methyl group is unlikely.[27, 28] It should be noted that DFT calculations were performed on the cyclization of the trienes, and although the *o*-xylene triene precursor cyclizes faster than the *p*-xylene triene precursor, the difference in cyclization rates is negligible.

Therefore, the hypothesis states that *o*-xylene precursors are consumed faster than the *p*-xylene precursors. Specifically, the cyclic diene intermediates A and B that are formed after cyclization of the previous trienes show why *o*-xylene formation is quick and levels off. For *o*-xylene precursor B, isomerization takes place to yield precursor B', which contains a conjugated pair of thermodynamically stable tertiary olefins. Intermediate B' can easily be directly dehydrogenated to give *o*-xylene. On the other hand, *p*-xylene precursor A will first isomerize to yield a non-conjugated pair of thermodynamically stable tertiary olefins (precursor A'). Intermediate A' cannot be directly dehydrogenated to give *p*-xylene. In order to reach *p*-xylene, one of the tertiary double bonds needs to be isomerized across the methyl group to produce precursor A''. Even though additional thermodynamic stability is imparted to intermediate A'' due to hyperconjugation of the double bonds, the relatively high kinetic barrier of isomerization across the methyl group slows down overall formation of *p*-xylene.

Also, it should be noted that a change in the active catalytic species is not the reason for *o*-xylene formation leveling off: the ratio of *o*-xylene to *p*-xylene after two hours is 1.8:1, and removing the catalyst from the solution and adding fresh reagents gives a ratio of 2.4:1 of *o*-xylene to *p*-xylene. If the catalyst was the cause for *o*-xylene leveling off, that ratio should decrease significantly to the point where *p*-xylene formation is favored. Therefore, a change in the active catalyst is not the cause of the interesting formation kinetics of *o*-xylene.

The amount of dimers formed after 120 hours during dehydroaromatization of 2-ethyl-1-hexene is exceedingly high (52 %). This number would have to be significantly

decreased for this process to be of commercial interest. Dimers are formed via Diels-Alder reactions between the multitude of olefin intermediates produced or via iridium-mediated dimerization. Dimer formation can be limited by increasing the temperature of the reaction, diluting the reaction, or by promoting gas phase reactions.

Dimer formation via Diels-Alder reactions can be limited by increasing the temperature of the reaction because Diels-Alder reactions are reversible at high temperatures.[29] Also, increasing the temperature of the reaction will increase the overall rate of dehydroaromatization so intermediate olefins will react faster and be less likely to undergo Diels-Alder dimerization or iridium-mediated dimerization. Attempts to limit dimer formation by increasing the temperature of dehydroaromatization are summarized in Table 5.3.

Table 5.3: Limitation of dimers through increased temperature after 120 hours

Reaction	Ethyl benzene	*o*-Xylene	*p*-Xylene	C_{16} Dimers
170 °C	2 %	7 %	38 %	52 %
200 °C	6 %	7 %	51 %	33 %
230 °C	5 %	8 %	45 %	42 %

Conditions: [(^{iPr}PCOP)Ir(C_2H_4)] = 10 mM; [2-ethyl-1-hexene] = 1.8 M; [TBE] = 5.6 M; 3 equivalents NaO^{t}Bu relative to catalyst. Dimers are formed via Diels-Alder reactions and iridium-mediated dimerization and are not well resolved on GC. Concentration of dimers are calculated based on missing 2-ethyl-1-hexene.

Increasing the temperature from 170 °C to 200 °C decreases total dimer formation to 33 % from 52 % and increases *p*-xylene concentration to 51 % from 38 %. Total *o*-xylene stays

the same while ethylbenzene increases from 2 % to 6 %. The overall reaction is much better because the dimer formation decreased while the ratio of *p*-xylene to *o*-xylene increased from 5.4:1 to 7.3:1. Interestingly, although the temperature to 230 °C does give better yields compared to the reaction at 170 °C, it does not give better yields of desired products compared to the reaction at 200 °C. This is likely due to slight catalyst decomposition at the elevated temperature.

Diluting the reaction in a solvent that is inactive towards the catalyst can also decrease dimer formation because the olefins in solution will be diluted and therefore less likely to react with other olefins. As the ($^{i\text{Pr}}$PCOP)Ir catalyst cannot C-H activate ortho to a methyl group, mesitylene can be conveniently used as a solvent in a 5:1 ratio to the reaction mixture to dilute the concentration of olefin species in solution.[30] Attempts to limit dimer formation through dilution are summarized below in Table 5.4.

Table 5.4: Limitation of dimers through dilution after 120 hours

Reaction	Ethyl benzene	*o*-Xylene	*p*-Xylene	C_{16} Dimers
170 °C[a]	2 %	7 %	38 %	52 %
170 °C[b] Diluted	3 %	13 %	43 %	27 %
200 °C[b] Diluted	7 %	11 %	60 %	20 %
230 °C[b] Diluted	8 %	12 %	54 %	23 %

Conditions: [a] [($^{i\text{Pr}}$PCOP)Ir(C_2H_4)] = 10 mM; [2-ethyl-1-hexene] = 1.8 M; [TBE] = 5.6 M; 3 equivalents NaO^{t}Bu relative to catalyst.

[b] [($^{i\text{Pr}}$PCOP)Ir(C_2H_4)] = 10 mM; [2-ethyl-1-hexene] = 0.36 M; [TBE] = 1.1 M; 3 equivalents NaO^{t}Bu relative to catalyst. Dimers are formed via Diels-Alder reactions and iridium-mediated dimerization and are not well resolved on GC. Concentration of dimers are calculated based on missing 2-ethyl-1-hexene.

Diluting the reaction by eighty percent in unreactive mesitylene leads to a significant decrease in dimer formation (52 % to 27 %) and an increase in C_8 aromatics (47 % to 59 %). However, there is a decrease in the ratio of *p*-xylene to *o*-xylene (5.4:1 to 3.3:1) and some unreacted starting material. Combining the idea of increasing the temperature of the reaction with diluting the reaction in mesitylene leads to a better reaction. At 200 °C and eighty percent dilution in mesitylene total dimer formation is down to 20 % while *p*-xylene formation is up to 60 %. Also, the ratio of *p*-xylene to *o*-xylene remains the same and there is very little unreacted starting material. The yield of ethylbenzene increases from 2 % to 7 % due to the rate of dehydrogenation increasing at higher temperatures and leading to less isomerization of 2-ethyl-1-hexene, which aromatizes to ethylbenzene (see Scheme 5.5). Again, increasing the temperature to 230 °C did not yield better results than the reaction at 200 °C due to slight decomposition of the catalyst at the elevated temperature.

The final method for decreasing dimer formation is to run the dehydroaromatization reaction in the gas phase based on work performed in the Goldman Group by Akshai Kumar and co-workers.[31] Running the reaction in the gas phase will limit dimer formation because the Diels-Alder dimerization will be entropically unfavorable and the equilibrium will shift towards the retro-Diels-Alder products.[32] Unfortunately, every attempt to run gas phase dehydroaromatization reactions led to catalyst decomposition and a large amount of unreacted starting material. Catalyst

decomposition was observed despite changes to reaction time, temperature, catalyst, NaO^tBu, volume, and reaction procedure. A dehydroaromatization reaction was run under gas phase conditions and typical liquid phase dehydroaromatization conditions from the same stock solution to compare yields of products (Table 5.5).

Table 5.5: Gas phase vs. liquid phase dehydroaromatization

Phase	Unreacted S.M.	Ethyl benzene	*o*-Xylene	*p*-Xylene	C_{16} Dimers
Liquid	2 %	3 %	9 %	43 %	40 %
Gas	46 %	2 %	9 %	35 %	1 %

Conditions: [(^{iPr}PCOP)Ir(C_2H_4)] = 10 mM; [2-ethyl-1-hexene] = 1.8 M; [TBE] = 5.6 M; 120 hours, 200 °C, 3 equivalents NaO^tBu relative to catalyst. Dimers are formed via Diels-Alder reactions and iridium-mediated dimerization and are not well resolved on GC. Concentration of dimers are calculated based on missing 2-ethyl-1-hexene.

Catalyst decomposition is observed for the gas phase reaction and not observed for the liquid phase reaction despite both reactions being run under the same conditions. The gas phase reaction has 46 % unreacted 2-ethyl-1-hexene compared to just 2 % for the liquid phase reaction. However, despite a large amount of unreacted starting material for the gas phase reaction, total dimer formation is drastically decreased compared to the liquid phase reaction (1 % vs. 40 %). Also, total C_8 concentration for the gas phase reaction is only marginally lower than the liquid phase reaction, again despite 46 % unreacted starting material for the gas phase reaction. Running the dehydroaromatization reaction in the gas phase successfully decreases total dimer formation, therefore preventing catalyst decomposition for this reaction is a worthwhile goal.

5.2.3 Dehydroaromatization of 4-Methylheptane

Although *m*-xylene is not as useful as *p*-xylene, there is some commercial interest in synthesizing *m*-xylene for use in synthesis of resorcinol.[33] Resorcinol is used for production of tires, resins, acne medications, and many other commercial products.[34] Based on previous results showing that 3-methylheptane can be dehydroaromatized to give *p*-xylene, 4-methylheptane should dehydroaromatize to form *m*-xylene. Because the triene formed from transfer dehydrogenation of 4-methylheptane is symmetrical, the only aromatic product that can be formed is *m*-xylene (Scheme 5.11).

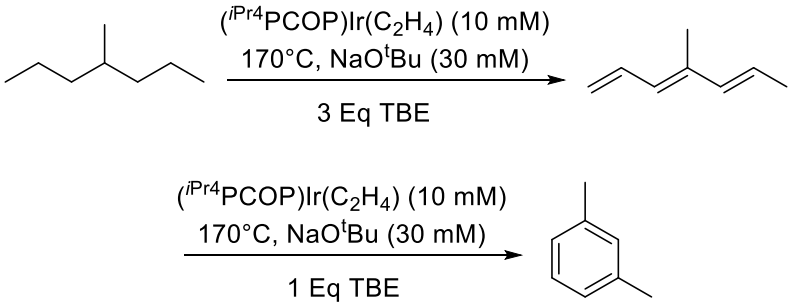

Scheme 5.11: Formation of *m*-xylene through dehydroaromatization of 4-methylheptane

Data for the formation of *m*-xylene from dehydroaromatization of 4-methylheptane is shown below in Scheme 5.12 and Table 5.6.

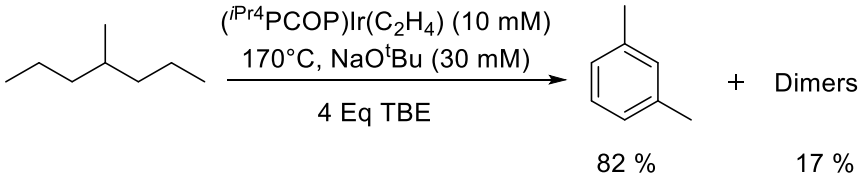

Scheme 5.12: Dehydroaromatization of 4-methylheptane

Table 5.6: Dehydroaromatization of 4-methylheptane (mM)

Time	TBE	TBA	4-methyl heptane	C_8 Olefins	*m*-Xylene	C_{16} Dimers
0 hr	6026	0	1459	0	0	0
2 hr	5050	1031	792	659	10	0
4 hr	4772	1243	728	752	23	0
7 hr	4456	1586	597	801	54	0
24 hr	2928	3122	303	724	335	50
48 hr	1376	4236	119	409	810	80
120 hr	17	5988	3	20	1171	130

Conditions: [($^{i\text{Pr}}$PCOP)Ir(C_2H_4)] = 10 mM; [4-methylheptane] = 1.43 M; [TBE] = 5.72 M; 120 hours, 170 °C, 3 equivalents NaO^{t}Bu relative to catalyst. Dimers are formed via Diels-Alder reactions and iridium-mediated dimerization and are not well resolved on GC. Concentration of dimers are calculated based on missing 4-methylheptane.

Interestingly, the total dimer formation for this reaction is significantly decreased compared to the dehydroaromatization of 3-methylheptane or 2-ethyl-1-hexene. Along with decreased dimers, there is a large amount of *m*-xylene (82 % yield). Applying the same ideas that gave decreased dimers for dehydroaromatization of 2-ethyl-1-hexene should also further decrease dimers for dehydroaromatization of 4-methylheptane.

Similar to 3-methylheptane, 4-methylheptane is an exotic starting material and lack of an economically viable synthetic procedure makes this reaction difficult to commercialize.

5.2.4 Dehydroaromatization of 2,5-Dimethylhexane

One of the disadvantages to using 2-ethyl-1-hexene as a starting material for dehydroaromatization to for *p*-xylene is that multiple C_8 aromatic products are possible from that reaction. Dehydroaromatization using 2,5-dimethylhexane as a starting material would give *p*-xylene as the only C_8 aromatic product (Scheme 5.13).

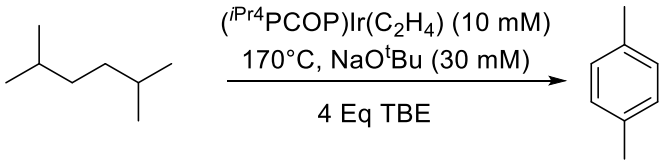

Scheme 5.13: Formation of *p*-xylene from dehydroaromatization of 2,5-dimethylhexane

Dehydroaromatization reactions using 2,5-dimethylhexane gave very little *p*-xylene and instead gave a large amount of 2,5-dimethyl-2,4-hexadiene, which does not go on to form *p*-xylene (Scheme 5.14).

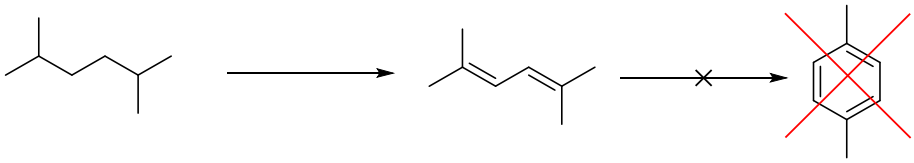

Scheme 5.14: 2,5-Dimethyl-2,4-hexadiene prevents *p*-xylene formation

Once the double bonds are in the 2,4 position, they are unlikely to be isomerized. This is due to the high stability imparted by both bonds being adjacent to tertiary carbons and that the diene is stabilized by hyperconjugation. Changing the temperature, catalyst, and reaction time had little effect on the overall concentration of *p*-xylene and it is unlikely that 2,5-dimethylhexane can be a viable starting material for dehydroaromatization.

5.3 Experimental

5.3.1 General Procedure for Dehydroaromatization

The representative procedure for dehydroaromatization reactions is as follows: In an argon-filled glove box, ($^{i\text{Pr}}$PCOP)Ir(η^2-C_2H_4) (5.6 mg, 0.01 mmol, 10 mM) was dissolved in substrate (e.g. 2-ethyl-1-hexene : 0.28 mL, 1.82 mmol, 1.8 M); TBE (3.1 equivalents with respect to 2-ethyl-1-hexene, 0.7 mL, 5.46 mmol, 5.5 M) and mesitylene (0.01 mL, internal standard) were then added to the solution. Aliquots of this solution (0.1 mL each) were transferred to several 5 mm glass tubes and the contents were cooled under liquid nitrogen and sealed under vacuum. The sealed tubes were heated simultaneously in a preheated oven. At regular intervals, a tube was brought to room temperature and the

sample was analyzed by gas chromatography in comparison with authentic products. The major products were confirmed by GC-MS.

All alkanes, alkenes, mesitylene, and TBE were distilled under vacuum from Na/K alloy after several freeze-pump-thaw cycles and stored in an argon glove box. Gas chromatography (GC) measurements were performed on a Varian 430 instrument fitted with a capillary column (30 m length x 0.25 mm inner diameter x 0.5 μm film thickness). Gas chromatography – mass spectrometry (GC-MS) measurements were performed on a Varian 3900 Saturn 2100T instrument fitted with a capillary column (30 m length x 0.25 mm inner diameter x 0.25 μm film thickness).

5.3.2 DFT Information

All calculations were carried out using the Gaussian 09 suite of quantum chemical programs and the Lee-Yang-Parr correlation functional B3LYP with a 6-311 + (d,g) basis set.[35] Rates were calculated using the Eyring equation.[36] The following tables and figures are DFT coordinates for calculations presented in Table 3.7 and Table 3.8.

5.4 Summary

Dehydroaromatization reactions were performed on non-linear starting materials to give different products. Specifically, 3-methylheptane and 2-ethyl-1-hexene were used to form the highly desirable molecule *p*-xylene. 2-Ethyl-1-hexene is a particularly

attractive starting material because it can be synthesized using known methods from ethylene. *p*-Xylene is the major product formed form these reactions and attempts to minimize all other products has led to a yield of sixty percent *p*-xylene. *m*-Xylene is useful as a precursor to resorcinol and can be synthesized using dehydroaromatization starting from 4-methylheptane. Attempts to synthesize *p*-xylene from 2,5-dimethylhexane starting material were unsuccessful due to the formation of the highly stable diene 2,5-dimethyl-2,4-hexadiene.

5.5 Appendix

The following figures are GC traces of dehydroaromatization reactions after 120 hours.

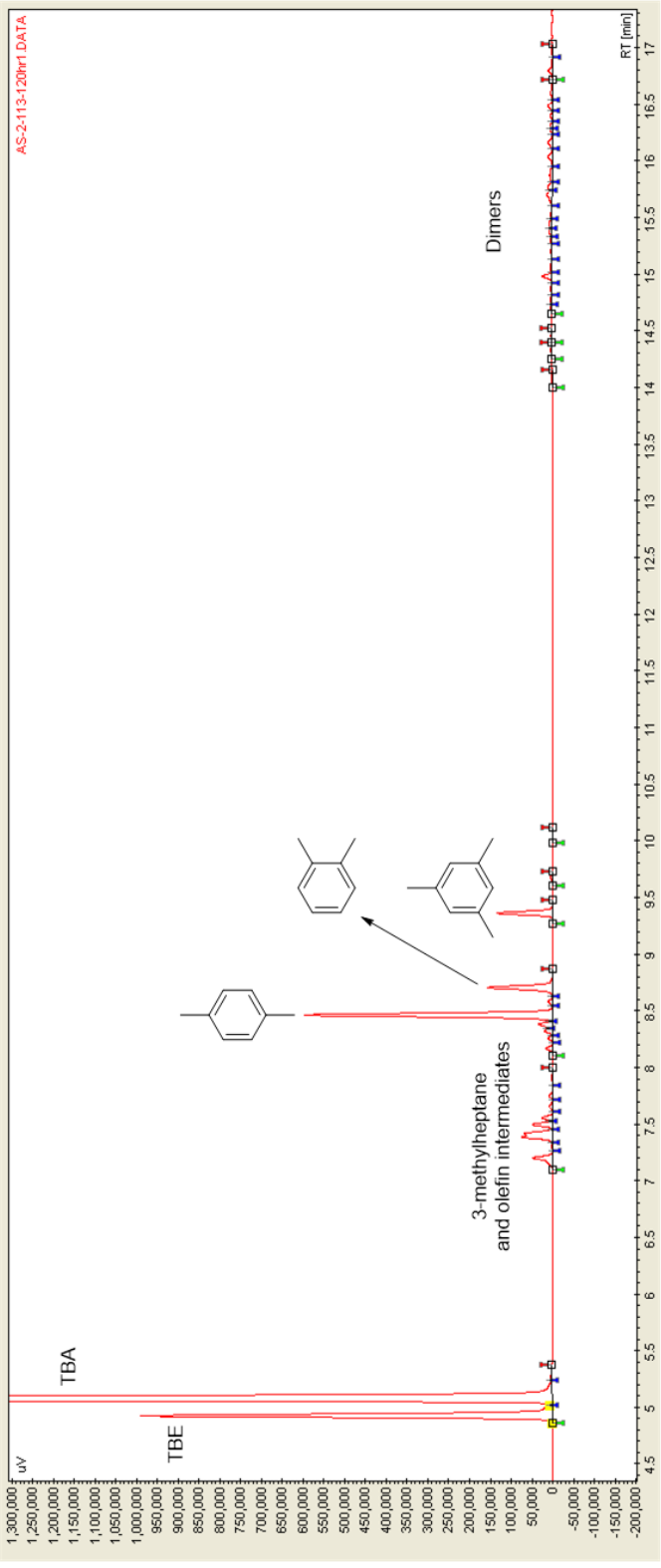

Figure 5.4: GC trace for dehydroaromatization of 3-methylheptane

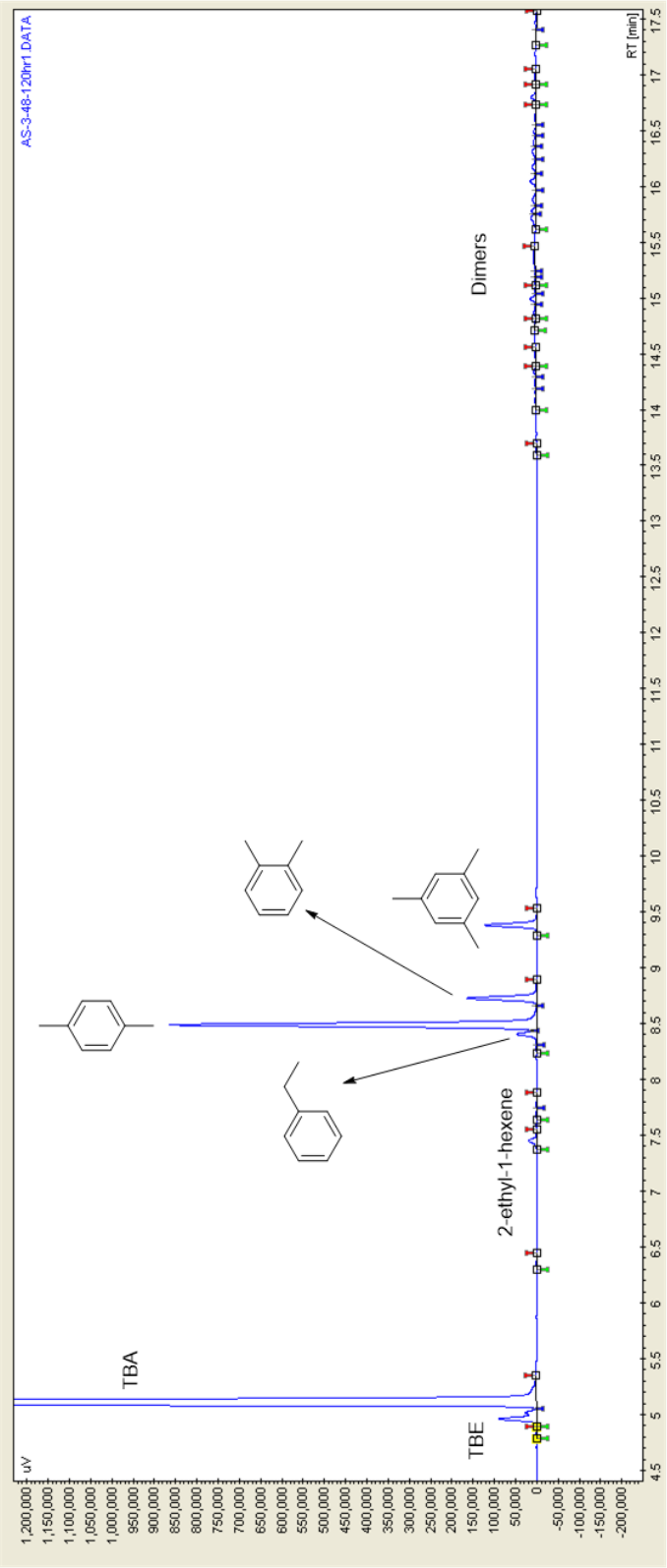

Figure 5.5: GC trace for dehydroaromatization of 2-ethyl-1-hexene

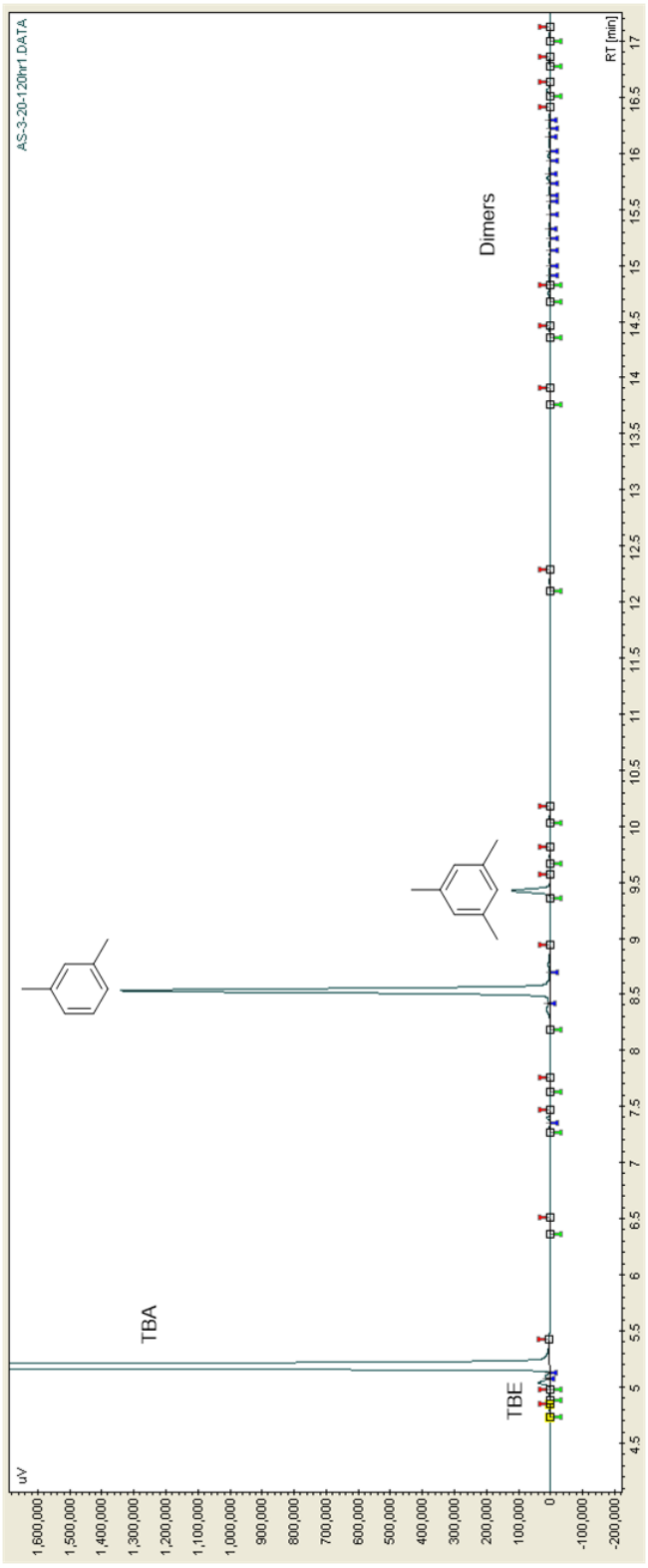

Figure 5.6: GC trace for dehydroaromatization of 4-methylheptane

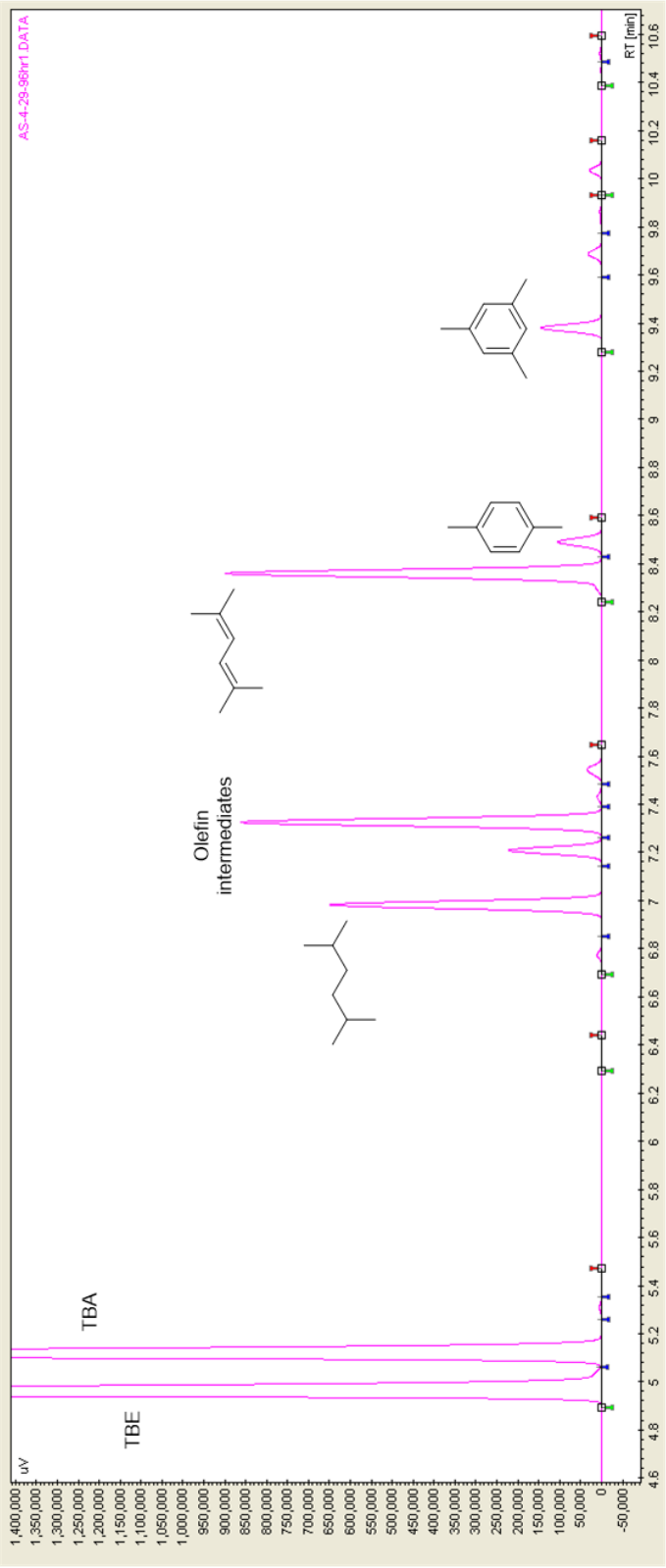

Figure 5.7: GC trace for dehydroaromatization of 2,5-dimethylhexane

5.6 References

[1] Witcoff, H. A.; Reuben, B. G.; Plotkin, J. S. *Industrial Organic Chemicals* 2nd edn (Wiley-IEEE, 2005).
[2] Fabri, J.; Graeser, U.; Simo, T. A. Xylenes, *Ullmann's Encyclopedia of Industrial Chemistry* (Wiley-VCH, Weinheim, 2000).
[3] Wantanachaisaeng, P.; O'Niel, K. *Capturing Opportunities for Para-Xylene Production*, **2010**.
[4] Ashraf, M. T.; Chebbi, R.; Darwish, N. A. *Ind. Eng. Chem. Res.* **2013**, *52*, 13730.
[5] Paraxylene. http://www.cpchem.com/bl/aromatics/en-us/Pages/Paraxylene.aspx (accessed September 14th 2015).
[6] Rahimpour, M. R.; Jafari, M.; Iranshahi, D. *Appl. Energy*, **2013**, *109*, 79.
[7] Egan, C. J.; Luthy, R. V. *Ind. Eng. Chem.* **1955**, *47*, 250.
[8] Uguina, M. A.; Sotelo, J. L.; Serrano, D. P. *Ing. Eng. Res. Chem.* **1993**, *32*, 49.
[9] PxMax (selective toluene disproportionation), http://www.exxonmobilchemical.com/Chem-English/brands/pxmax-selective-toluene-disproportionation.aspx?ln=productsservices (accessed September 14th 2015).
[10] Raibu, S.; Al-Khattaf, S. *Ind. Eng. Chem. Res.* **2008**, *47*, 39
[11] Breen, J. P.; Burch, R.; Kulkarni, M.; Collier, P.; Golunski, S. *J. Am. Chem. Soc.* **2005**, *127*, 5020.
[12] Aboul-Gheit, A. K.; Hanafy, S. A.; Aboul-Enein, A. A.; Ghoneim, S. A. *J. Taiwan Inst. Chem. Eng.* **2011**, *42*, 860.
[13] Chen, N. Y.; Kaeding, W. W.; Dwyer, F. G. *J. Am. Chem. Soc.* **1979**, *101*, 6783.
[14] Nunan, J.; Cronin, J.; Cunningham, J.; *J. Catal.* **1984**, *87*, 77.
[15] Van Vu, D.; Miyamoto, M.; Nishiyama, N.; Egashira, Y.; Ueyama, K. *J. Catal.* **2006**, *243*, 389.
[16] Li, Y. G.; Xie, W. H.; Yong, S. *Appl. Catal., A.* **1997**, *150*, 231.
[17] Faramawy, S. *Pet. Sci. Technol.* **1999**, *17*, 249.
[18] Mirth, G.; Cejka, J.; Lercher, J. A. *J. Catal.* **1993**, *139*, 24.
[19] Breen, J. P.; Burch, R.; Kulkarni, M.; McLaughlin, D.; Collier, P. J.; Golunski, S. E. *Appl. Catal., A* **2007**, *316*, 53.
[20] Sotelo, J. L.; Uguina, M. A.; Valverde, J. L.; Serrano, D. P. *Ind. Eng. Chem. Res.* **1993**, *32*, 2548.
[21] Ahuja, R.; Punji, B.; Findlater, M.; Supplee, C.; Schinski, W.; Brookhart, M.; Goldman, A. S. *Nature Chem* **2011**, *3*, 167.
[22] Roy, D.; Sunoj, R. B. *Org. Biomol. Chem.* **2010**, *8*, 1040-1051.
[23] Zhang, W.; Li, C.; He, R.; Han, X.; Bao, X. *Catal. Lett.* ***2000,*** 64*,* 147-150.
[24] Kissin Y.V. *Macromol. Chem. Phys*. **2009**, *210*, 1241.
[25] Kissin, Y. V.; Schwab, F. C. *J. Appl. Pet. Sci.* **2009**, *111*, 273.
[26] Karinen, R. S.; Krause, A. O. I.; Tikkanen, E. Y. O.; Pakkanen, T. T. *J. Mol. Catal.: A Chem.* **2000**, *152*, 253.
[27] Hubert, A. J.; Reimlinger, H. *Synthesis*, **1969**, 97.
[28] Hubert, A. J.; Reimlinger, H. *Synthesis*, **1970**, *1*, 405.
[29] Kwart, H.; King, K. *Chem. Rev.* **1968**, *68*, 415.
[30] Golberg, K. I.; Goldman, A. S. *Activation and Functionalization of C-H Bonds*; Oxford University Press, 2004.
[31] Kumar, A.; Zhou, T.; Emge, T. J.; Mironov, O.; Saxton, R. J.; Krogh-Jespersen, K.; Goldman, A. S. *J. Am. Chem. Soc.* Paper submitted, **2015**.
[32] Huybrechts, G.; Rigaux, D.; Vankeerberghen, J.; van Mele, B. *Int. J. Chem. Kinet.* **1980**, *12*, 253.
[33] Suzuki, S (Chevron Res, USA). Resorcinol Process. US Patent 3903177 A, September 2nd, 1975
[34] Rubber Chemicals, Resorcinol. http://www.sumitomo-chem.co.jp/kaseihin/english/rubber_chemicals/ (accessed 5/28/14), part of Sumitomo Chemical Specialty Chemicals Division.
[35] Lee, C.; Yang, W.; Parr, R. G. *Phys. Rev. B* **1988**, *37*, 785.
[36] Eyring, H. *J. Chem. Phys.* **1935**, *3*, 9.